IMPERIAL COLLEGE LONDON

DEPARTMENT OF ELECTRICAL AND ELECTRONIC ENGINEERING

Energy Demand Management of Electric Vehicles

Qazi Rashid Hamid

13th January 2014

A thesis submitted in partial fulfillment of the requirements for the degree
of Doctor of Philosophy and the Diploma of Imperial College London

Declaration of Originality

I declare that the work presented in this thesis is my own and that all else is appropriately referenced.

Qazi Rashid Hamid

Copyright Declaration

Abstract

The aim of this thesis is to investigate novel recharging schemes for energy demand management (DM) of electric vehicles (EVs). While there has been a lot of work highlighting the importance of energy DM of EVs, most of the reported works do not expand on suggesting how such a DM system may be implemented. In this thesis the focus is on two aspects of DM system implementation. At the instantaneous control time scale, an alternative mechanism for frequency regulation with the aim of neutralising sudden changes in output power of electric generators is presented. At the recharge planning time scale, the aim is to avoid congestion and undesirable voltage drops in the distribution system, and a novel approach is presented that can improve voltage profiles. The problem of considering both voltage congestion and frequency regulation in a composite DM framework is also addressed.

At the instantaneous control time scale, a novel distributed recharging rate controller is presented that is based on non-linear control and that yields a real time and distributed solution. This controller minimises communication overheads and allows EVs to join and leave at arbitrary times. From the perspective of recharging rate allocation, the controller achieves a Pareto efficient allocation which is also proportionally fair. The proposed controller is then applied to a system with a single, isolated, and unregulated synchronous machine and it is shown that the frequency can be used as proxy to the imbalance between produced and consumed electric power and hence communication overhead can be eliminated in such cases. A protocol is also discussed that can modify the controller and can implement the modified controller in a multi-machine system. Simulation is used to show the frequency regulation and fairness of recharging rates of EVs when the protocol and the modified controller are used. Subsequently, the integration of the recharging rate controller with the legacy protection system is also discussed.

At the recharge planning time scale, the problem of congestion in the distribution system is addressed. Most of published literature on distribution system voltage issues deals with control of various network elements, for instance, on-load tap changers or banks of shunt capacitors on the distribution feeders. In this thesis, a complementary approach

is presented that can also improve voltage profile by scheduling EV load in such a manner that undesirable voltage drops are avoided or their severity is diminished. In this context, a novel approach is presented for recharging EVs in the same geographic neighbourhood that share the same secondary circuits when recharging. The approach is based on a numerical method called Smoothed Particle Hydrodynamics (SPH) that has been previously used by other researchers to solve the equations of fluid dynamics. The characteristics of the method used for the proposed approach as well as its performance in term of improvement in the reduction of voltage drops and its adaptation to elastic and non-elastic loads is highlighted via simulation. Finally, the approach is extended to also provide a frequency control reserve service.

Acknowledgements

Contents

List of Figures

List of Tables

List of Acronyms

DM   Demand Management.

DR   Demand Response.

DSM   Demand Side Management.

DSO   Distribution System Operator.

EDP   Energy Demand Particle.

EDPS   Energy Demand Particle System.

EV   Electric Vehicle.

FP   Fluid Particle.

FPS   Fluid Particle System.

SPH   Smoothed Particle Hydrodynamics.

List of Symbols

$\Delta\omega$ Frequency deviation of electric power system

a   Acceleration of fluid particle (FP) in fluid particle system (FPS)

P   Vector of recharging rates=$[p_1, \; p_2, \; \ldots p_N]$

v   Velocity of FP in FPS

x   Position of FP in FPS

ρ density

τ FPS simulation time

$C(t)$ Net power capacity available to recharge EVs in G2V mode

$ED_{j,k}$ Energy demand specified by $EV_{j,k}$

$EV_{j,k}$ kth EV connected to secondary circuit node j

I_j Current injection at bus j

m Mass of FP in FPS

N Number of recharging EVs

Nb Number of buses in the distribution system

p_i Recharging rate of ith EV

P_j Net active power injection at bus j

p_{edp} The amount of active power associated with a EDP

P_{EV} Aggregate recharging rate=$\sum_{i=1}^{N} p_i$

$p_{imaxV2G}$	The maximum discharge rate of *ith*
p_{imax}	Maximum recharging rate of *ith* EV
$p_{j,k}$	Recharging rate of $EV_{j,k}$
$P_{NEV}(t)$	Power demand from non-EV loads,
$P_{SCH}(t)$	Scheduled Power
$P_{V2G}(t)$	Aggregate power drawn from EVs in V2G mode
Q_j	Net reactive power injection at bus j
S_j	Net apparent power injection at bus j
$t\_A_{j,k}$	Arrival time of $EV_{j,k}$
$t\_D_{j,k}$	Departure time of $EV_{j,k}$
t_{edp}	The time for which active power flow is sustained when an EDP is activated
$V(t)$	Set of EVs recharging at time t
V_j	Voltage at bus j
$V_{V2G}(t)$	Set of EVs willing to participate in V2G when needed
W_1	Vector of payment rates=$[w_{1,1},\ w_{2,1},\ \dots w_{N,1}]$
$w_{i,1}$	*ith* EV's payment rate (paid by EV) for recharging
$w_{i,2}$	*ith* EVs payment rate (paid to EV) for discharging in V2G mode
$Y_{i,j}$	Mutual admittance between bus i and bus j
$Y_{j,j}$	Self admittance of bus j
$Z_{i,j}$	Impedance between bus i and bus j

Chapter 1

Introduction

1.1 Motivation and Background

Climate change is one of the most compelling issues that the world is facing today. The challenges imposed by climate change are driving research and development in a wide range of technical, economical and operational aspects of human made systems. The underlying aim in this thesis is to investigate alternative and complementary ways of reducing the emission of green house gases such as CO2. Currently two human made systems that are significant contributors to the CO2 emissions, and that are of interest for this thesis, are, i) the electric power system, and ii) the transportation system. It is now widely recognised that these two systems, when linked together by means of electric vehicles (EVs)[1], can overcome outstanding barriers faced by climate change adaptation using mechanisms to better manage electric power demand.

1.1.1 Electric Power System and Electric Vehicles

Independent of recent technological developments in the transportation system, the electric power system is going through a phase of significant changes in order to address the challenges of climate change. Significant research effort has been directed towards producing technologies that will enable transition to emission free generation of electric

---

[1]We use the term EVs to refer to all types of vehicles that have a battery and can connect to electric grid. Thus, EVs include battery electric vehicles (BEVs), plug-in electric vehicles (PEVs) and plug-in hybrid electric vehicles (PHEVs).

power. Governments around the world have taken initiatives to encourage development, deployment and integration of renewable energy sources. Examples include Renewable Portfolio Standard adopted by various states in the United States that requires that a utility must produce at least a certain percentage of its electricity from renewable energy sources [1] like hydro, wind and solar. However, It is widely acknowledged that reliance on renewable energy sources for the generation of electric power poses many technical, economic, and operational challenges. These challenges arise because of the underlying uncertain availability of renewable energy sources [2].

Variability of renewable energy sources is a term that is used to refer to the uncertainty in the output power of the turbines and the electric generators due to changes in the availability of renewable energy sources, which cannot be predicted accurately. Several aspects can be cited as sources of variability, for example, [2]: a) the intermittent nature of the availability of the output power because, for example, wind turbines will not operate if wind speed is too high or too low; b) the sudden variations in the output power because of the sudden and unpredictable changes in wind speed and direction; and c) the rate of change in output power because of slow or fast changes in wind speed and direction.

From the above highlighted renewable energy sources, wind is the most prominent renewable energy source for future electric power generation [3]. It is estimated that potential wind energy is sufficient to meet most of global electricity demand [4]. World Wind Energy Association's (WWEA) 2009 report [5] indicates that the installed nameplate capacity of wind power is estimated to reach 1,500,000 MW by year 2020. It is, therefore, very important to address the challenges that arise because of variability renewable energy sources.

Various solutions that cope with variability of renewable energy sources have been suggested in the literature. For example, operating large electric generators as reserves has been investigated in [6], storage of energy is considered in [7] and the use of Demand Side Management (DSM) is addressed in [8]. Recently, using EV batteries as part of storage systems to counterbalance the variability of renewable energy sources has been proposed [9]. Ideally, EV based storage systems should be managed in such a way that the transportation system and the electric power system are integrated [10, 11]. We refer to these systems as EV energy demand management (DM) systems.

Researchers agree that unmanaged recharging of EVs can cause many problems for electric power system [12, 13]. The impacts of unmanaged recharging of EVs may include: increase in energy losses, increase in voltage drops in the distribution system, and overloading of transformers and cables [14]. In addition, when the variability of wind and its impacts on electric power system are taken into account, the unmanaged recharging of EVs will require upgrade of transmission lines and very large installed capacity of electric power generation [15, 16]. In contrast, proactively managing the recharging of EVs has several benefits. Since household vehicles remain parked for most of their life time, it has been broadly noticed that the batteries of EVs can act as storage units for electricity. In this context, the recharging rates of EVs can be controlled to not only neutralise the problems described previously, but also to improve the utilisation of electric generators and infrastructure of electric power system [11]. Moreover, EVs can act as small electric generators and feed electric power back to the electric grid in a vehicle-to-grid (V2G) regime [17]. EVs can also be used for providing ancillary services such as frequency control reserves [18], frequency regulation [19], and reactive power compensation [20]. Furthermore, EV owners can generate revenue by allowing the use of EVs for peak shaving and frequency regulation [21].

1.1.2 Transportation System and Electric Vehicles

At present transport is heavily dependent on liquid fossil fuels, which are unsustainable sources of energy [22]. Moreover, environmental concerns, security of supply of liquid fossil fuels, and volatility of prices of oil are major concerns in the transport sector [23]. Therefore, advancement on electric vehicles (EVs) technology is part of a global strategy to transform the transport sector [24] to reduce its dependency (which could be up to 94 % [22]) on oil.

It is estimated that the bulk of total CO_2 emissions in transportation system is associated to light duty passenger vehicles [25], and that the global car ownership and associated energy use will continue to increase because of growth in emerging economies like China and India [26]. Electrifying light duty passenger vehicles could achieve deep cuts in CO_2 emissions [22] and can also decrease over all energy usage because: i)electric motors operate highly efficiently as compared to internal combustion engines, ii)the internal combustion engines keep running in idle mode even when the vehicle is stationary,

whereas electric motors don't need to run in idle mode, and *iii*)energy can be recovered through regenerative braking when an EV is stopped by applying brakes [27]. Electrification of transport will also reduce pollution in cities and improve air quality [28]. However, Several barriers need to be overcome before a large proportion of car owners can own EVs [22, 29, 28]. For example, the cost of EVs has been historically considered the most significant economic barrier in the process of acceptance and mass introduction of EVs [30]. Some steps by various governments throughout the world have been aimed at reducing the first cost by means of government subsidies [28]. Furthermore, if EVs are mass produced, then economies of scale should also reduce the costs of EV.

The limitations of the EV battery technology ,as it is, is the most significant technical barrier in the large scale adoption of EVs [31]. As compared to liquid fossil fuels, the energy density of the batteries is very low. The batteries age with time and their capacity to store energy decreases with age [32]. In respect to the life expectancy of the batteries, among several factors that impact the life span are operating temperature, overcharging, rate of charge/discharge and depth of discharge in each charge/discharge cycles [33, 34].

From the perspective of end-user, the distance an EV can travel per recharge (called the range of EV) is considered a major psychological barrier [35], called the range barrier. Even though range of most EVs is sufficient to meet most travel needs of average users, the perception of small range plays an important role. It might be possible to overcome the range barrier through proactive education, information, training, and better user interfaces for EVs [35]. In this context, the refuelling infrastructure and services for liquid fossil fuel based vehicles are very well developed and convenient to use. In contrast, such infrastructure and services do not exist for EVs, which is also a barrier in large scale adoption of EVs. To overcome this barrier, novel business solutions such as battery replacement services have been suggested. These business solutions also address the range barrier and cost of ownership of the batteries [36].

Last but not least, for successful realisation of EVs and their potential benefits, coordinated action by governments, research institutions, automobile industry, and consumers is required [22].

1.1.3 Benefits of Linking Electric Power System and Transportation System by Means of EVs

Many benefits of proactively managing the recharging of EVs have been discussed in the literature. Among the most discussed we have: improved utilisation of electric generators and infrastructure of electric power system [11], peak shaving [17, 21], and ancillary service provision such as frequency control reserves [18], frequency regulation [19], and reactive power compensation [20]. The intrinsic benefits to the transportation system include: reduced reliance on fossil fuels, reduction in CO_2 emissions [22], improved energy efficiency [27], and improved air quality in urban environments [28]. In addition, electrification of transportation will reduce the emission of CO_2 and shift the reduced emission from the transportation system to the electric power system, where more effective mechanisms for monitoring and regulating the CO_2 emissions could be implemented [36].

1.1.4 Current Trends in Electric Vehicles Sales

According to International Energy Agency's (IEA) report, in 2012, more than 100,000 EVs were sold globally [37]. The sales of EVs more than doubled in the year 2012 as compared to the year 2011 [37]. It is expected that EVs sales will continue to increase as the cost of batteries decreases. For example, in the year 2008, the costs of batteries were estimated to be 1000 [\$/kwh], which had decreased steadily to 485 [\$/kwh] by the year 2012 [37]. Figure 1.1 [37] [2] shows the sales targets for select countries that are expected to have significant number of EVs. U.S. Department of Energy has estimated that the cumulative sales of electric vehicles in the U.S. will have exceeded 1,000,000 by the year 2015.[38]. In the U.K. more than 8,000 EVs had been registered by the end of year 2012[37].

1.2 Electric Vehicle Energy Demand Management Problem

Let us consider a typical EV, which comes with a software agent (referred to as the EV agent) that manages the battery of the EV. Let us also assume that the EV agent

---

[2]This figure has been taken from a report [37] published by IEA. The report used the Electric Vehicle Initiative (EVI) as the data source for this figure.
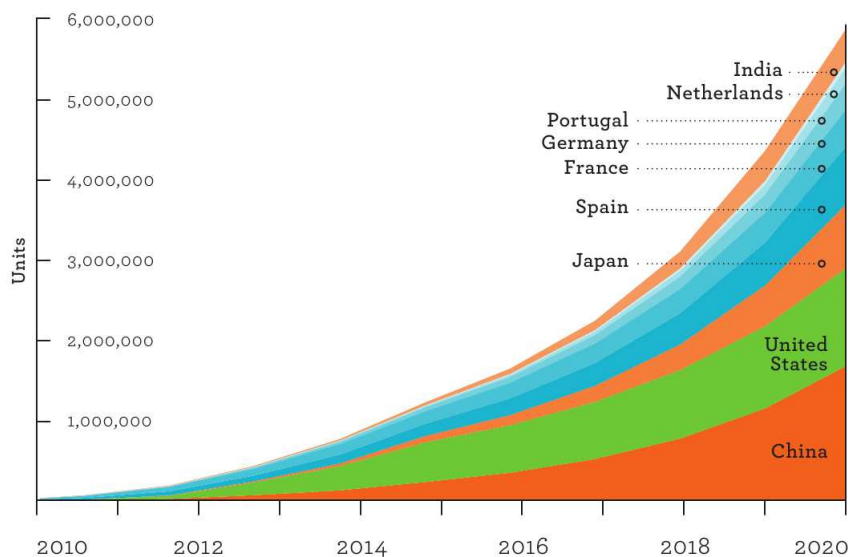
FIGURE 1.1: EV Sales targets for select countries [37]

can interact with the EV owner who can schedule journeys that he/she plans to take. Moreover, the EV agent is capable of monitoring the usage pattern of the EV and learn to schedule the usual journeys without the intervention of the EV owner. The EV agent is then able to communicate with a recharging information management centre and inform the centre about the planned journeys of the EV and its energy demand in each of the periods of connection in advance.

When the EV has completed a journey and it is anticipated that it will remain parked for a significant duration of time, the EV is plugged into a recharging socket. The EV agent informs the recharging socket about: *i*) the anticipated departure time, *ii*) current state of charge of battery, and *iii*) the desired state of charge of battery at the departure time. Depending on the recharging policy used by the distribution system operator (DSO), the recharging socket may: a) Inform the EV agent about the price of electric power flow, or b) Send the information to a schedule builder which builds a recharging schedule considering the EV and its energy demand in relation to other EVs. In response to a) above, the EV agent may either accept the price and decide a recharging rate or decide to wait if it is anticipated that price will decrease later in time. In response to b) above, the EV agent may inform the EV owner. The EV agent is also able to receive updates from the EV owner in case the travel plan has changed.

The objective of the EV agent is to manage the battery state of charge such that the

EV owner can complete his/her desired journeys without inconvenience. The objective of the recharging policy used by DSO is to ensure that the recharging activity of the population of EVs as a whole, would not introduce operational challenges to the electric power system and/or would provide some service to the electric power system. The objective of EV energy demand management system is to implement the recharging policy of the DSO and reconcile the objectives of an EV agent (which depend on the state of a particular EV) and the objectives of recharging policy (which depend on the state of whole population of EVs).

1.3 Aims and Objectives of the Thesis

The aim of this thesis is to research and develop novel recharging schemes for energy demand management of EVs. To this end the following objectives have been identified.

1. To design a distributed recharging rate controller that can facilitate the participation of EVs in frequency regulation mechanisms to improve the security of electric power system.

2. To create an incentive policy for autonomous EVs that gives EVs a degree of control over their participation timing and their recharging rates.

3. To devise a schedule for recharging EVs that would avoid congesting the secondary circuits in the distribution system.

4. To design a recharging scheme that can provide a primary frequency control reserve, as well as avoid congesting the secondary circuits in a composite framework.

1.4 Contributions

The contributions of the work presented in this thesis are:

- In Chapter 2, a novel distributed recharging rate controller is presented that allocates proportionally fair recharging rates to EVs and requires only to measure (or to receive information about) the frequency of electric power system. This contribution has been published in [39].
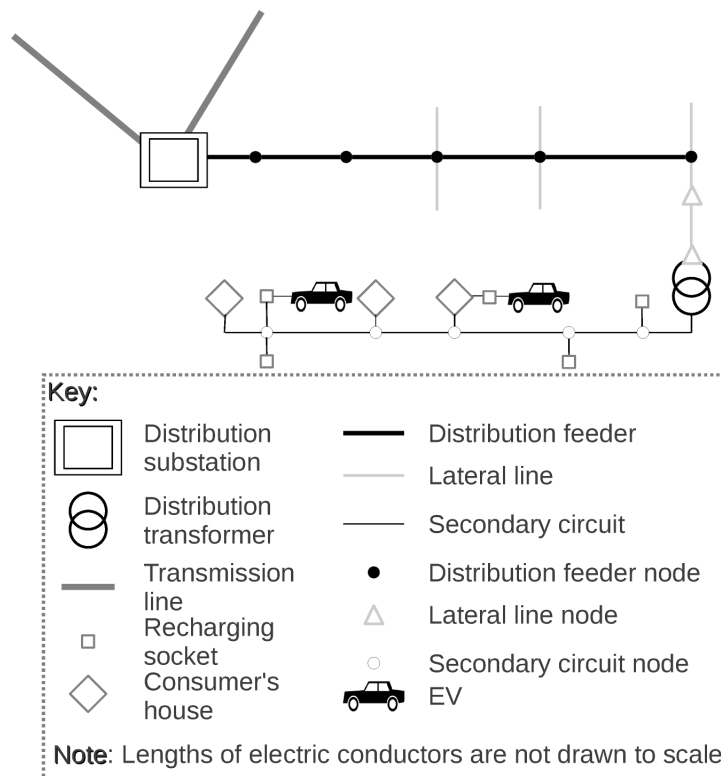
FIGURE 1.2: Electric power distribution system

- In Chapter 3, a novel approach is presented that can construct recharging schedules for EVs that avoid congesting the secondary circuits.

- In Chapter 4, the approach presented in Chapter 3 is extended to impart to it the ability of responding to a drop in the frequency of electric power system and the ability of emulating a frequency control reserve. The work in Chapter 3 and Chapter 4 is the subject of another journal publication.

1.5   Terminology and Definitions

In this section, the terms that will be used later in the thesis are introduced and explained.

Electric Power Distribution System

Electric power distribution system is the part of electric power system that carries electric power from the electric power transmission system to the consumer of electric power.

We may refer to electric power distribution system as *"distribution system"*. Figure 1.2 will be used to relate various terms used in this thesis in relation to a distribution system. Most of these terms used for electric power distribution system have been taken from [40].

A distribution system is typically composed of two subsystems, namely: 1) primary distribution system and 2) secondary distribution system. The definitions of primary and secondary distribution system as as follows.

Primary Distribution System

A primary distribution system is the subsystem of the distribution system that transports electric power from a node in the electric power transmission or sub-transmission system to the distribution transformers. A primary distribution system is composed of a distribution substation, distribution feeders, and lateral lines. A primary distribution system can be either a radial system where there is only one path along distribution feeders between the substation and a distribution transformer or it can be a network where several paths along distribution feeders can exist between a the substation and a distribution transformer.

Secondary Distribution System

Secondary distribution system is the part of the distribution system that transports electric power from a distribution feeder node or a lateral line node to consumer's premises. It is composed of distribution transformers and secondary circuits. Secondary distribution system operates at utilisation voltage. Secondary distribution systems are often radial systems where only one path exists between a distribution transformer and customer premises.

Distribution Substation

A distribution substation is the part of electric power system that connects a primary distribution system to a node in electric power transmission system. It contains transformers that step down the transmission level voltages (69–1,100 (kV)) to the distribution level voltages (2.2–34.5 (kV))[40]. We may also refer to distribution substation as *"substation"*. The transformers at the substation typically have taps that can be used to change the winding ratio of the transformer and hence the output voltage. These tap changing transformers are used to regulate voltage on one end of distribution feeders.

Distribution Feeder

A distribution feeder is a set of electrical conductors that is used to transport electric power from a distribution substation to a load area, where a load area is an area of land in which electric power loads are located. Several feeders may emanate from a substation. A distribution feeder can be several miles in length. A distribution feeder may be tapped at several points along its length. These points are called *"distribution feeder nodes"*. A distribution feeder is tapped by connecting each of its conductors to an electrical conductor called *"bus bar"* which is often referred to as *"bus"*[3].

The part of the distribution feeder between two distribution feeder nodes is called a *"distribution feeder segment"*. A distribution transformers can be connected to a distribution feeder node. Distribution feeders typically have a shunt capacitor bank at a distribution feeder node. Shunt capacitors are used to regulate voltage on the distribution feeder node by changing reactive power flow.

Lateral line

A lateral line is a set of electrical conductors that is connected to a distribution feeder node at one end and is tapped along its length at *"lateral line nodes"*. The segment of lateral line between two lateral line nodes is called a *"lateral line segment"*. Distribution

---

[3]Depending on the context, the term *"bus"* may refer to a node in the transmission system, a distribution feeder node, a lateral line node, or a secondary circuit node.

transformers are typically connected to lateral line nodes. Both lateral lines and distribution feeders operate at distribution level voltages and typically carry 3-phase electric power.

Distribution Transformer

A distribution transformer is an electric transformer that is used to step down distribution level voltage to utilisation voltage where *"utilisation voltage"* is the voltage at which electrical appliances operate. A distribution transformer may also be referred to as a *"service transformer"*.

Secondary Circuit

A secondary circuit is a set of electrical conductors that is connected to a distribution transformer at one end and is tapped at several points called *"secondary circuit nodes"* along its length. Secondary circuits operate at utilisation voltage. Consumer's houses are connected to secondary circuit nodes. We may also refer to secondary circuit nodes as load feeding points for EVs since EVs are connected to recharging sockets which in turn are connected to secondary circuit nodes. Secondary circuits typically carry single phase electric power.

Recharging Socket

A recharging sockets is a socket/plug to which an EV connects for recharging. Recharging sockets are connected to the secondary circuit nodes or load feeding points.

Congestion in the Distribution System

All types of electrical conductors used in distribution feeders, lateral lines, and secondary circuits have certain current carrying capacities. If large currents are drawn through conductors, then conductors can overheat and might get damaged. If electrical load is such that the resulting current approaches or exceeds the capacity of the conductors, then we say that *"congestion"* has occurred. Congestion and voltage drops are closely linked because voltage drops along conductors are directly proportional to the current

carried by the conductor. We refer to drop in voltage as "voltage congestion". For voltage congestion to occur, it is not necessary for any conductor to have reached its current carrying capacity. Voltage congestion can occur if utilisation voltage in any part of distribution system drops below the standard limits even if no conductor is carrying a current greater than its current carrying capacity.

Recharging Rate Profile

A recharging rate profile is an active power flow $p(t)$ [kw] or [kwh/h] that transports energy to the battery of an EV. A recharging rate profile is *"admissible"* if it transports a given fixed amount of energy to the battery of an EV in a given fixed window of time.

Recharging Schedule

A recharging schedule is a set of recharging rate profiles such that each EV under consideration has an associated recharging rate profile in the recharging schedule. A recharging schedule represents a plan according to which each EV under consideration will be recharged. A recharging schedule is *"admissible"* if all recharging rate profiles in it are admissible.

A recharging schedule is *"congestion avoiding schedule"* if its planned recharging activity is aimed at actively reducing congestion and voltage drops in the distribution system.

Elastic and Non-Elastic Loads

Elastic loads are those loads whose instantaneous electric power consumption can be varied safely and controlled. All loads with batteries, and hence EVs are considered elastic loads. Non-elastic loads are those that consume a fixed amount of electric power and might not operate properly if input power is varied. Therefore, all constant power loads are non-elastic loads. In addition, the electric power consumption of some loads may depend on the voltage on the terminals or frequency of electric power (for example, loads using induction motors). Such loads are also considered non-elastic because their electric power consumption may vary but is not controlled.

Reliability of Electric Power System

Reliability of electric power system is a term which is used to indicate, in a general sense, the ability of power system to perform its function [41]. Reliability has two aspects: 1) security, and 2) adequacy.

Security of Electric Power System:
Security of electric power system is its ability to respond to dynamic and transient disturbance arising within the system. The disturbance can be caused by many possible events, for example, sudden failure of a large generator and loss of a transmission line [41].

Adequacy of Electric Power System:
Adequacy of electric power system is its ability to satisfy customer load demand within the operational constraints. Adequacy is related to the existence of sufficient generation, transmission, and distribution facilities. Adequacy is associated with static conditions and does not include system dynamics and/or transient disturbances [41]. Adequacy can be assessed at the level of: *i*) generation facilities, *ii*) transmission facilities, and *iii*) distribution facilities.

Demand Response (DR)

U.S. Department of energy has defined demand response (DR) as [42]: "Demand response is a tariff or program established to motivate changes in electric use by end-use customers in response to changes in the price of electricity over time, or to give incentive payments designed to induce lower electricity use at times of high market prices or when grid reliability is jeopardised."

Frequency Control Reserve

Frequency control reserve refers to the capacity that can be used to supply electric power or to reduce load in case of loss of electric generators or unexpected changes in electric power generation caused by the variability of renewable energy sources. Frequency control reserve can be the provided by electric generators that can increase electric power generation, or by loads that can decrease the load by changing their consumption pattern or time.

System of Fluids

A system of fluids is a volume of at least two fluids of different densities contained in a container which acts as boundary through which fluids cannot flow.

Pressure:

Pressure is defined as force per unit area. We denote pressure in a system of fluids as q $[N/m^2]$. This unusual notation is necessitated by the fact that we have used P [kw] for active electric power and p [kw] for recharging rate of an EV.

Density:

Density is defined as mass per unit volume. We denote the density as ρ $[kg/m^3]$.

Relationship between density of a fluid and pressure in a fluid:

In a static fluid, the density and pressure are related as

$$q_h = q_s + \rho g h \tag{1.1}$$

where, q_s $[N/m^2]$ is the pressure at surface of fluid, q_h is the pressure at depth h, ρ $[kg/m^3]$ is the density of fluid, g $[m/s^2]$ is the acceleration of gravity and $g = 9.8 \ m/s^2$, and h $[m]$ is the depth of fluid as measured from the surface.

1.6   Outline of the Thesis

The thesis is divided into five chapters as follows.

In **Chapter 2**, a novel distributed recharging rate control algorithm is presented, which combines the objectives of regulating frequency and improving the utilisation of electric generators. An incentive policy κ is created that encourages electric vehicles (EVs) to demand energy when non-EV demand is low and the electric generators are under-utilised. EVs also act as frequency regulators which can control their participation role by modifying their respective payment rate w_i. The proposed distributed recharging rate control algorithm can realise a DM solution for EVs and does not require explicit real time communication from the electric generators or between the recharging sockets. Simulation is used to assess the algorithm and to highlight its embedded characteristics.

In **Chapter 3**, a novel approach is presented that can be used to construct recharging schedule that avoid congestion in the secondary circuits in the distribution system. The approach is based on particle systems and numerical methods that are typically used to solve fluid flow equations. A two stage process is presented that can construct recharging schedules of desired characteristics. A metric is proposed that can compare various recharging schedules in terms of their impacts on the voltages in the secondary circuits. Two examples are presented to compare the presented approach with the existing approaches in the related literature.

In **Chapter 4**, the particle system introduced in Chapter 3 is extended to provide frequency control reserve, which allows EVs to take part in frequency control services and demand response schemes, and at the same time avoids congesting the secondary circuits. The extension of the particle system is used to also handle non-elastic loads and their impact on recharging of EVs.

In **Chapter 5**, the conclusions are summarised and the future work is suggested.

Chapter 2

Distributed Recharging Rate Control

2.1 Introduction

As already described in the previous chapter, proactively managing the energy demand for electric vehicles (EVs) has many benefits. In this chapter, a recharging schemes is proposed that recharges EVs and provides a frequency regulation service to the electric grid. The EVs are integrated as a subset of demand side management (DSM) technologies as suggested in [9, 11] and [43]. Although these works highlight the importance of EV energy DM, they hardly expand on suggesting how such a DM system may be implemented.

The DM system proposed in this chapter aims at exploiting the following characteristics of EVs to manage their demand.

1. EVs are indifferent to the exact time of recharge completion as long as usual/scheduled journeys are not affected.

2. EV population has heterogeneous energy needs.

   - Not all EVs need to recharge their battery to the maximum capacity each day.

   - Not all EVs have the same journey patterns

3. Many EVs can tolerate uncertainty in the exact battery state of charge provided that they can achieve a minimum battery state of charge.

A recharging rate control algorithm is presented for parked EVs, where a large percentage of these EVs behave as variable power and delay tolerant loads that coexist with other types of loads. The proposed recharging rate control algorithm *i*) can realise a DM solution to reconcile energy demand from autonomous EVs with the output of, for example, renewable energy sources and *ii*) can realise an alternate mechanism for frequency regulation in the event of, for example, changes in output power of electric generators.

2.2   Organisation of the Chapter

This chapter is organised as follows: Section 2.3 presents a review of the related work. Section 2.4 describes the architecture of system under consideration, components of the system, and their inter relationship. Section 2.5 presents a distributed recharging rate control algorithm for recharging EVs. Section 2.6 provides implementation of recharging rate control and simulation results. Section 2.7 uses an example to relate the recharging rate control with the recharging strategy of EVs and generation capacity control. We conclude this chapter in Section 2.8 and comment on the future work.

2.3   Related Work

In this chapter, an EV energy DM problem is essentially a scheduling problem which manifests two key features: *i*) Each EV battery is recharged to the desired state of battery charge during the period between two consecutive journeys; *ii*) The aggregate demand from EVs could fill the valley that non-EV demand produces. Feature *ii*) can also be interpreted to be aiming at minimising the difference between the instantaneous marginal cost of generation and its average over 24 hours. Such interpretation includes the availability of renewable energy sources and hence the aggregate demand from EVs may not necessarily be seen as a flat valley filling demand.

The work on EV energy DM can be broadly classified into two distinct categories depending on the level of autonomy of EVs: *i*) the recharging schedule is controlled by the

electric grid *ii*) the recharging schedule control is delegated to autonomous EV agents. In the first case EVs report their recharge requirements to a dispatch centre which in turn produces a recharging schedule for each EV [44]. Despite the apparent simplicity of the electric grid controlled scheduling, to the best of our knowledge, polynomial time algorithms that compute optimal recharging schedules have not been published. In the second case each EV is allowed to self-schedule the recharging time according to the criterion known only to the respective EV agent [10, 45].

The research work on DM with autonomous EVs can be further divided into two classes: *i*) day ahead negotiation and *ii*) real time bargaining. The former class includes works where EVs can bid for energy the day before the actual demand [46, 47]. The algorithm developed in this chapter belongs to the latter class where EV agents bargain in real time and learn from historic demand patterns. The publications relevant to the work presented in this chapter are reviewed in the remainder of this section.

Galus *et al.* [10] present a framework for recharging EVs using an energy hub system. They note that EVs must be granted autonomy in recharging decisions and suggest use of a multi-agent system (MAS). In principle, we support the use of a MAS framework for EV energy DM and pursue a similar broader objective of integrating transport and power systems. However, our solution is quite different: Galus *et al.* [10] integrate EVs into multi carrier energy networks by solving an optimal energy dispatch problem whereas in this chapter we propose to integrate EVs as frequency regulators. Also, in [10] a hub manager aggregates several hundred EVs and requires information from each EV to provide a solution. The hub manager maintains a list of arriving/departing EVs and allows new EVs to join only at the start of 15 minute intervals. The solution proposed in this chapter works with or without aggregation of EVs and allows EVs to join at arbitrary times.

Though the economic aspects of DM with autonomous EVs can be understood using classical economics and game theory, the mechanics of resulting energy transactions and the impacts on the operation of the system have received little attention in the literature. For example, Vytelingum *et al.* [48] and Wei *et al.* [49] attempt to present MAS based solution to manage micro storage devices including EVs. However, they do not consider the actual mechanism by which agents acquire energy and assume that agents can buy

it at market price. Such MAS can be integrated on top of the algorithm described in this chapter.

Ma *et al.* [45] use non-cooperative game theory to analyse the recharging strategies of EVs and make the observation that the recharging games for EVs are conceptually similar to the routing games in networks. They consider EVs as cost minimising rational agents coupled through a common energy price where each agent solves its local optimisation problem. In the limit of infinite population, the decentralised strategies of EVs result in a unique Nash equilibrium that has the property of filling valleys in non-EV demand. In comparison to [45], our work addresses a few novel aspects of decentralised recharging of EVs. We show not only that EVs can decide strategy in a decentralised manner, but also that the impact of the strategy and resulting incentive can also be computed using decentralised recharging rate controllers. This chapter presents a novel attempt to include in a unified framework: the recharging strategies of EVs, operational aspect of frequency regulation and the utilisation of the electric generators.

Many studies on Load Frequency Control (LFC) or frequency regulation can be found in the literature [50]. Recently, researchers have become interested in using EVs to provide frequency regulation services [19, 51]. The recharging rate control proposed in this chapter may also be classified as an LFC mechanism. However, the mechanism suggested here is novel in that it combines frequency regulation with incentive policy provision for autonomous EV agents.

2.4   System Architecture

2.4.1   Physical Architecture

Electric vehicles connect to the distribution system through recharging sockets. Each recharging socket has its own recharging rate controller (socket agents). In the proposed architecture, recharging sockets are enabled round the clock and do not adhere to a centralised recharging policy. Each EV has an agent that can communicate with a recharging socket and make a demand for energy. Recharging sockets receive these demands and provide energy accordingly. Thus EVs may be considered as autonomous buyers and the recharging sockets as points of sale.

After completing their journeys EVs will connect to recharging sockets. The *ith* EV agent will send a signal $w_{i,1}$ [\$/h] to the socket agent indicating its preferred rate of payment to get recharged, and in return the socket agent will allocate a recharging rate of p_i [kw] and will broadcast on the current policy $1/\kappa$ [\$/kwh]. From now on we will also refer to p_i [kw] as the recharging rate of *ith* EV. EVs may also indicate their willingness to discharge in V2G mode and communicate $w_{i,2}$ [\$/h] to recharging sockets which will indicate their desired rate of payment for discharging.

When connecting to the recharging socket an EV agent may decide a value of $w_{i,1}$ [\$/h] based on its current status and requirements for the next journey, which may include; current battery state of charge, expected remaining time to a new journey (T_{L_i}), expected travel time of next journey and total budget for recharging (Bd).

2.4.2   Logical Architecture

We can decompose the EV energy DM system into three inter related components, namely:

1. Distributed recharging rate control,

2. On line resource acquisition,

3. Capacity control.

Figure 2.1 shows the relationship between these components which are organised at two levels. Level 1 represents the activities on the demand side and level 2 represents activity on the generation side. We now briefly describe the function of each component.

Component 1: Distributed Recharging Rate Control

Component 1 controls the energy transfer rate for EVs based on real time availability of energy. Its aim is to balance the aggregate demand with the time varying generation capacity set by Component 3. In the event that non-EV energy demand exceeds the generation capacity, Component 1 reduces the recharging rate of all EVs to zero and possibly allocates negative recharging rates (V2G mode of operations [17]). If generation capacity exceeds the non-EV demand, then recharging rates are allocated to EVs
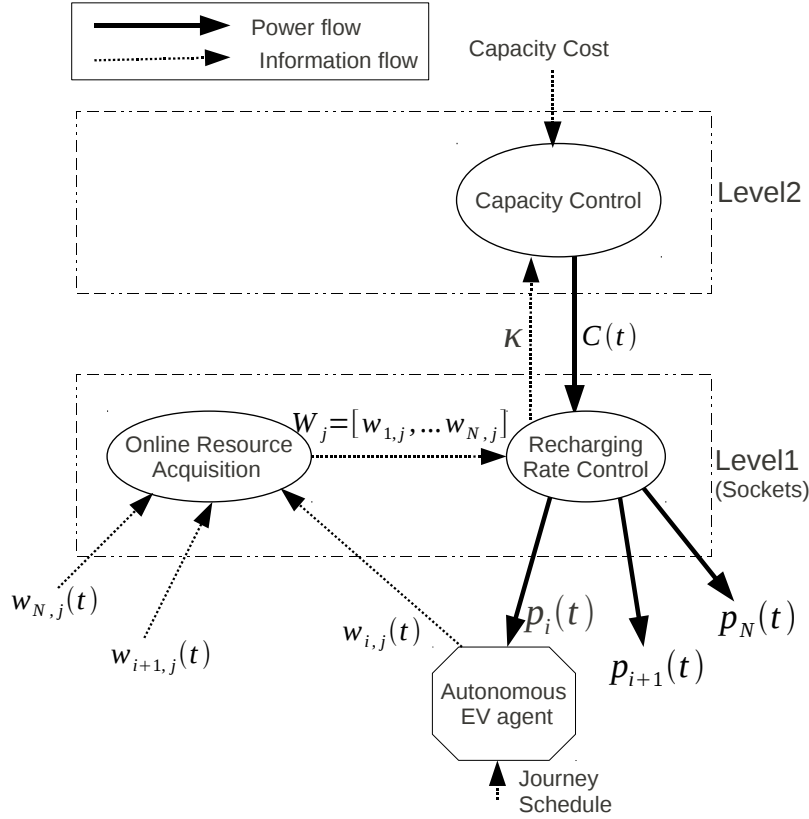
FIGURE 2.1: Components of the demand management system

according to their respective payment rate $w_{i,1}$ [\$/h]. This chapter will mainly focus on the solution of Component 1 of EV energy DM system.

Component 2: On line Resource Acquisition

This component is intended to capture the behaviour of autonomous EV agents when they submit $w_{i,1}$, and to analyse the equilibrium properties of the system. Given a generation capacity, it is possible for an autonomous EV agent to increase its payment rate $w_{i,1}$ relative to other EVs. Increasing $w_{i,1}$, however, does not mean that the recharging rate p_i of that the EV will necessarily increase because competing EVs agents can also decide to increase their respective $w_{k,1}$. This situation can be modelled as a game [52] and in Section 2.7 we present a simple instance of such game.

Component 3: Capacity Control

Component 1 uses capacity as an exogenous variable and cannot control it. A scenario may be constructed where capacity is zero and Component 1 can only reach one solution which is to reduce the recharging rate to zero for all EVs. Component 1 will enforce this solution irrespective of what the EVs wish to pay. Hence, to ensure that EVs may receive sufficient power, decision on the generation side is needed, which is the capacity control. This capacity control problem can be modelled as a Revenue Management (RM) problem.

2.4.3 Remarks on EV agents and Recharging Sockets

In regards to the interaction between the EV agents and the socket agents, upon connection the EV agent can submit to the socket agent an arbitrary small value of $w_{i,1}$ [\$/h] which is the payment rate at which the EV agent is willing pay for recharging. In turn, the EV agent obtains from the socket agent a signal $1/\kappa$ [\$/kwh] which can be interpreted as the instantaneous price of unit of energy. In this setting the EV agent's action of submitting a $w_{i,1}$ [\$/h] is equivalent to submitting a demand for $p_i = \kappa * w_{i,1}$ [kw]. After this initial interchange of signals EV agents can continuously monitor changes in $1/\kappa$ [\$/kwh], and they can decide autonomously if their rate of payment w_i [\$/h] needs modification.

We assume that EV agents are continuously trying to reconcile their internal goals, as for example, their predicted battery state of charge ($BSOC$) at the start of their next journey with their remaining budget and current payment rate. On the other hand, the sockets are continuously solving a Nash bargaining problem that will allocate to each EV a recharging rate that is proportionally fair. At equilibrium, $1/\kappa$ [\$/kwh] should be such that no EV changes its payment rate $w_{i,1}$ [\$/h]. Note that with the above mechanism EVs need only to communicate to the local socket $w_{i,1}$ [\$/h] and can discover their equilibrium charging rates p_i [kw] in a distributed manner. We further note that from the perspective of a recharging socket, the equilibrium payment rates $w_{i,1}$ [\$/h] are still exogenous variables and can be considered arbitrary.

There are unlimited ways in which EV agents and socket agents can agree to more elaborated ways of interchanging information. For example, the socket agents could

broadcast forecasts of near future $1/\kappa$ [\$/kwh] values. This line of research is out of the scope of this chapter but is certainly worth further investigation.

The price signal κ is to be calculated by the recharging sockets locally, therefore, the recharging sockets should be made resistant to tampering. If recharging sockets are tampered with, the fairness in the allocated recharging rates could be compromised.

2.5 Distributed Recharging Rate Control

2.5.1 Problem Formulation

Notation

$V(t)$ = set of EVs recharging at time t,

$V_{V2G}(t)$ = set of EVs willing to participate in V2G when needed,

N = Number of recharging EVs,

p_i = Recharging rate (at which energy is accumulating in the *ith* EV battery [kw] (or otherwise, when not specified, [p.u.]) [1],

$w_{i,1}$ = *ith* EV's payment rate (paid by EV) for recharging [\$/h],

$w_{i,2}$ = *ith* EVs payment rate (paid to EV) for discharging in V2G mode [\$/h],

$P_{SCH}(t)$ = Scheduled power [p.u],

$P_{NEV}(t)$ = Power demand from non-EV loads [p.u.],

$C(t) = P_{SCH}(t) - P_{NEV}(t)$ = Net power capacity available to recharge EVs in G2V mode [p.u.],

$P_{V2G}(t)$= Aggregate power drawn from EVs in V2G mode [p.u.],

p_{imax} = Maximum allowed power at which *ith* EV's battery can be recharged [p.u.],

$p_{imaxV2G}$ = The maximum allowed power at which *ith* EV's battery can be discharged [p.u.],

---

[1] p.u = per unit. Hence, these units have been normalised

$\Delta\omega=$ frequency deviation of electric power system[p.u.],

$P_{EV} = \sum_{i=1}^{N} p_i$ [p.u.],

$\mathbf{P} = [p_1, \ p_2, \ \ldots p_N]$ [p.u.],

$W_1 = [w_{1,1}, \ w_{2,1}, \ \ldots w_{N,1}]$ [\$/h].

Recharging sockets may advertise two modes of operation for EVs:

- Mode 1: If $C(t) > 0$, the EVs in $V(t)$ act as energy sinks.

- Mode 2: If $C(t) < 0$, EVs in $V_{V2G}(t)$ act as energy sources.

In addition to the EVs considered in sets $V(t)$ and $V_{V2G}(t)$, some EVs may choose to discharge their batteries while $C(t) > 0$. In the framework here presented, we can add their discharging rates to $C(t)$ and consider them as virtual generators maximising their revenue. Similarly, some EVs are allowed to recharge when $C(t) < 0$. If this is the case, they are assimilated as non-EV loads and their recharging rates are added to P_{NEV}.

We now introduce the two objective functions of the two optimisation problems that the socket agents are continuously solving. The choice of these two objective functions has its foundations in the Nash bargaining mechanism from cooperative game theory [53, 54]. The Nash bargaining solution framework enables the implementation of fair allocation of resources among contending agents and it can be seen as a generalisation of the widely studied proportional fairness principle. For example, in [55] the proportional fairness principle was used to assign rates fairly to different contending elastic data traffic demands. For more information on fairness in resource allocation, the reader is referred to [56, 57]. With this choice of the two objective functions in mind, the socket controllers (agents) set the recharging rate of connected EVs by solving the following optimisation problems.

Mode 1

$$
\begin{aligned}
&\underset{\mathbf{P}}{\text{maximise}} && \sum_{i|v_i \in V(t)} w_{i,1}(t) log(p_i(t)) \\
&\text{subject to} && \sum_{i|v_i \in V(t)} p_i(t) \leq C(t) \\
& && 0 \leq p_i(t) \leq p_{imax} \ \ \forall \ i|v_i \in V(t)
\end{aligned}
\tag{2.1}
$$

Mode 2

$$\underset{\mathbf{P}}{\text{maximise}} \quad \sum_{i|v_i \in V_{V2G}(t)} w_{i,2}(t) log(-p_i(t))$$

$$\text{subject to} \quad \sum_{i|v_i \in V_{V2G}(t)} -p_i(t) \leq P_{V2G}(t) \tag{2.2}$$

$$- p_{imaxV2G} \leq p_i(t) \leq 0 \;\; \forall \; i|v_i \in V_{V2G}$$

Note that for the proposed recharging rate control $w_{i,1}(t)$, $w_{i,2}(t)$, $C(t)$ and $P_{V2G}(t)$ are exogenous variables and cannot be controlled: $w_{i,1}$, $w_{i,2}$ are determined by autonomous EV agents while $C(t)$ and $P_{V2G}(t)$ are set by the capacity controller.

In respect to equations (2.1) and (2.2), it can be verified that these equations represent two convex optimisation problems [58]. Many numerical methods are able to provide the instantaneous solution, but the dynamic nature of the problem, the geographical spread of the EV population and scalability of solution can present difficulties when centralised solvers are used. We note that equations (2.1) and (2.2) represent two problems that change with time. EVs/non-EV loads arrive and depart at random times. A centralised solver would need to collect data and solve the problem every time some change occurs. Therefore, our interest is in distributed and on-line optimisation approaches since recharging sockets need to solve the problem in real time with minimum communication overhead. We choose a solution approach based on solving convex optimisation problems using sliding mode control [59] which yields an on-line distributed solution that requires only binary information about the state of the system which in our case is the frequency deviation of electric power system. Using results from [60], it can be shown that the following differential inclusions converge to the solutions of the problems described by equations (2.1) and (2.2).

Mode 1

$$\frac{d(p_i(t))}{dt} = \frac{\alpha w_{i,1}(t)}{p_i(t)} \bar{\theta}_1 \; \overline{\phi_1(p_i(t))} - \beta(\theta_1 + \phi_1(p_i(t))) \tag{2.3}$$

where

$$\theta_1 = \begin{cases} 1 & \text{if } \sum_{i|v_i \in V(t)} p_i(t) \geq C(t), \\ 0 & \text{otherwise} \end{cases} \tag{2.4}$$

$$\phi_1(p_i(t)) = \begin{cases} 1 & \text{if } p_i(t) \geq p_{imax} \text{ ,} \\ -1 & \text{if } p_i(t) \leq 0 \text{ ,} \\ 0 & \text{otherwise} \end{cases} \tag{2.5}$$

and

$$\overline{\phi_1(p_i(t))} = \begin{cases} 1 & \text{if } \phi(p_i(t)) = 0, \\ 0 & \text{otherwise} \end{cases} \tag{2.6}$$

Mode 2

$$\frac{d(p_i(t))}{dt} = \frac{\alpha w_{i,2}(t)}{p_i(t)} \overline{\theta_2} \, \overline{\phi_2(p_i(t))} + \beta(\theta_2 + \phi_2(p_i(t))) \tag{2.7}$$

where

$$\theta_2 = \begin{cases} 1 & \text{if } -\sum_{i|v_i \in V_{V2G}(t)} p_i(t) \geq P_{V2G}(t), \\ 0 & \text{otherwise} \end{cases} \tag{2.8}$$

$$\phi_2(p_i(t)) = \begin{cases} 1 & \text{if } p_i(t) \leq -p_{imaxV2G} \text{ ,} \\ -1 & \text{if } p_i(t) \geq 0 \text{ ,} \\ 0 & \text{otherwise} \end{cases} \tag{2.9}$$

Here $\alpha > 0$ and $\beta > 0$ are tunable parameters which are the same for all recharging sockets.

2.5.2 Remarks about Selection of α and β

The values of parameters α and β need to be chosen carefully. A necessary requirement is that all recharging sockets must use the same values of α and β. The magnitude of values of α and β determines the rate of convergence of recharging rates to the equilibrium point of (2.3). The larger magnitudes allow faster convergence. However, there is a limit on how large the values of α and β can be, because the recharging rates, after having converged, oscillate around the equilibrium point of (2.3). The amplitude of these sustained oscillations increases when the magnitude of values of α and β is increased. Moreover, if the amplitude of these oscillations in recharging rates is large,

and there is a large number of recharging EVs, the oscillations might be observed in the frequency of electric power system, which is undesirable.

It is suggested that values of α and β be dynamically adapted. For example, after a sudden drop in frequency, large values of α and β may be allowed to reach the new equilibrium quickly. Having once reached near the new equilibrium, the values of α and β could be reduced to small values to avoid oscillations around the equilibrium point. The socket manager, introduced in Section 2.6.3, can adapt these values by observing the frequency of electric power system. It can then broadcast the new values α and β so that all recharging sockets can use the same values.

2.5.3   Optimal Recharging Rate

In Mode 1, at the optimal point of Eq. (2.1) the recharging rate of *ith* EV is given by

$$
p_i = \begin{cases} \kappa w_i & \text{if } \kappa w_i < p_{i,max}, \\ p_{imax} & \text{otherwise} \end{cases} \tag{2.10}
$$

where κ is some constant which is the same for all EVs and has units of $[kwh/\$]$. We refer to $1/\kappa$ as price per unit of energy.

Proof. First note that $p_i \leq p_{i,max}$ as this condition is enforced by the second constraint in Eq. (2.1). To show the recharging rate at the optimal point of the problem in Eq. (2.1), we start by considering all the EVs. let $N_j = N$, $C_j = C$ and $V_j = V$ and $j = 1$ where j indicates the iteration number of the following procedure (referred to as Procedure A), where Sj is used as abbreviation of Step j.

2.5.3.1   Procedure A

S1) Assume that second constraint is absent. We solve Eq. (2.1) only with first constraint. Dropping the second constraint, we transform the optimisation problem in Eq. (2.1) into an equivalent problem by a change of variable.

$$
x_i(t) = log(p_i(t)) \tag{2.11}
$$

and formulate an equivalent problem to the original problem as follows

$$
\begin{aligned}
&\underset{x_i}{\text{maximise}} && \sum_{i \mid v_i \in V_j(t)} w_{i,1}(t)x_i(t) \\
&\text{subject to} && \sum_{i \mid v_i \in V_j(t)} e^{x_i(t)} \leq C_j(t)
\end{aligned}
\tag{2.12}
$$

Since the objective is linear in $x(t)$, we can use vector notation to represent it. Let us define $\mathbf{W_{1,j}} = [w_{1,1}, \ldots, w_{N_j,1}]^T \in \mathbb{R}^{N_j}$, $\mathbf{X_j} = [x_1, \ldots, x_{N_j}]^T \in \mathbb{R}^{N_j}$, $\mathbf{E_{x,j}} = [e^{x_1}, \ldots, e^{x_{N_j}}]^T$ and $\mathbf{P_{max,j}} = [p_{1max}, \ldots, p_{N_jmax}]^T$. For simplicity we can drop the notation that shows dependence on t and write

$$
\begin{aligned}
&\underset{X_j}{\text{maximise}} && \mathbf{W_{1,j}}^T\mathbf{X_j} \\
&\text{subject to} && \mathbf{1}^T\mathbf{E_{x,j}} \leq C_j
\end{aligned}
\tag{2.13}
$$

Note that we are maximising a linear function over a convex feasible region. Thus at the optimal point, the hyper plane $\mathbf{W_{1,j}}^T\mathbf{X} = b$ must be tangent to the feasible region where $b \in \mathbb{R}$. We note that at the optimal point, $\mathbf{W_{1,j}}^T\mathbf{X} = b$ is tangent to a level curve of function $\mathbf{1}^T\mathbf{E_{x,j}}$ corresponding to the level curve defined by $\mathbf{1}^T\mathbf{E_{x,j}} = C_j$. Now since the gradient of a function is normal to its level curves, we conclude that $\mathbf{W_{1,j}}$ is parallel to the gradient of $\mathbf{1}^T E_{x,j}$.

Note that $\nabla(\mathbf{1}^T\mathbf{E_{x,j}}) = \mathbf{E_{x,j}} = \mathbf{P_j} = [p_1, \ldots, p_{N_j}]^T$ Thus we can write

$$
\frac{\mathbf{W_{1,j}}}{\|\mathbf{W_{1,j}}\|} = \frac{\mathbf{P_j}}{\|\mathbf{P_j}\|}
\tag{2.14}
$$

where $\|.\|$ is the Euclidean Norm and hence, $p_i = \kappa_j w_i$ for $i = 1, \ldots, N_j$ where $\kappa_j = \dfrac{\|\mathbf{W_{1,j}}\|}{\|\mathbf{P_j}\|}$

S2) We divide EVs into two sets G_1 and G_2 depending on the solution of the most recent iteration of S1. An EV is assigned a set using following equation.

$$
v_i \in
\begin{cases}
G_{1,j} & \text{if } \kappa_j w_{i,1} < p_{i,max}, \\
G_{2,j} & \text{otherwise}
\end{cases}
\tag{2.15}
$$

Where all EVs in $G_{2,j}$ are those whose recharging rates would violate the second constraint in Eq. (2.1) if it was present.

S3) If $G_{2,j}$ is empty then go to S4. otherwise, for all EVs in $G_{2,j}$, assign $p_i = p_{i,max}$. For these EVs we have found the optimal solution because the objective is concave increasing in p_i and it is shown in Appendix A that $\kappa_{j+1} \geq \kappa_j$ for all $j \geq 1$. For rest of EVs in $G_{1,j}$, if $G_{1,j}$ is empty, then go to S5. Otherwise set $C_{j+1} = C_j - \sum\limits_{i|v_i \in G_{2,j}} p_{i,max}$, $V_{j+1} = G_{1,j}$, $N_{j+1} = |G_{1,j}|$ and go to S1 with reduced problem under consideration.

S4) Now for all EVs left under consideration, none must be recharging such that the second constraint in Eq. (2.1) can be violated. Hence we have reached the solution. Go to S6.

S5) Since $G_{1,j}$ is empty, we stop because for all EVs $p_i = p_{i,max}$ and go to S6.

S6) Suppose we reach S6 in qth iteration. It follows that we can define $G_1 = G_{1,q}$ and $G_2 = \cup_{j=1}^q G_{2,j}$ which contains all EVs recharging at maximum possible recharging rate and $\kappa = \kappa_q$ where

$$
v_i \in
\begin{cases}
G_1 & \text{if } p_i = \kappa w_{i,1} < p_{i,max} \\
G_2 & \text{if } p_i = p_{i,max}
\end{cases}
\tag{2.16}
$$

Since a given EV in $V(t)$ must be either in G_1 or in G_2, the equation (2.10) follows.

$\square$

The EVs in G_1 are the recipients of the proportional service because their recharging rates are directly proportional to their respective payment rates. We consider EVs in G_2 as the recipients of the priority service since they are recharged at the maximum possible recharging rate.

2.5.4 Value of κ in jth Iteration of Procedure A

During jth iteration of step 1 of procedure A,

$$
p_i = \frac{w_{i,1}}{\sum_{k=1}^{N_j} w_{k,1}} C_j
\tag{2.17}
$$

.

Proof. Here we show that

$$p_i = \frac{w_{i,1}}{\sum_{k=1}^{N_j} w_{k,1}} C_j \Leftrightarrow p_i = w_{i,1} \frac{\|\mathbf{P_j}\|}{\|\mathbf{W_{1,j}}\|} \tag{2.18}$$

suppose

$$p_i = \frac{w_{i,1}}{\sum_{k=1}^{N_j} w_{k,1}} C_j$$

then

$$p_i = \frac{w_{i,1}}{\sum_{k=1}^{N_j} w_{k,1}} \frac{\|\mathbf{W_{1,j}}\|}{\|\mathbf{W_{1,j}}\|} C_j$$

thus

$$p_i = \frac{w_{i,1}}{\|\mathbf{W_{1,j}}\|} \sqrt{\left(\frac{w_{1,1} C_j}{\sum_{k=1}^{N_j} w_{k,1}}\right)^2 + \cdots + \left(\frac{w_{N_j,1} C_j}{\sum_{k=1}^{N_j} w_{k,1}}\right)^2}$$

hence

$$p_i = \frac{w_{i,1}}{\|\mathbf{W_{1,j}}\|} \sqrt{p_1^2 + \cdots + p_{N_j}^2}$$

thus

$$p_i = w_{i,1} \frac{\|\mathbf{P_j}\|}{\|\mathbf{W_{1,j}}\|}$$

Alternately suppose

$$p_i = w_{i,1} \frac{\|\mathbf{P_j}\|}{\|\mathbf{W_{1,j}}\|} \text{ for } i = 1 \ \ldots \ N_j \tag{2.19}$$

then

$$\sum_{k=1}^{N_j} p_k = \sum_{k=1}^{N_j} w_{k,1} \frac{\|\mathbf{P_j}\|}{\|\mathbf{W_{1,j}}\|}$$

hence

$$\frac{\|\mathbf{P_j}\|}{\|\mathbf{W_{1,j}}\|} = \frac{\sum_{k=1}^{N_j} p_k}{\sum_{k=1}^{N_j} w_{k,1}}$$

Using this value in Eq. (2.19), we get

$$p_i = w_{i,1} \frac{\sum_{k=1}^{N_j} p_k}{\sum_{k=1}^{N_j} w_{k,1}}$$

but $\sum_{j=1}^{N_j} p_j = C_j$ at the optimal point since objective is concave increasing in p_i

$$p_i = \frac{w_{i,1}}{\sum_{k=1}^{N_j} w_{k,1}} C_j$$

Which completes the proof. $\qquad\square$

Note that this result is true for *qth* iteration and hence true for every EV in G_1 and allows us to view the recharging rate controller as a discriminatory scheduler. Thus for EVs in G_1 we can write

$$p_i = \frac{w_{i,1}}{\sum_{k|v_k \in G_1} w_{k,1}} C_{G_1} \tag{2.20}$$

and

$$\kappa = \frac{C_{G_1}}{\sum_{k|v_k \in G_1} w_{k,1}} \tag{2.21}$$

where C_{G_1} is capacity being used to recharge EVs in G_1.

2.5.5   Characteristics of κ

Using the proposed recharging rate control, autonomous EV agents are encouraged to submit demand at the time of high availability of energy and to disperse in time their demand relative to each other. From Eq. (2.21), the following characteristics of the incentive policy κ can be identified.

1. κ is directly proportional to the available generation capacity. For a given payment rate, EVs get better recharging rates if their demand time matches with the time of high availability.

2. κ is a monotonically decreasing function of the number of recharging EVs. When large number of EVs submit demand at the same time, the recharging rates reduce for all EVs. For a given payment rate, EVs can achieve better recharging rates if they disperse in time their demand relative to each other instead of submitting it at the same time.

2.5.6   Pareto Efficiency

Let $u_i(p_i, w_{i,1})$ be the utility of *ith* EV which is concave increasing in p_i and decreasing in $w_{i,1}$. Using the results presented in [61], it is shown in Appendix A that, assuming that all EVs are rational and autonomous, and that they observe the same value of κ for their chosen $w_{i,1}$, the equilibrium recharging rates are Pareto efficient.
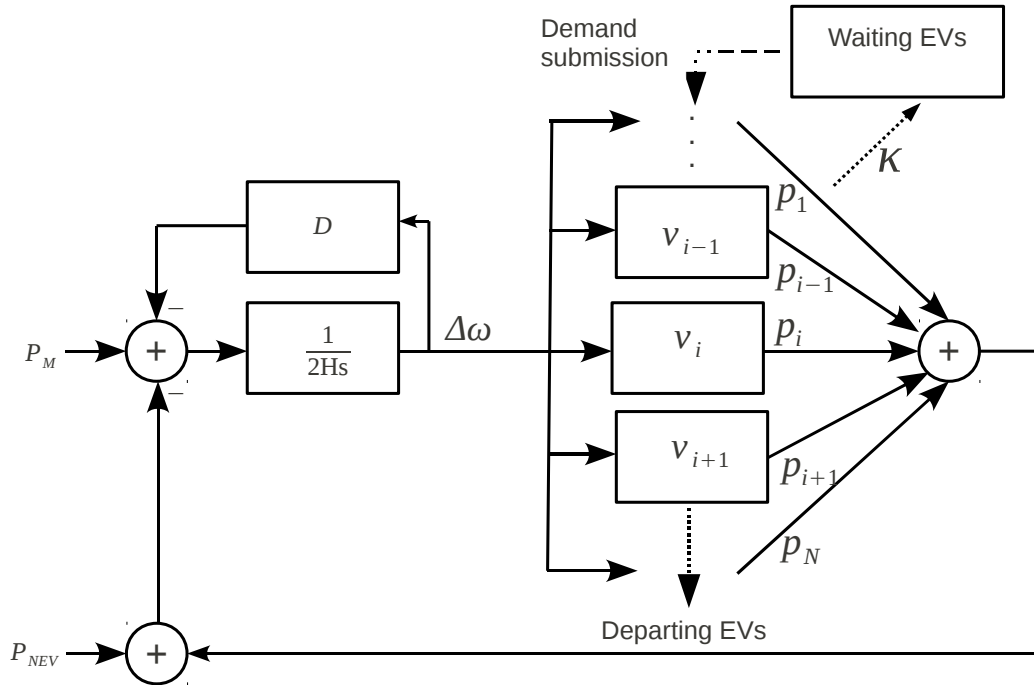
FIGURE 2.2: Implementation using a single turbine and isolated synchronous machine

2.5.7 Proportional Fairness

Let $\mathbf{P_0} = [p_{01}, p_{02}, \ldots, p_{0N}]$ be a recharging rate vector for N EVs that is feasible. For a given payment rate vector $\mathbf{W_1} = [w_{1,1}, w_{2,1}, \ldots, w_{N,1}]$, we say that $\mathbf{P_0}$ is proportionally fair if for any other feasible $\mathbf{P_1} \neq \mathbf{P_0}$ the aggregate weighted proportional change is negative. *i.e.*,

$$\sum_{i=1}^{N} w_{0i} \frac{p_{1i} - p_{0i}}{p_{0i}} < 0 \tag{2.22}$$

Using a similar argument as presented in [55], it is shown in Appendix A that the optimal recharging rates are proportionally fair.

2.6 Implementation

2.6.1 Single Machine Implementation

We first consider an isolated and unregulated synchronous machine who's rotor is initially rotating at synchronous speed and arbitrary initial EV recharging rates such that initial net torque on rotor is zero. Such a machine can be modelled by the following linear

differential equation [62]

$$2H\frac{d(\Delta\omega(t))}{dt} + D\Delta\omega(t) = P_M(t) - P_{NEV}(t) - \sum_{i=1}^{N} p_i(t) \tag{2.23}$$

Where H [p.u] is the inertia constant of machine, D [p.u] is the damping torque, $\Delta\omega$ [p.u] is the frequency deviation and P_M[p.u] is the input mechanical torque to the machine which is the scheduled power. Figure 2.2 shows a diagram of depicting such a synchronous machine and EVs.

It will be shown now that the frequency deviation of electric power system can be used to allocate the recharging rates as in Eq. (2.10). Let $0 \leq P_M \leq 1, 0 < D \leq 1, H > 0$ and $0 < P_{NEV} \leq 1$ be constants such that $P_M - P_{NEV} < \sum_{i=1}^{N} p_{imax}$ and $P_M - P_{NEV} - \sum_{i=1}^{N} p_i(0) \approx 0$ then from any given initial values of $0 < p_i(0) \leq p_{imax}$ for $i = 1, \ldots N$, the system of differential inclusions in Eq. (2.24) converges to $p_i(t)$ as in Eq. (2.10) with κ as in Eq. (2.21) such that $|\Delta\omega| \leq \Delta\zeta$ where $\Delta\zeta$ is small as compared to the statutory frequency deviation.

$$2H\frac{d(\Delta\omega(t))}{dt} + D\Delta\omega(t) - P_M(t) + \sum_{j=1}^{N} p_j(t) + P_{NEV}(t) = 0$$

$$\frac{d(p_i(t))}{dt} - \frac{\alpha w_{i,1}(t)}{p_i(t)}\overline{\theta_1(t)}\ \overline{\phi_1(p_i(t))} - \beta(\theta_1(t) + \phi_1(p_i(t))) = 0 \tag{2.24}$$

for $i = 1, 2, \ldots,$ N

Because computing the values of θ_1 and θ_2 using equations (2.4) and (2.8) will require knowledge of recharging rates p_i of all EVs, to ensure scalability, we compute the value of θ_1 and θ_2 by using the frequency deviation $\Delta\omega$.

$$\theta_1 = \begin{cases} 1 & \text{if } \Delta\omega < 0, \\ 0 & \text{otherwise} \end{cases} \tag{2.25}$$

and

$$\theta_2 = \begin{cases} 0 & \text{if } \Delta\omega < \Delta\omega_{V2G}, \\ 1 & \text{otherwise} \end{cases} \tag{2.26}$$

Proof. The first equation in Eq. (2.24) can be rewritten as

$$2H\frac{d(\Delta\omega(t))}{dt} + D\Delta\omega(t) = C(t) - P_{EV}(t) \tag{2.27}$$

where $C(t) = P_M(t) - P_{NEV}(t)$ and $P_{EV}(t) = \sum_{j=1}^{N} p_j(t)$

Dividing both sides of Eq. (2.27) by $2H$, multiplying by integrating factor $e^{\left(\frac{D}{2H}\right)t}$, integrating and multiplying by $e^{-\left(\frac{D}{2H}\right)t}$ after integration, we get

$$\Delta\omega(t) = e^{-\left(\frac{D}{2H}\right)t}\left[\int_0^t \frac{e^{\left(\frac{D}{2H}\right)\tau}}{2H}\left(C(\tau) - P_{EV}(\tau)\right)d\tau + c_0\right] \tag{2.28}$$

We can write

$$\Delta\omega(t) = g_1(t)g_2(t) \tag{2.29}$$

where $g_1(t) = e^{-\left(\frac{D}{2H}\right)t}$ and

$$g_2(t) = \left[\int_0^t \frac{e^{\left(\frac{D}{2H}\right)\tau}}{2H}\left(C(\tau) - P_{EV}(\tau)\right)d\tau + c_0\right] \tag{2.30}$$

Now let us consider the only two possible values that θ_1 can take. Suppose $0 < \Delta\omega(0) = c_0 < \Delta\zeta$, we take $\theta_1 = 0$. Hence, using Eq. (2.3), $p_j(t) = min(\int_0^t \left(\frac{\alpha w_i(t)}{p_j(t)}dt\right), p_{j,max})$. Hence $P_{EV}(t) = \sum_{j=1}^{N} min(\int_0^t \left(\frac{\alpha w_i(t)}{p_j(t)}dt\right), p_{j,max})$ is a monotonically increasing function of time. Since $C(t) < \sum_{i=1}^{N} p_{imax}$, it follows that $C(t) < P_{EV}(t)$ for some $t > t_0$. If $C(0) < P_{EV}(0)$, then $t_0 = 0$. It follows from Eq. (2.30), that $g_2(t)$ increases monotonically for $t < t_0$ and starts decreasing for $t > t_0$. This decrease is rapid because $e^{\frac{D}{2H}t}$ increase rapidly although $C(t) - P_{EV}(t) < 0$ is very small. Thus we conclude that $\Delta\omega(t) < 0$ for some $t > t_1 > t_0$ and hence $\theta_1 = 1$ for $t > t_1$.

Alternately, suppose $-\Delta\zeta < \Delta\omega(0) = c_0 < 0$, we take $\theta_1 = 1$. Hence, using Eq. (2.3), $p_j = max(p_j(0) - \beta t, 0)$. Here $P_{EV}(t) = \sum_{j=1}^{N} max(p_j(0) - \beta t, 0)$ is a monotonically decreasing function of time. Since $C(t) > 0$, it follows that $C(t) > P_{EV}(t)$ for some $t > t_3$. If $C(0) > P_{EV}(0)$, then $t_3 = 0$. It follows from Eq. (2.30), that $g_2(t)$ decreases for $t < t_3$ and then increases for $t > t_3$. Hence $\Delta\omega(t) > 0$ for some $t > t_4 > t_3$ and hence $\theta_1 = 0$ for $t > t_4$.
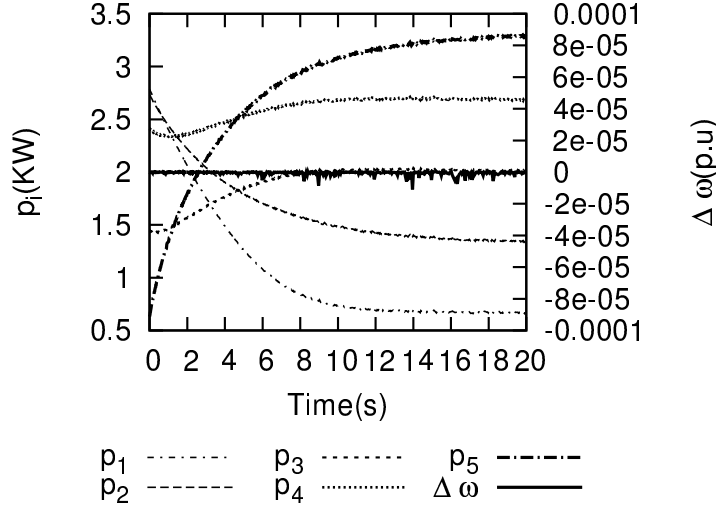
FIGURE 2.3: Recharging rates and frequency deviation for single machine case

We note that if use the condition $\Delta\omega(t) = 0$ to create a sliding mode, then it also creates a corresponding sliding mode on the condition $C(t) = P_{EV}(t)$. Hence, the equilibrium point of Eq. (2.24) is the same as the equilibrium point of Eq. (2.3).

$\square$

In respect to the previous proof, we note that the frequency deviation follows a differential equation and lags the imbalance between generation and demand as it is shown by Eq. (2.28).

We have noted that it is possible to use the frequency deviation $\Delta\omega(t)$ as proxy to compute θ_1 instead of using Eq. (2.4). Thus, the recharging rates that converge to Eq. (2.10) can be calculated in a distributed manner.

We note that alternative methods for extracting the required information on power imbalance may exist but we leave this line of investigation for future research.

Figure 2.3 shows the recharging rates p_i and frequency deviation $\Delta\omega$ when recharging 5 EVs using $P_{base} = 100$ (kw) electric generator. Here, $H = 1$ (s), $D=1$ (p.u), $P_{NEV} = 0.9$ (p.u), $\sum_{i=1}^{N} p_i(0) = 0.1$ (p.u) with random $p_i(0)$, $\mathbf{W_1} = [1, 2, 3, 4, 5]$ ($/h), $\alpha = 1$, $\beta = 1$. It can be observed from Fig. 2.3 that if total load is initially balanced then the recharging rate controller achieves intra EV redistribution of recharging rates such that the recharging rates converge to $\mathbf{P} = [0.67, 1.33, 2, 2.67, 3.33]$ (kw) which are in accordance with their respective payment rates. The redistribution is achieved in such a
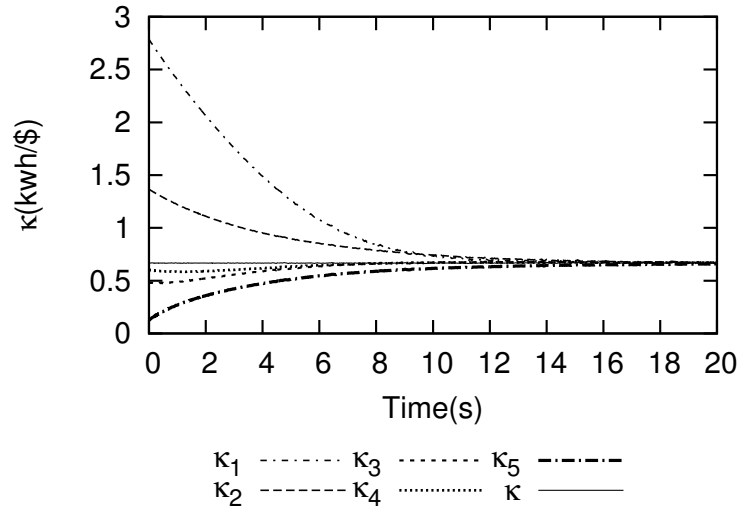
FIGURE 2.4: Value of κ as observed at individual recharging sockets

way that the rotor of the synchronous machine rotates at synchronous speed and hence a change in input torque is not required and $1/\kappa$ converges to 0.67 (kwh/\$) at all the recharging sockets as shown in Fig. 2.4

We note that the following are special cases when an intra-EV redistribution of recharging rates will occur

    i) Demand submitted by a new EV

   ii) Completion of a demand or departure of an EV

 iii) A change in $w_{i,1}$ by *ith* EV agent.

 iv) A change in Non-EV load

2.6.2 EV Agent's Budget and Decentralised Billing

When an EV connects to the socket, the EV agent knows the budget Bd [\$] that it has at its disposal to achieve, for example, a target battery state of charge $BSOC_i$ [kwh] before the next journey. What the EV agent does not know is the state of the electric grid and hence it is unaware of the value of $1/\kappa$. However, the EV agent can submit a small $w_{i,1}$ and within a few seconds (Section 2.6.5, Fig. 2.6) it will receive from the socket agent the signal $1/\kappa$. From this point onwards the EV agent can start making informed decisions by tracking its remaining budget and estimating the total cost of

recharging: as a first approximation at the moment of connection $Bd \geq \overline{MP_i} \approx w_{i,1} * T_L$ where $T_L = t_1 - t_0$ is the total time available to recharge the battery. Here, t_0 is the EV initial time of connection to socket and t_1 is the time of departure of the EV. Therefore, the EV agent and the sockets agent can estimate the cost incurred (current value of bill) using Eq. (2.31).

$$MP_i(t_0, t_n) = \int_{t_0}^{t_n} w_{i,1}(t)dt \qquad (2.31)$$

The EV agent will also be able to monitor at all times the battery state of recharge using Eq. (2.32):

$$\Delta BSOC_i(t_0, t_n) = \int_{t_0}^{t_n} p_i(t)dt \qquad (2.32)$$

Thus, the EV agent can continuously monitor the changes in $1/\kappa$ and dynamically adapt the value of $w_{i,j}$ to satisfy its internal objectives. For example, it could be constantly aiming at saving as much as possible from its remaining budget $(Bd - MP_i(t_0, t_n) \geq 0)$ as long its target $BSOC_i(t_0, t_n)$ is being achieved.

A rational EV agent will stop paying once its battery has been recharged to the target capacity. Hence the EV agent can set $w_{i,1} = 0$ and this will instantly stop recharging the EV battery. At the time of disconnection, the socket agent will have no further information on $w_{i,1}$ and the bill can be transmitted to a centralised location.

2.6.3   A Protocol Based on the Recharging Rate Controller

In order to deploy the recharging rate controller in a multi-machine system, we will need to take into account the following considerations.

1. The frequency deviation as estimated by a recharging socket is based on voltage and current at the recharging socket. The voltage and current will contain various harmonics due to intra machine rotor oscillations, distortion and noise. It might not be possible to measure the frequency deviation to the desired accuracy with high resolution at each recharging socket.

$$p_i(t_k \le t \le t_{k+1}) = \begin{cases} p_i(t_k) + \int_{t_k}^{t} \left(\frac{w_{i,1}\alpha}{p_i(\tau)} \right) d\tau - \beta\phi(p_i(t))(t - t_k) & \text{if } m(t_k) = FAN \text{ and } p_i(t_k) \ne 0 \\ \Delta\gamma & \text{if } m(t_k) = FAN \text{ and } p_i(t_k) = 0 \\ p_i(t_k) - \beta(1 + \phi(p_i(t)))(t - t_k) & \text{if } m(t_k) = FBN \\ 0 & \text{if } m(t_k) = SSL \\ p_i(t_k) & \text{if } m(t_k) = LSS \text{ or message loss in tr} \end{cases}$$

(2.33)

2. Different sections of electric power system may have slight mismatch in frequency at a given instant in time. The frequency deviations as individually estimated by all recharging sockets are not necessarily the same.

Therefore, we modify the recharging rate controller and propose a socket management protocol. We consider a socket manager agent that can communicate with the sockets and other controllers in the power system. The socket manager broadcasts a pseudo frequency signal to all sockets. Two messages are sufficient to send the pseudo frequency signal.

i) **FAN** frequency above nominal

ii) **FBN** frequency below nominal

In addition the socket manager broadcasts two messages that are not part of the original control. These messages can temporarily hold the socket state or shed its load when needed.

iii) **LSS** lock socket state

iv) **SSL** shed socket load

let $m(t_k)$ be a message received by *ith* socket at time t_k. The recharging rate for *ith* socket is given by Eq. (2.33), where $\Delta\gamma > 0$ is an arbitrarily small constant.

The socket manager has the following key functions.

1. Generates the pseudo frequency signal for recharging rate controllers

2. Allows any critical control to act without interference from recharging rate controllers by allowing locking of sockets.
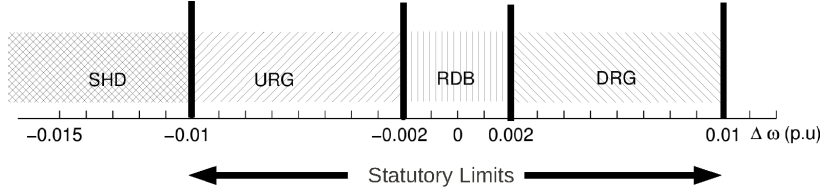
FIGURE 2.5: Frequency to function map for the socket manager

3. Integrates with the protection system to shed all EV load or sheds all EV load if frequency falls below the statutory limit and switches the sockets to Mode 2. Those EVs which are willing to discharge are used as V2G sources.

To generate the pseudo frequency the socket manager maps the frequency to functions as shown in Fig. 2.5 where the functions, their descriptions and the corresponding messages are shown in the following text.

1. **SHD** sheds all EV load. A **SSL** messages is transmitted every T [ms].

2. **URG** Decreases the recharging capacity for EVs. A **FBN** message is transmitted every T [ms].

3. **RDB** Redistributes recharging rates among EVs according to their respective payment rates. A **FAN** message is transmitted and a **FBN** message follows it by T_f [ms] where $T_f \leq T$. The pattern is repeated every T [ms]. T_f is computed such that $T_f = 0$ at the lower boundary of **RDB** region of map in Fig. 2.5 and increases linearly to $T_f = T$ at the upper boundary of **RDB** region.

4. **DRG** Increase the capacity for recharging EVs. A **FAN** message is transmitted very T [ms].

2.6.4   Benefits of Proposed Protocol

1. All sockets act on the same information and do not need to accurately measure the frequency deviation with high resolution.

2. Message communication to all sockets is broadcast, hence, addressing of individual sockets is not needed.

3. Recharging sockets can temporarily use local frequency measurements if communication link is broken and can revert to using global measurement when link is re-established

4. Exact measurement of frequency is not required at each socket and pseudo frequency can be generated using an approximation of exact frequency

5. Interference to critical controls in the power system is avoided by locking sockets when needed.

2.6.5 Simulation Results

In this section we present simulation results with the recharging rate control implemented together with the socket management protocol. We use a power system with primary frequency regulation provided by steam reheat turbines with droop based governors as modelled in [63]. The average frequency deviation $\Delta\omega$ can be expressed by the following equation as derived in [63].

$$\Delta\omega = \left(\frac{R\omega_n^2}{DR+1}\right)\left(\frac{(1+F_H T_R)P_{SP} - (1+T_R s)P_e}{s^2 + 2\zeta\omega_n s + \omega_n^2}\right) \tag{2.34}$$

Where

$$\omega_n^2 = \frac{DR+1}{2HRT_R} \tag{2.35}$$

$$\zeta = \omega_n\left(\frac{2HR + (DR+F_H)T_R}{2D_R+1}\right) \tag{2.36}$$

and

$$P_e = P_{SCH} - P_{NEV} - P_{EV} \tag{2.37}$$

Where

$R =$ Speed droop or regulation,

$F_H =$ Fraction of power from high pressure section of turbine,

$T_R =$ Reheat time constant [s],

$P_e =$ Electrical power [p.u],
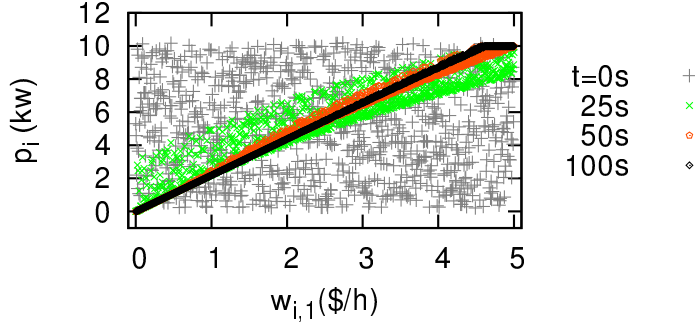
FIGURE 2.6: Snapshot of recharging rates as function of $w_{i,1}$
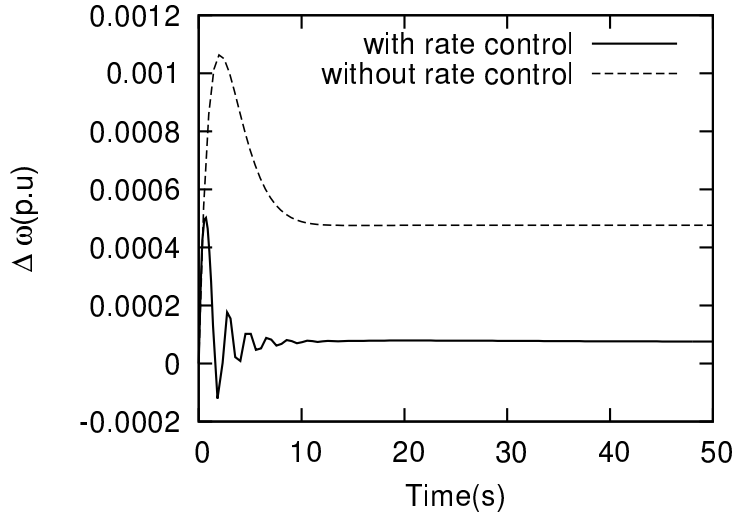
FIGURE 2.7: Frequency deviation with and without proposed recharging rate control

P_{SP} = Incremental set point [p.u],

The configuration parameters are: $N = 1000$, $P_{base} = 50$ (Mw) $\alpha = 1$, $\beta = 1$, $P_{NEV}(t_0)$ = 0.9 (p.u), $P_M(t_0) = 0$, $t_0 = 0$, w_i are uniformly distributed random variables between 0 and 5 (\$/h) (considered constant during the simulation), $p_i(t = 0)$ are uniformly distributed between 0 and 10 (kw) such that $\sum_{i=1}^{N} p_i = 0.1$ (p.u) (to ensure initial balance condition), $p_{imax} = 10$ (kw) $H = 3.5$ (s), $R = 0.05$, $F_H = 0.3$, $D=1$, $T_R = 8$ (s), $P_{SP} = 0$, $T = 20$ (ms) and RDB region has boundaries at $\Delta\omega = \pm 0.0002$ (p.u)

Figure 2.6 shows the snapshots of recharging rates p_i as function of w_i at t = 0, 25, 50, and 100 (s) respectively. Thus recharging rates are redistributed and EVs are dynamically partitioned into G_1 and G_2 with $\kappa \approx 2.2$ (kwh/\$).

Figure 2.7 shows the frequency deviation for a 1% sudden non-EV load loss at t = 0 (s). This step change in $C(t)$ contains a wide spectrum of frequencies. When the high frequency components of $C(t)$ are significant, $P_{EV}(t)$ may not be able to follow $C(t)$, which is reflected in the values of $\Delta\omega$ when ($t \le 10$ (s)). When the magnitude of high frequency components of $C(t)$ becomes negligible compared to its moving average value over a few minutes, $P_{EV}(t)$ follows $C(t)$, which is reflected in the values of $\Delta\omega$ when ($t \le 10$ (s)). In the case of this example, it can be seen that, when the proposed recharging rate control is used, the peak frequency deviation is reduced by 50%. Hence, a smaller primary frequency regulating turbine can be used to provide frequency regulation. We note that the highlighted characteristics can be very helpful in reducing the turbine size that is needed to regulate the fluctuations of, for example, the output of renewable energy sources.

For the multiple machine case, we can observe that if the size of $RDB > 0$ (Fig. 2.5) this will result in a steady state value $|\Delta\omega| > 0$ which is constant (Fig. 2.7) and bounded by half of the width of the RDB band. We note that as the width of the RDB region approaches zero, the controller in Eq. (2.33) will in the limit behave as the controller used in the single machine case in Eq. (2.24) except in rare circumstances when the EV load is shed because of the frequency falling below the statutory limit.

Since steady state frequency deviation is constant, we observe that $C(t) = P_{EV}(t)$ but a small power will flow from generators providing droop based regulation. However, we would like to point out that had the parked EVs not been present, a much larger power flow from regulating generators would have occurred as observed in Fig. 2.8.

2.7 Recharging Strategies, Demand Deferment and Capacity Control

As previously mentioned, the socket agents will broadcast the same value of $1/\kappa$. Assuming that EV agents are perfectly rational and autonomous with utility $u_i(p_i, w_{i,1})$ such that each EV can exchange $p_i = \kappa w_{i,1}$ [kw] with $w_{i,1}$ [\$/s] in an environment where the energy providers are maximising their revenue, the EV agents will choose $w_{i,1}$ such that the resulting equilibrium recharging rates are Pareto efficient and proportionally fair.
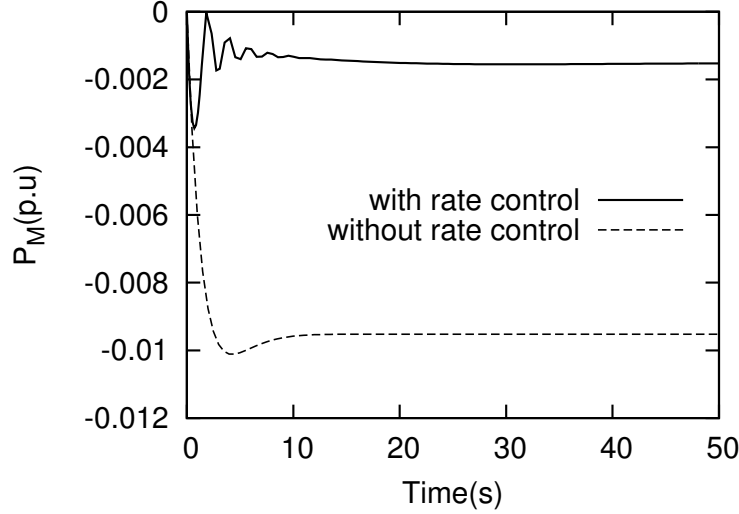
FIGURE 2.8: Output power of the frequency regulating turbine

Let $CCR(C)[\$/h]$ be the generation cost rate of C [kw]. In general, the cost rate is a convex function and the marginal cost rate of generation $\frac{\partial CCR}{\partial C}$ is increasing function of C. Thus in the context of a competitive generation market, a generator will maximise revenue if:

$$\frac{\partial CCR}{\partial C}\big|_{C=P_{NEV}+C_0} = \frac{1}{\kappa} = \frac{\sum_{i|v_i \in G_1} w_{i,1}}{C_0} \tag{2.38}$$

To show why κ encourages deferment of demand by some EVs, we focus on Mode 1 of operations and consider a simple game. Let us consider rational and selfish EV agents which try to maximise their $BSOC$ and minimise their total incurred cost. We note that all rational EVs will be in G_1 as any EV in G_2 can decrease its payment rate without decreasing its recharging rate. As we have previously introduced, the total cost incurred by the ith EV agent over a time $t_n - t_0$ will be $MP_i(t_0, t_n)$ as in Eq. (2.31), and the corresponding change in battery state of charge $\Delta BSOC_i(t_0, t_n)$ as in Eq. (2.32). From Fig. 2.6, we can see that p_i converges to $\kappa w_{i,1}$ in a few seconds even when EVs submit random values of $w_{i,1}$ at the same time, hence. [2]

$$\Delta BSOC_i(t_0, t_1) = \int_{t_0}^{t_1} p_i(t)dt \approx \int_{t_0}^{t_1} \kappa(t)w_{i,1}(t)dt \tag{2.39}$$

---

[2] p_i will converge to κw_i even faster than the rate of convergence shown in Fig. 2.6 when the number of arriving/departing EVs are small compared to the number of already parked EVs.

Lets now consider a game with two EVs: V_1, V_2 and two time slots t_1 and t_2 of same time width T_c. We denote a recharging strategy as (t_i, t_j) where V_1 chooses the *ith* time slot and V_2 chooses the *jth* time slot. In this game, there are four recharging strategies namely $a_1 = (t_1, t_1), a_2 = (t_1, t_2), a_3 = (t_2, t_1)$ and $a_4 = (t_2, t_2)$. For simplicity, we assume that P_{NEV} is the same in both time slots. Also let the equilibrium value of κ be κ_A when EVs choose the same time slot, and κ_B when they choose different time slots. We define the payoffs of EVs as the ratio $\Delta BSOC/MP_i$, which, in a steady system, is the value κ. We will now show that a_1 and a_4 are unstable and a_2 and a_3 are pure strategy Nash equilibria. The payoff matrix can be written as

V_1, V_2	t_1	t_2
t_1	κ_A, κ_A	κ_B, κ_B
t_2	κ_B, κ_B	κ_A, κ_A

TABLE 2.1: Payoff matrix for two EVs

When the EVs choose the same time slots, the collective revenue rate of the electric generator from recharging both EVs at the same time is $2w$ and it will be w when the EVs choose different time slots. Let C_A denote the capacity allocated by the electric generator when the EVs choose the same time slots and C_B denote the capacity allocated by the electric generator when the EVs choose different time slots. C is zero in a time slot if no EV chooses that slot. For slots chosen by at least one EV, we now determine C_A and C_B. Thus we can write

$$\frac{\partial CCR}{\partial C}\Big|_{C=P_{NEV}+C_A} = \frac{2w}{C_A} \tag{2.40}$$

$$\frac{\partial CCR}{\partial C}\Big|_{C=P_{NEV}+C_B} = \frac{w}{C_B} \tag{2.41}$$

Multiplying Eq. (2.41) by 2, rearranging and comparing with a rearranged version of Eq. (2.40), we get

$$\frac{\partial CCR}{\partial C}\Big|_{C=P_{NEV}+C_A} C_A = 2\frac{\partial CCR}{\partial C}\Big|_{C=P_{NEV}+C_B} C_B \tag{2.42}$$

All quantities in Eq. (2.42) are positive. Furthermore, $\frac{\partial CCR}{\partial C}$ is a convex increasing function of C. It follows that $C_A > C_B$ and

$$\frac{\partial CCR}{\partial C}\Big|_{C=P_{NEV}+C_A} > \frac{\partial CCR}{\partial C}\Big|_{C=P_{NEV}+C_B} \qquad (2.43)$$

Now rearranging Eq. (2.42) we get

$$C_A = 2\frac{\frac{\partial CCR}{\partial C}\big|_{C=P_{NEV}+C_B}}{\frac{\partial CCR}{\partial C}\big|_{C=P_{NEV}+C_A}}C_B \qquad (2.44)$$

From equations (2.44) and (2.43), we conclude that $C_A < 2C_B$. Noting that $\frac{1}{\kappa_A} = \frac{2w}{C_A}$ and $\frac{1}{\kappa_B} = \frac{w}{C_B}$, we can write

$$\kappa_A = \kappa_B \frac{C_A}{2C_B} \qquad (2.45)$$

and hence,

$$\kappa_A < \kappa_B \qquad (2.46)$$

Using Eq. (2.46), we can interpret the payoff matrix of the game in Table 2.1 and observe that a_1 and a_4 are unstable, and that a_2 and a_3 are two pure Nash equilibria strategies. Hence both EVs will benefit if only one of them defers its demand. Furthermore, we note that there are an unlimited number of equivalent strategies as any EV does not need to recharge continuously in one session.

If we consider EVs as players in this iterative game, each EV agent will endeavour to achieve, for example, a desired $\Delta BSOC(t_0, t_n)$ before it's next journey commences while minimising the total cost incurred. These EV agents are hence allowed to make arbitrary learning moves in real time to experiment without compromising the load balance as socket agents will ensure that policy κ is complied at all times. [3]

There is a vast amount of technical literature on game theory [52] which is at the core of the solution to the game highlighted in this section. For example in [64], and in the

---

[3]Note that since EV agents will learn their recharging strategies based on the value of κ, they should restrain from learning when either message **SSL** or message **LSS** is active.

context of multi-agent learning framework, the use of game theory [52] and reinforcement learning [65] was investigated. In [64] the authors study how to learn to play a Pareto-optimal Nash equilibrium when there exist multiple equilibria and agents may have different preferences. It is beyond the scope of this thesis to further expand on more elaborated aspects of this game and its solution.

2.8 Final Remarks

In this chapter, a distributed recharging rate control algorithm has been proposed that combines the objectives of regulating frequency and improving utilisation of electric generators by creating an incentive policy for autonomous EV that are randomly connecting to and disconnecting from the electric grid. The incentive policy κ encourages EVs to demand energy when non-EV demand is low and utilisation of electric generators needs to be improved. EVs also act as frequency regulators which can control their participation role by modifying their respective payment rate $w_{i,1}$ as individual EVs connect and disconnect at arbitrary times.

The proposed recharging rate control algorithm can be used to realise a DM solution to, for example, reconcile EVs energy demand profiles with the output of available energy sources. Furthermore, encouraging results show that the proposed recharging rate control algorithm can help decrease the required size of frequency regulating turbines.

Chapter 3

Distribution Voltage Congestion Avoidance

3.1 Introduction and Motivation

Consider a typical neighbourhood in a city that is composed of several homes that can be characterised by their corresponding electricity consumption profiles. The electric power distribution system operator (DSO) that supplies the electricity to this neighbourhood would have had estimated, using historical data, the aggregate electricity demand profile and expected growth of electricity demand in the neighbourhood. With the appropriate energy demand forecast the DSO would have installed the appropriate infrastructure elements like, the distribution feeders, the distribution transformer and the secondary circuits. At the planning stage, a margin of safety would have been considered to decide the capacities of the infrastructure elements. Subsequently, at the operations phase of the system, the operator will constantly monitor electric power flow profiles in the system and take necessary action when instantaneous load rises above the design capacity of the system.

In this chapter, this scenario is extended by considering that several houses in the neighbourhood also own electric vehicles (EVs). If this is the case, then on a typical weekday, household owners will return home at roughly the same time in the evening and they will plug in their EVs, which by default might start recharging immediately. As it is known that recharging a typical EV can become a substantial load (10kW to

71

30kW) on the distribution system, if several of these EVs happen to recharge at the same time, the secondary circuits and the distribution transformer can get overloaded [66]. Under these circumstances, the voltage at customer premises might drop below statutory limits. Moreover, in case of severe overload, the distribution conductors might be damaged because of overheating.

There are several mechanism to avoid overload in the distribution system. For example, the DSO may upgrade the network infrastructure by installing bigger transformers and thicker conductors, but such upgrade is often very costly. Moreover, if the durations of overload are short and the infrastructure has underutilised assets for most of the time, the benefits of infrastructure upgrade might not justify the economic costs. An alternative approach is to install software components in the recharging sockets that allow EVs to coordinate their recharging activities [67]. In this chapter and the next, we study mechanisms to shape the recharging rate profile of EVs with explicit consideration for the voltage profile in the distribution system. This investigation also allows us to search for a solution that will enhance the voltage security as compared to the case of random uncoordinated recharging.

3.2   Organisation of the Chapter

In Section 3.3, the literature is reviewed and relevant research work is identified. In Section 3.4, the fundamentals of electric power flow and the load flow problem are reviewed. In Section 3.5, the relationship between voltage drops and active power flow is explored and an analogy between voltage drops in the secondary circuits and the pressure in a system of fluids is presented. In Section 3.6, energy demand is approximated by an energy demand particle system (EDPS) and a correspondence is established between an EDPS and a fluid particle system (FPS). In Section 3.7 a two stage framework is presented that can be used to construct recharging schedules for EVs that are aimed at avoiding congestion in the secondary circuits. In Section 3.8 a method, called smoothed particle hydrodynamics (SPH), for solving equations of fluid dynamics is reviewed and an algorithm that applies SPH method to the FPS is presented. Finally, in Section 3.9 the proposed approach is evaluated and compared with the state of the art approaches using two examples.

3.3 Literature Review

Recently, there has been great amount of interest in EV recharging schemes and specifically in the impacts of integration of these recharging schemes with the electric power system. Depending on the particular role that EVs are expected to play, researchers have pursued different lines of investigation. For example, several papers can be found that try to flatten the aggregate (EV + non-EV) demand on electric power system [68, 69]. Other researchers have: a) studied the use of EVs as small electric power generators to supply electric power at peak times [9, 21], b) investigated the impacts of uncontrolled or uncoordinated recharging of EVs on electric power system [70, 71], c) proposed algorithms for scheduling the recharging of EVs to reduce impacts on the distribution system [72, 73] In this section, we restrict ourselves to a review of those works which directly address the impacts on distribution system voltages taking into consideration the recharging profiles of EVs.

Clement *et. al.* [71, 74] appear to be the first to have suggested coordinated recharging of EVs based on consideration of voltage in the distribution system. Their study in [74] is based on stochastic simulation of EV energy demand and hence it might be useful in studying the impacts of recharging EVs and suggesting upgrade of infrastructure where necessary. In [74] the problem is formulated by scaling down an IEEE 34 node distribution feeder and considering it as a secondary circuit. EVs are recharged during two periods of time in a day and during those periods an EV is either considered connected or disconnected throughout the period. The energy demand from each EV is considered to be the same and equal to the battery capacity of the EV and at the start of a recharging period, all EVs are assumed to have empty batteries. In this chapter, we present an alternative scheduling method for recharging EVs with a more general formulation in that EVs can recharge at any time in the day and EVs can demand different amounts of energy in different periods of time. The work presented in [74] is focused on calculating impacts of recharging EVs using stochastic simulation of various scenarios. In contrast, the work presented in this chapter is focused on a scheduling method that avoids congestion in the secondary circuit.

Sortomme *et. al.* [72] have suggested an optimal scheduling method for recharging EVs. They use the notion of equivalence of *i*) minimising voltage impacts, *ii*) minimising losses, *iii*) minimising load variance and *iv*) maximising load factor. The authors in [72]

propose to schedule recharging EVs based on minimising load variance or maximising load factor. In the same paper it is suggested that the optimisation problems corresponding to *i*) minimising load variance and *ii*) maximising load factor are convex, but there is no reference to the proof. The argument in [72] also relies on remarks from references [71, 74] to assume equivalence between loss minimisation and the minimisation of voltage drop and its associated impacts. The equivalence relationship between load factor and losses is based on Buller and Woodrow formula [75] which in turn relies on empirical study of few distribution systems. Unfortunately Buller and Woodrow formula has been criticised by Mikić [76] as unreliable for general use. We also note that the equivalence relationship derived between minimising losses and minimising load variance neglects the topology of distribution system and assumes nominal voltages at each node in the distribution system. According to [72], this assumption yields a convex optimisation problem but Taleski *et. al.* [77] have shown that the assumption of nominal voltage at each node significantly reduces the accuracy of estimates of losses. The work presented in this chapter avoids relying on these equivalence relationships and highlights, through a simple example in Section 3.5.1, that there might be multiple recharging schedules that have the same load factor but different impacts on voltages. Therefore, maximising the load factor does not necessarily minimise the impacts on voltages.

Deilami *et. al.* [73] have presented a real time coordinated recharging scheme for improving voltage profiles and reducing losses, and a similar approach has been presented in [78]. In these studies EVs are considered as non-elastic loads. Note also that the work in [73] can be seen as an admission control problem rather than a scheduling problem, because EVs that can cause voltage constraint violations are denied admission and are recharged with a delay. An EV can have one of three priority levels and all EVs with higher priority level are admitted before the EVs in the next lower priority level are considered. EVs that have the same priority level are selected based on the sensitivity terms obtained from the Jacobian matrix in a load flow problem and the EVs whose recharging rate causes the least sensitivity to voltage are admitted earlier. EVs whose admission can cause a violation of constraints are not admitted and are recharged with a delay. The work in [73] considers the full topology of distribution system and hence avoids approximations used in [72]. However, because the underlying nature of problem in [73] is of admission control, the output recharging schedules might be improved by taking a different scheduling approach such as the one presented in this chapter. The

examples presented in Section 3.9 highlight cases where we first use [73] and [72] to construct an initial recharging schedule and then improve it.

Despite the limitations with the formulation in [72] the advantage of reduction in required computation is significant. Hence, in this chapter we propose a rescheduling strategy that uses a two stage framework. We first use the two objectives of i) minimising load variance and ii) maximising load factor, to obtain an initial schedule as phase 1. Subsequently, in phase 2, the initial schedule is further improved by using characteristics of the topology of the distribution system.

The proposed approach is inspired by a system of particles seeking equilibrium. The idea is to discretise the energy demand and map it into a particle system. The equations modelling the dynamics of the particle system can then be solved using a appropriate numerical method. We note however, that to solve equations of a particle system might be computationally expensive if they are solved on a Central Processing Unit (CPU), but if the behaviour of each particle is simulated on a thread on a Graphics Processing Unit (GPU), then particle systems of large number of particles can be solved in real time by taking advantage of GPU's parallel computation. For example, up to 64,000 particles have been reported to be simulated in real time at 60 frames per second (that is, 60 iterations of SPH method per second where each iteration involves 64,000 particles) [79]. We note that the simulation reported above also includes computational cost of rendering complex fluid surfaces in 3D. In contrast, we will need only a 2D simulation of fluid particles and no graphic rendering is necessary, therefore particle systems with even higher number of particles can be simulated in real time.

To compare the characteristics of the relevant published solutions and the proposed approach, we use the following features as guidelines.

- **Topology Aware:** A scheduling scheme is topology aware if it does not neglect the topology of the distribution system

- **Elastic Demand:** A scheduling scheme is based on elastic demand from EVs if the recharging rate of EVs can be varied over a given range.

- **Computational cost:** It is the computational time required by the algorithm used in the scheme.

- **Voltage Improvement:** It is the expected improvement in voltage (relative to uncoordinated scheduling) that the scheme might achieve.

Types	Topology Aware	Elastic Demand	Computational Cost	Voltage Improvement
Loss minimisation [72, 74]	Yes	Yes	High	Significant
Variance minimisation, load factor maximisation [72]	No	Yes	Low	Moderate
Admission control based [73]	Yes	No	Moderate	Light
Particle system based	Yes	Yes	Low [1]	Significant

TABLE 3.1: Comparative view of relevant solutions published in the literature

The works reviewed in this section are those which stated that the objective of scheduling solution was to reduce the impact of recharging EVs on voltages in the distribution system. Thus, we have not considered, for example, [80] as strongly related to our work because it's stated objective is to maximise the profit of distribution network operator (DNO) although it does include voltage as a constraint in the formulated optimisation problem.

Finally, it is not simple to compare works in [72, 73] and [74] as there is no metric that can be used to assess the prepared output recharging schedules. These schemes rely on visual inspection of voltages and power losses to show that coordinated recharging achieves better results when compared with uncoordinated recharging, but it is very difficult to gauge the relative performance of schedules based on visual inspection alone. A metric to compare our solution with other relevant solutions is proposed in Section 3.9.2.

---

[1]potentially low with parallel computing (see, for example, [79])

3.4   Relationship of Voltage to Power Transfer

The relationship between electric power transfer and voltage in a distribution system is in general non-linear. For an Nb bus electric power system, we can write the relationship between bus current injection and bus voltage using the $(Nb \times Nb)$ network admittance matrix Y.

$$\begin{pmatrix} Y_{1,1} & Y_{1,2} & \cdots & Y_{1,Nb} \\ Y_{2,1} & Y_{2,2} & \cdots & Y_{2,Nb} \\ \vdots & \vdots & \ddots & \vdots \\ Y_{Nb,1} & Y_{Nb,2} & \cdots & Y_{Nb,Nb} \end{pmatrix} \begin{pmatrix} V_1 \\ V_2 \\ \vdots \\ V_{Nb} \end{pmatrix} = \begin{pmatrix} I_1 \\ I_2 \\ \vdots \\ I_{Nb} \end{pmatrix} \tag{3.1}$$

Where $V_i = |V_i| \angle \delta_i$ is the voltage on bus i, $Y_{i,i} = |Y_{i,i}| \angle \theta_{i,i}$ is the self admittance or "driving point admittance" of bus i and $Y_{i,k} = |Y_{i,j}| \angle \theta_{i,j}$ is the mutual admittance between bus i and bus k. And noting that the net apparent power injection in bus k can be given by

$$S_k^* = P_k - jQ_k = V_k^* I_k \tag{3.2}$$

Where S_k, P_k, and Q_k are respectively the net apparent power, net active power, and net reactive power injected to bus k. Now we can write

$$P_k - jQ_k = V_k^* \sum_{n=1}^{N} Y_{k,n} V_n \tag{3.3}$$

and

$$P_k = \sum_{n=1}^{Nb} |Y_{k,n} V_k V_n| \cos(\theta_{k,n} - \delta_n - \delta_k) \text{ for } k = 1, \ldots Nb \tag{3.4}$$

$$Q_k = -\sum_{n=1}^{Nb} |Y_{k,n} V_k V_n| \sin(\theta_{k,n} - \delta_n - \delta_k) \text{ for } k = 1, \ldots Nb \tag{3.5}$$

The $2Nb$ equation in Eq. (3.4) and Eq. (3.5) taken together, are called *power flow equations* and they specify the exact relationship between all power flows and voltages

in the electric power system. These equations can be solved numerically by using various methods, for example, the Newton Method and the Gauss Seidel Method. Given the power injections at (Nb-1) buses and a reference voltage on a bus, a solution of the power flow equations is called the solution of *load flow problem.*

3.5 Relating Voltage Drops in the Secondary Circuits With Active Power Flow

Electric vehicles are connected to recharging sockets at the secondary circuit nodes as shown in Fig. 1.2. In this setting, secondary circuits can be most vulnerable to congestion and voltage drops due to the addition of EV loads and their uncoordinated recharging. Some of the reasons for this vulnerability of the secondary circuits are:

1. The distribution feeder typically has a tap changing transformer at the substation end and a shunt capacitor bank at a distribution feeder node. Both the tap changing transformer and the shunt capacitors can be used to regulate voltage on the distribution feeder. In contrast, secondary circuits typically have no voltage regulating equipment and a voltage drop in secondary circuit is reflected as a drop in utilisation voltage.

2. Distribution feeders and lateral lines can carry large currents. In contrast, the current carrying capacities of secondary circuits is often quite limited.

3. The cost of upgrading a distribution feeder is small when compared with the cost of upgrading all secondary circuits associated to it.

Because of the reasons stated above, in this chapter, we focus on the impacts of recharging EVs on voltage drops in the secondary circuits. In this context, we note that the voltages in a distribution system are affected by both active power P and reactive power Q. However, when considering recharging of EVs, our interest lies in controlling active power P and not the reactive power Q since a flow of reactive power Q cannot be stored as energy in the batteries of EVs.

To represent a secondary circuit we will use a simplified one line diagram shown in Fig. 3.1. In this figure the short vertical line is referred to as *bus*, which represents a
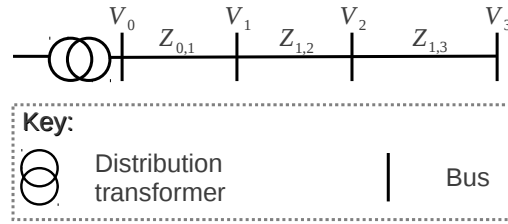
FIGURE 3.1: A simplified diagram for secondary circuit

secondary circuit node. The bus connected to the output of distribution transformer is numbered zero. Hence, the voltage at this bus is V_0, and is also referred to as V_s (source voltage). All buses are numbered and voltage on a bus is specified as V_j where j is the bus number. The impedance of the secondary circuit segment between secondary circuit nodes i and j is $Z_{i,j}$ and the segment is labelled as $Z_{i,j}$ in Fig. 3.1.

3.5.1 Remarks on the Impact of Recharging Schedules the Secondary Circuit Voltages

Consider two EVs connected to two recharging sockets in the same secondary circuit but at two different nodes. Let EV 1 be connected to a recharging socket at node 1 and EV 2 be connected to a recharging socket at node 2. We note that there are many possible ways in which EVs can be recharged. For example, in Fig. 3.2 (a) and (b), we show two possible ways of recharging the two EVs. Let $p_1(t)$ represent the recharging rate of EV 1 and $p_2(t)$ represent the recharging rate of EV2, then $\sum p_j(t)$ denotes the aggregate recharging rate of the two EVs. Let us represent the active power flow caused by recharging EV 1 as the height of blue rectangles in Fig. 3.2 (a) and (b) and the active power flow caused by recharging EV 2 as the height of the red rectangle 3.2 (a) and (b). Note that the area of blue rectangles in Fig. 3.2 (a) and (b) is the energy delivered to the battery of EV 1 and the area of the red rectangles 3.2 (a) and (b) is the energy delivered to the battery of EV2.

Let us refer to the schedule in Fig. 3.2 (a) as Schedule 1 and the schedule in Fig. 3.2 (b) as Schedule 2. We note that, Schedule 1 and Schedule 2 are equivalent in terms of meeting demand from EVs and both have load factor equal to 1. These schedules, however, are different in terms of their start and end times of recharge, and the their impacts on the voltage drops in the secondary circuit.
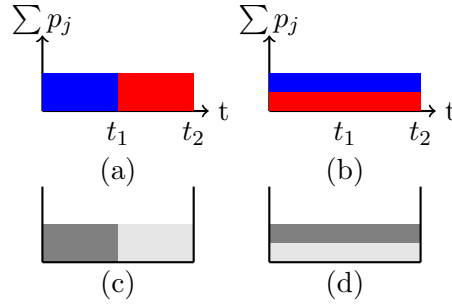
FIGURE 3.2: Two maximum load factor recharging schedules (a) Schedule 1 and (b) Schedule 2, and two containers in (c) and (d) each with two fluids

This very simple example illustrates an important aspect that the results presented in [72] have overlooked. We note that there may exist many load factor maximising recharging schedules when all loads are not at the same secondary circuit node. However, not all of these load factor maximising schedules are optimal with respect to the voltage drops in the secondary circuit. Therefore this is further evidence that the search for a recharging schedule that minimise voltage drop, cannot be formulated as a convex program based on maximising load factor.

In the remainder of this chapter, we present a novel approach for constructing recharging schedules that uses an analogy between the recharging schedule of different EVs connected to different secondary circuit nodes and a system of fluids with different fluids of different densities. Fig. 3.2 (c) and (d) show two containers each filled with two fluids with different densities. Lets assume that the density of white fluid is greater than the density of grey fluid. The configuration of fluids in Fig. 3.2 (d) corresponds to Schedule 2 in Fig. 3.2 (b), and is an equilibrium for the system of fluids under the only influence of gravity. While configuration of system of fluids in Fig. 3.2 (c) corresponds to Schedule 1 in Fig. 3.2 (a), and would be an unstable configuration under the same assumption of different density of the constituent fluids. If we use the behaviour and the equilibrium of the system of fluids in Fig. 3.2 (c) and (d) as an analogy to select a recharge scheduling policy for two EVs, then we would select Schedule 2 (stable configuration) and rejects Schedule 1 (unstable configuration).
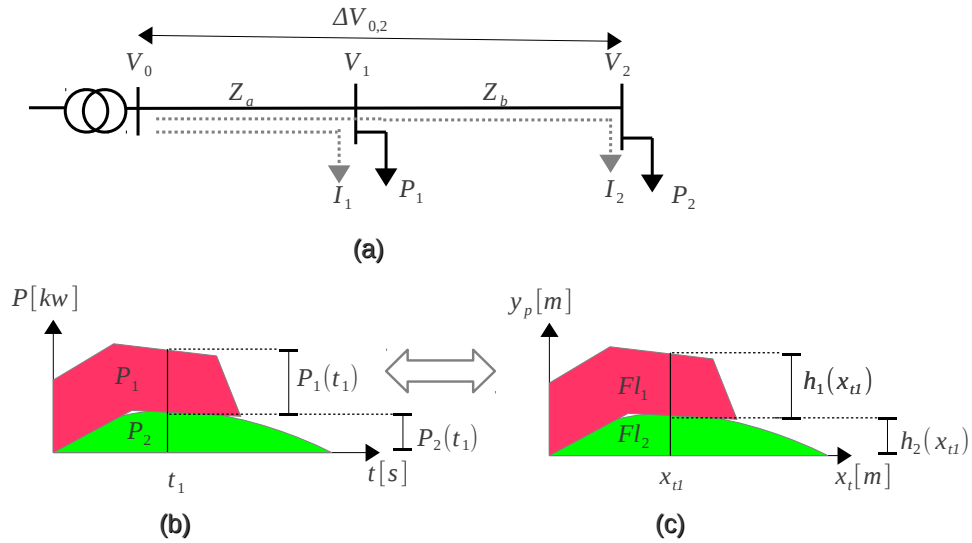
FIGURE 3.3: Analogy of recharging schedules to a system of fluids

3.5.2 Analogy of Recharging Schedule to a System of Fluids

Consider the one line diagram for a secondary circuit as shown in Fig. 3.3 (a). Let $\Delta V_{0,2}(t)$ be the voltage drop between bus 0 and bus 2 caused by the power flow corresponding to the recharging schedule shown in Fig. 3.3 (b). Then we can write [2]

$$\Delta V_{0,2}(t) = I_1(t)Z_a + I_2(t)(Z_a + Z_b) \tag{3.6}$$

Now consider Fig. 3.3 (c) which is a system of fluids with two fluids. Fluid 1 (Fl_1) has density ρ_a $[kg/m^3]$ and fluid 2 (Fl_2) has density $\rho_a + \rho_b$ $[kg/m^3]$. Then, from Fig. 3.3 (c), we notice that we can write the expression for pressure q $[N/m^2]$ in the system of fluids as

$$q(x_t, y_P)\big|_{y_P=0} = q(x_t, 0) = gh_1(x_t)\rho_a + gh_2(x_t)(\rho_a + \rho_b) \tag{3.7}$$

where $h_1(x_t)$ $[m]$ is the height of fluid 1, $h_2(x_t)$ $[m]$ is the height of fluid 2, g $[m/s^2]$ is the acceleration of gravity, and x_t $[m]$ and y_P $[m]$ are the two coordinate axis of the system of fluids.

---

[2]V, I, and Z are phasors

Assuming that the force of gravity is normal to coordinate axis x_t, we know from fluid statics that a necessary condition for equilibrium of fluid is given by Eq. (3.8).

$$\frac{\partial q(x_t, 0)}{\partial x_t} = 0 \qquad (3.8)$$

The condition in Eq. (3.8) could be interpreted to mean that at equilibrium the system of fluids will choose, from among all possible configurations, a configuration that minimises the maximum value of pressure $q(x_t, 0)$ subject to containment of its fluid within boundaries and subject to conservation of its volume. That is, there is no other configuration of system of fluids for which the maximum value of pressure $q(x_t, 0)$ is strictly less than the maximum value of pressure $q(x_t, 0)$ for the configuration at equilibrium.

By observing the structure of expressions in equations (3.7) and (3.6) and their similarity, it is our conjecture that if we a construct a recharging schedule from the equilibrium configuration of the system of fluids, then the maximum voltage drop $|\Delta V_{0,2}(t)|$ is a minimum among maximum voltage drops caused by all other schedules.

The analogue of Eq. (3.8) for voltage drops in the secondary circuit can be given as

$$\frac{\partial |\Delta V_{0,2}(t)|}{\partial t} = 0 \qquad (3.9)$$

In order to get more insight into the physical interpretation of Eq. (3.9), let us now reconsider the example studied in Section 3.5.1 and assume that both EVs arrive at corresponding recharging sockets at the same time and depart at the same time. It will be verified in Section 3.5.2.1 that Eq. (3.9) holds for all t for Schedule 2 except for arrival and departure times of EVs. It can also be verified that Eq. (3.9) does not hold for Schedule 1 in Fig. 3.2 (a) for at least one point in time t which is not the arrival or departure time of either of the EVs. Therefore, we can expect that

$$\max(|\Delta V_{0,2}(t)|_2) \leq \max(|\Delta V_{0,2}(t)|_1) \qquad (3.10)$$

where $\max(|\Delta V_{0,2}(t)|_k)$ is the maximum voltage drop between secondary circuit node 0 and secondary circuit node 2 for Schedule k. It will be verified in Section 3.5.2.1 that

this is indeed the case and that

$$\max |\Delta V_{0,2}(t)|_2 < \max |\Delta V_{0,2}(t)|_1 \tag{3.11}$$

3.5.2.1 Analytic Verification for Constant Current Loads

Let us consider the Schedule 1 and Schedule 2 as schedules for constant current loads. Without loss of generality, we can write the expressions for currents drawn and associated voltage drop $\Delta V_{0,2}$ due to both Schedule 1 and Schedule 2.

Schedule 1

$$I_1(t) = (u(t) - u(t - t_1)) \, e^{j\alpha_1} \tag{3.12}$$

$$I_2(t) = (u(t - t_1) - u(t - t_2)) \, e^{j\alpha_2} \tag{3.13}$$

where $u(t)$ is the unit step function.

$$u(t) = \begin{cases} 0 & \text{if } t < 0 \\ 1 & \text{otherwise} \end{cases} \tag{3.14}$$

hence,

$$\Delta V_{0,2}(t) = (u(t) - u(t - t_1)) \, Z_a e^{j\alpha_1} + (u(t - t_1) - u(t - t_2)) \, (Z_a + Z_b) \, e^{j\alpha_2} \tag{3.15}$$

Differentiating Eq. (3.15) with respect to t, we get:

$$\frac{\partial \Delta V_{0,2}(t)}{\partial t} = (\delta(t) - \delta(t - t_1)) \, Z_a e^{j\alpha_1} + (\delta(t - t_1) - \delta(t - t_2)) \, (Z_a + Z_b) \, e^{j\alpha_2} \tag{3.16}$$

Therefore, $\frac{\partial \Delta V_{0,2}(t)}{\partial t} = 0$ over the open intervals $(0, t_1)$ and (t_1, t_2), and $\frac{\partial \Delta V_{0,2}(t)}{\partial t} \neq 0$ for $t = t_1$.

To calculate the maximum value of $|\Delta V_{0,2}(t)|$, we calculate its value in both interval $(0, t_1)$ and interval (t_1, t_2) and choose the greater of the two.

$$|\Delta V_{0,2}(t)| = |Z_a| \text{ for } t \in (0, t_1) \tag{3.17}$$

and

$$|\Delta V_{0,2}(t)| = |Z_a + Z_b| \text{ for } t \in (t_1, t_2) \tag{3.18}$$

Let $Z_a = |Z_a| \angle \gamma_a$, and $Z_b = |Z_b| \angle \gamma_b$,

Since the resistance of secondary circuit cannot be negative or zero and secondary circuits are inductive,

$$|\gamma_a - \gamma_b| < \frac{\pi}{2} \text{ rad} \tag{3.19}$$

Now, for any two complex numbers Z_a and Z_b, we can write

$$|Z_a + Z_b|^2 = |Z_a|^2 + |Z_b|^2 + 2|Z_a||Z_b|\cos(\gamma_a - \gamma_b) \tag{3.20}$$

Using Eq. (3.19), from Eq. (3.20), we conclude,

$$|Z_a + Z_b| > |Z_a| \tag{3.21}$$

Therefore,

$$\max(|\Delta V_{0,2}(t)|_1) = |Z_a + Z_b| \tag{3.22}$$

Schedule 2

In Schedule 2, relative to Schedule 1, the magnitude of currents can be halved and duration of currents can be doubled.

Thus,

$$I_1(t) = \frac{1}{2}\left(u(t) - u(t - t_2)\right)e^{j\alpha_1} \tag{3.23}$$

$$I_2(t) = \frac{1}{2}\left(u(t) - u(t - t_2)\right)e^{j\alpha_2} \tag{3.24}$$

hence,

$$\Delta V_{0,2}(t) = \frac{1}{2}\left(u(t) - u(t - t_2)\right)Z_a e^{j\alpha_1} + \frac{1}{2}\left(u(t) - u(t - t_2)\right)\left(Z_a + Z_b\right)e^{j\alpha_2} \tag{3.25}$$

Differentiating Eq (3.25) with respect to t, we get:

$$\frac{\partial \Delta V_{0,2}(t)}{\partial t} = \frac{1}{2}\left(\delta(t) - \delta(t - t_2)\right)Z_a e^{j\alpha_1} + \frac{1}{2}\left(\delta(t) - \delta(t - t_2)\right)\left(Z_a + Z_b\right)e^{j\alpha_2} \tag{3.26}$$

Therefore, $\frac{\partial \Delta V_{0,2}(t)}{\partial t} = 0$ over the open interval $(0, t_2)$.

To calculate the maximum value of $|\Delta V_{0,2}(t)|$, we evaluate it at any time in the interval $(0, t_2)$.

$$\max\left(|\Delta V_{0,2}(t)|_2\right) = |\frac{1}{2}\left(Z_a e^{j\alpha_1}\right) + \frac{1}{2}\left(Z_a + Z_b\right)e^{j\alpha_2}| \tag{3.27}$$

Now using the triangular inequality, we can write

$$\max\left(|\Delta V_{0,2}(t)|_2\right) \leq |\frac{1}{2}\left(Z_a\right)| + |\frac{1}{2}\left(Z_a + Z_b\right)| \tag{3.28}$$

Now once again using Eq. (3.21)

$$\max\left(|\Delta V_{0,2}(t)|_2\right) < |\frac{1}{2}\left(Z_a + Z_b\right)| + |\frac{1}{2}\left(Z_a + Z_b\right)| \tag{3.29}$$

and hence,

$$\max\left(|\Delta V_{0,2}(t)|_2\right) < |\left(Z_a + Z_b\right)| \tag{3.30}$$

We note that the right hand side of Eq. (3.30) is the same as the right hand side of Eq. (3.22), therefore,

$$\max|\Delta V_{0,2}(t)|_2 < \max|\Delta V_{0,2}(t)|_1 \tag{3.31}$$

Hence, we have verified Eq. (3.11).

3.6 Energy Demand Particle System (EDPS) and Fluid Particle System (FPS)

We use particle systems to simulate the dynamics of system of fluids and to construct recharging rates from the system of fluids at equilibrium. For convenience in exposition, we need to distinguish between two particle systems: Energy Demand Particle System (EDPS) contains particles which represent energy demands; and Fluid Particle System (FPS) represents a collection of particles of matter. Where necessary, we will clearly specify which particle system we are referring to. However, the term *"particle system"* is used often without exact specification where the context of its use is sufficient to makes the meaning clear. The relationships of recharging schedules, EDPS, FPS and system of fluids is shown in Fig. 3.4.

3.6.1 Energy Demand Particles (EDPs)

An energy demand particle (EDP) is an imaginary particle that represents an active power flow of p_{edp} [kw] sustained over a time of t_{edp} [h] and hence delivers $p_{edp} * t_{edp}$ [kwh]
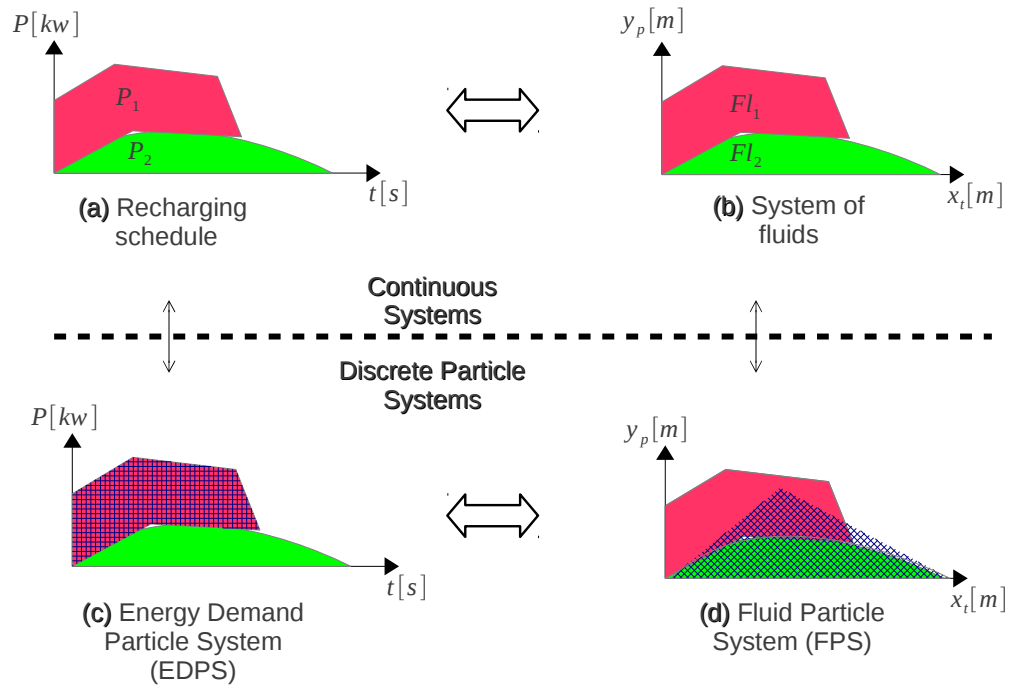
FIGURE 3.4: Relationships among (a) recharging schedules, (b) system of fluids, (c) Energy Demand Particle System (EDPS), and (d) Fluid Particle System (FPS)

of energy. Energy demand particles are used by recharging sockets to deliver energy to the batteries of EVs. Therefore, EDPs acts as a load of p_{edp} [kw] at a secondary circuit node.

Energy Demand Particles belong in a (t,P) plane, where t (h) represents time and P (kw) represents electric power. The t-coordinate of an EDP in (t,P) plane denotes the planned time at which the recharging socket will start delivering p_{edp} (kw) of electric power to the battery of the EV. When a recharging socket has started delivering electric power corresponding to an EDP and has not finished yet (because electric power flow must be sustained for t_{edp} (h)), we say that the EDP is *"active"* at the recharging socket. Several EDPs may be active at a recharging socket at a given time. The aggregate electric power delivered because of all active EDPs at a recharging socket is the recharging rate of the EV connected to the recharging socket. Each EDP is associated to a single secondary circuit node (to which the recharging socket using the EDP is connected) in the distribution system. When an EDP becomes active, a load of p_{edp} (kw) is added to the load at associated secondary circuit node.

A recharging socket may deactivate an EDP at any time and stop the flow of electric power corresponding to that EDP. This can happen if other controllers in the electric

power system send commands to recharging sockets requiring them to deactivate some EDPs. The EDPs can be deactivated as a reaction to events like, for example, the event of a drop in frequency, or the event of overload in the secondary circuit. An EDP is deactivated automatically if it has been active for t_{edp} (h) because the recharging socket would have delivered the energy for this EDP to the battery of EV.

3.6.2   Fluid Particles (FPs)

A fluid particle (FP) represents, in the context of this thesis, a very small volume of fluid that we consider as a particle. A FP has a mass which is a function of the density of fluid that FP represents. For each EDP in (t,P) plane, there corresponds a fluid particle (FP) in a (x_t,y_p) plane. The type and characteristics of the FP corresponding to a given EDP depends on the secondary circuit node to which EDP is associated.

Given an EDP at (t_1,P_1) associated with secondary circuit node j and EV k, we construct a FP at (x_{t1},y_{p1}) as follow:

$$x_{t1} = K_{t,x}t_1 \tag{3.32}$$

$$y_{p1} = K_{p,y}P_1 \tag{3.33}$$

where $K_{t,x}$ and $K_{p,y}$ are constants that are used to transform a point in (t, P) plane to a point in (x_t, y_p) plane. The mass assigned to a FP is calculated using Eq. (3.34)

$$m = K_{0,m} + K_{Z,m}|ZT_{j,0}| \tag{3.34}$$

where $K_{0,m}$ and $K_{Z,m}$ are constants, and $ZT_{j,0}$ is the sum of all impedances between secondary circuit node j and the distribution transformer. The choice of values of these constants will be discussed in Section 3.9.1.

In all the cases that we study, initial velocity and acceleration of FP are set to zero.

$$v(\tau = 0) = 0 \tag{3.35}$$

$$a(\tau = 0) = 0 \tag{3.36}$$
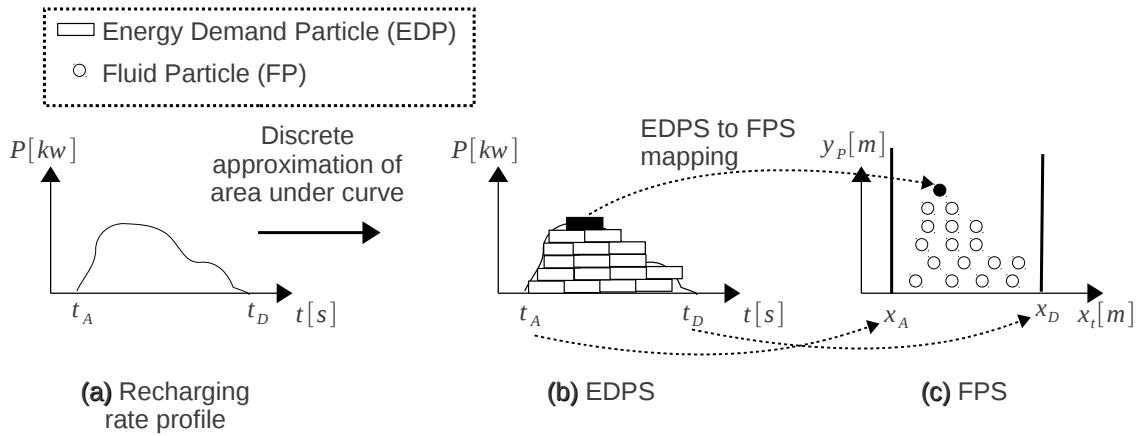
FIGURE 3.5: Constructing Energy Demand Particles (EDPs) and Fluid Particles (FPs) from a recharging rate profile

where τ is the simulation time in the FPS.

3.6.3 Constructing EDPS and FPS for a Recharging Schedule

Figure 3.5 shows the process of transforming a recharging rate profile into EDPs in the EDPS and then constructing FPs in the FPS. First note that the area under the curve of the recharging rate profile is approximated by the aggregate area of EDPs. Thus the energy delivered by the recharging rate profile and as the energy delivered by the collection of EDPs are equal up to the error of approximation. Where the error of approximation is the difference between the area under a recharging rate profile and the aggregate ares of all EDPs for the recharging rate profile.

For a recharging schedule, the EDPS and the corresponding FPS are constructed by constructing EDPs and corresponding FPs for each recharging rate profile in the recharging schedule.

3.6.4 Constructing a Recharging Rate Profile from EDPS

A recharging rate profile can be constructed once we have done the mapping of FPS into the EDPS. We can use the following steps to calculate recharging rate of $EV_{j,k}$ at time t_1 :

1. Count the number $N_{j,k}(t_1)$ of EDPs belonging to $EV_{j,k}$ that are active at time t_1

2. Obtain the recharging rate $p_{j,k}(t_1)$ of $EV_{j,k}$ by multiplying the number of the active EDPs and the electric power per EDP $p_{j,k}(t_1) = N_{j,k}(t_1) * p_{edp}$.

Here $EV_{j,k}$ is the *kth* EV connected to secondary circuit node j, $p_{j,k}$ is the recharging rate of $EV_{j,k}$, and p_{edp} is the electric power associated with an EDP.

3.6.5 Transformation of Constraints on Energy Demand to Constraints on EDPs and FPs

There are two constraints on the energy demand from a given EV that need to be considered.

The first constraint ensures that the energy delivered to the $EV_{j,k}$ is equal to the energy demand specified by the $EV_{j,k}$.

$$\int_{t\_A_{j,k}}^{t\_D_{j,k}} p_{j,k}(t)dt = ED_{j,k} \tag{3.37}$$

Where $t\_A_{j,k}$ is the arrival time of $EV_{j,k}$ at the recharging socket, $t\_D_{j,k}$ is the departure time of $EV_{j,k}$ from the recharging socket, and $ED_{j,k}$ is the energy demand specified by $EV_{j,k}$.

The second constraint ensures that electric power is scheduled only in a window of time for which EV is connected to a recharging socket.

$$p_{j,k}(t) = \begin{cases} 0 & \text{if } t < t\_A_{j,k} \\ \geq 0 & \text{if } t\_A_{j,k} < t < t\_D_{j,k} \\ 0 & \text{if } t\_D_{j,k} < t \end{cases} \tag{3.38}$$

These two constraints on energy demand, namely Eq. (3.38) and Eq. (3.37), can be translated into two properties of particle systems by observing:

1. The EDPs associated with $EV_{j,k}$ should not move outside the boundaries defined by $t\_A_{j,k}$ and $t\_D_{j,k}$. Thus FPs associated to these EDPs should not move outside the boundaries $x\_A_{j,k}$ and $x\_D_{j,k}$ that are obtained by transforming $t\_A_{j,k}$ and $t\_D_{j,k}$ using Eq. (3.32).

2. The EDPs associated with $EV_{j,k}$ are constructed such that their aggregate area in (t, P) plane equals $ED_{j,k}$. As each EDP has an area that does not change and it is not allowed for an EDP to be destroyed at any time, the aggregate area of EDPs will remain constant.

3.7   Proposed Approach

Now we use the particle systems introduced in the previous sections to build congestion avoiding recharging schedules for EVs. A two stage framework will be used to build recharging schedules. The output of Stage 1 is an intermediate schedule that, though feasible, can be improved with respect to the impact on voltages at the secondary circuit nodes. Stage 2 takes a initial feasible recharging schedule and modifies it such that: a) The EV energy demands are conserved, and b) The extreme values of voltage drops in the secondary circuits are reduced.

3.7.1   The Two Stage Framework

- **Stage 1: Feasible Solution**

  1. Obtain an initial recharging schedule by solving a problem with the objective of, for example, minimising load variance or maximising load factor [72]. With regards to voltages at the secondary circuit nodes, Stage 1 needs only to check the feasibility of the recharging schedule which can be done by solving a sequence of load flow problem where a load flow problem is solved for each time slot in the schedule.

- **Stage 2: Voltage Drop Reduction**

  1. Construct an EDPS from the initial recharging schedule and map it to a FPS.

  2. Allow the FPS to seek equilibrium. This step relies on a numerical method based on Smoothed Particle Hydrodynamics (SPH) to simulate the dynamics of FPs in FPS (Algorithm 1 in Section 3.8.3).

  3. Update positions of EDPs in EDPS in accordance with the positions of their corresponding FPs in FPS using equations (3.32) and (3.33).
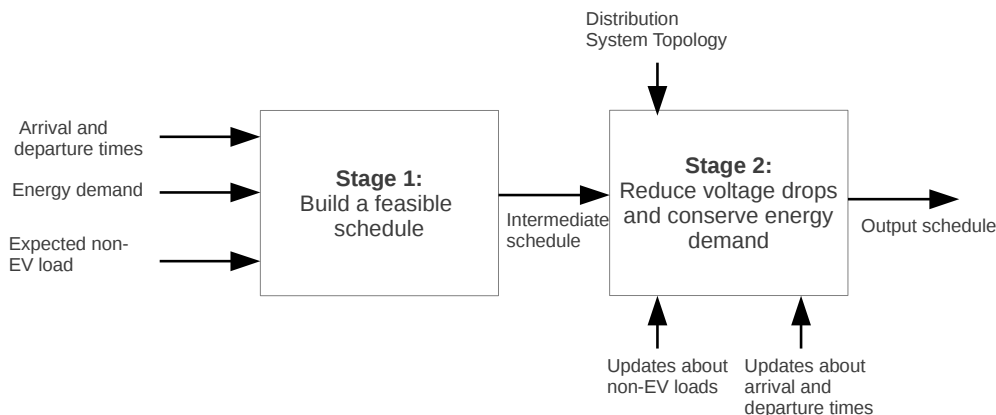
FIGURE 3.6: Two stage process for building congestion avoiding recharging schedules

    4. Build a recharging schedule corresponding to the EDPS.

A block diagram of the two stage process is shown in Fig. 3.6.

The Stage 1 can be performed off-line. We note that if Stage 1 builds a schedule that is optimal with respect to the voltage drops, then Stage 2 will not change it unless updates are received by Stage 2 that imply that the schedule built by Stage 1 is no longer optimal.

3.7.2   Remarks about Communication Requirements

Both stages of the two stage framework in Section 3.7.1 require communication of information between the recharging socket and the schedule building process. Therefore, particle system based scheduling will also require communication of information between recharging sockets and the FPS solver, which could be located near the distribution transformer. We note that, at the level of secondary circuits the population of loads as well as the distances from the physical locations of the loads to the distribution transformer are small. Therefore, Field Area Networks (FAN) can provide communication services [81]. Field Area Networks may use various technologies and media like cellular networks such as GSM and WIMAX, and wired networks like cable broadband and digital subscriber lines (DSL) [82].

3.8 Review of Smoothed Particle Hydrodynamics Method

In this section we describe the numerical method based on smoothed particle hydrodynamics (SPH) method that allows the FPS to pursue equilibrium. SPH method was first suggested by astrophysics researchers [83], and, since has also found many other applications in engineering and sciences [84]. We first review the Navier Stokes equations which model the dynamics of fluids. Then, we review the SPH method which can be used to solve a simplified version of the Navier Stokes equations [85][3].

The general form of the Navier Stokes equations is given by:

$$\rho \left(\frac{\partial \mathbf{v}}{\partial t} + \mathbf{v}.\nabla \mathbf{v} \right) = -\nabla q + \nabla.\mathbf{T} + \mathbf{f} \tag{3.39}$$

Where

$$\nabla = \frac{\partial}{\partial x}\hat{i} + \frac{\partial}{\partial y}\hat{j} + \frac{\partial}{\partial z}\hat{k} \tag{3.40}$$

and ρ $[kg/m^3]$ is the density of fluid, $\mathbf{v} = [v_x, v_y, v_z]^T$ $[m/s]$ is the velocity field, q $[N/m^2]$ is the pressure, $\mathbf{f} = [f_x, f_y, f_z]^T$ $[N/m^3]$ is the body force that acts throughout the volume of fluid, and $\mathbf{T}$ $[N/m^2]$ is the stress tensor.

For many applications, the exact behaviour of fluid may not be of interest and simplified version of the Navier Stokes equations can be used. Since we are interested in taking a system of fluids to an equilibrium position and the fluids are not necessarily real fluids, we can use a simplified version that is often used in simulation of fluids in computer graphics [85]:

$$\rho \left(\frac{\partial \mathbf{v}}{\partial t} \right) = -\nabla q + \mu \nabla^2 \mathbf{v} + \rho \mathbf{g} \tag{3.41}$$

Where $\mathbf{g}$ $[m/s^2]$ is the external force density field and μ $[Ns/m^2]$ is the viscosity of the fluid.

Before we review the application of SPH method to solve Eq. (3.41), we review some basics of SPH method as presented in [83].

---

[3]Both the Navier Stokes equations and the SPH method are very well known in the literature on fluid dynamics and astrophysics. Müller appears to be the first to have applied the SPH method for solving a simplified version the Navier Stokes equations in [85].

3.8.1   Background of the SPH Method

Let us consider a particle system in a space in $\mathbf{R}^3$, a scalar field $A(\mathbf{r})$, and the identity in Eq. (3.42), which is the sifting property of Dirac delta function.

$$A(\mathbf{r}) = \int A(\mathbf{r'})\delta(\mathbf{r} - \mathbf{r'})d\mathbf{r} \tag{3.42}$$

where $\mathbf{r} = [r_1, r_2, r_3]^T \in \mathbf{R}^3$, and $\delta(\mathbf{r})$ is the Dirac delta function with the following properties: $\delta(\mathbf{r}) = 0$ if $\mathbf{r} \neq \mathbf{0}$, and $\int_{-\infty}^{\infty} \delta(\mathbf{r})d\mathbf{r} = 1$.

Now, consider the following approximation for the scalar field $A(\mathbf{r})$.

$$A_s(\mathbf{r}) = \int A(\mathbf{r'})w(\mathbf{r} - \mathbf{r'}, h)d\mathbf{r'} \tag{3.43}$$

where $w(\mathbf{r} - \mathbf{r'}, h)$ is an interpolating kernel with the properties in Eq. (3.44) and Eq. (3.45) and h is called the smoothing length of kernel.

$$\int w(\mathbf{r}, h)d\mathbf{r} = 1 \tag{3.44}$$

and

$$\lim_{h \to 0} w(\mathbf{r}, h) = \delta(\mathbf{r}) \tag{3.45}$$

Let us now consider the density field (mass per unit volume) $\rho(\mathbf{r})$ in the considered space, and rewrite Eq. (3.43) as:

$$A_s(\mathbf{r}) = \int \frac{A(\mathbf{r'})}{\rho(\mathbf{r'})}w(\mathbf{r} - \mathbf{r'}, h)\rho(\mathbf{r'})d\mathbf{r'} \tag{3.46}$$

Let us now divide the volume which contains the particle system into N small elements with masses $m_1, m_2, \ldots, m_N$, then the contribution to the integral in Eq. (3.46) from an element k with mass m_k and centre of mass r_k can be given by:

$$\frac{A(\mathbf{r}_k)}{\rho(\mathbf{r}_k)}w(\mathbf{r} - \mathbf{r}_k, h)m_k \tag{3.47}$$

Hence, the scalar field $A(\mathbf{r})$ in Eq. (3.46) can be now written in terms of discrete particles masses as:

$$A_s(\mathbf{r}) = \sum_{k=1}^{N} \frac{A(\mathbf{r}_k)}{\rho(\mathbf{r}_k)} w(\mathbf{r} - \mathbf{r}_k, h) m_k \qquad (3.48)$$

Using Eq. (3.48) any field $A(\mathbf{r})$ can be approximated by analytic function $A_s(\mathbf{r})$ provided that $w(\mathbf{r}, h)$ is differentiable [83]. If this is the case, the density of particle system can be estimated as [83]:

$$\rho_s(\mathbf{r}) = \sum_{k=1}^{N} m_k w(\mathbf{r} - \mathbf{r}_k, h) \qquad (3.49)$$

The gradient and Laplacian of $A(\mathbf{r})$ can also be estimated using SPH as [85]:

$$\nabla A_s(\mathbf{r}) = \sum_{k=1}^{N} \frac{A(\mathbf{r}_k)}{\rho(\mathbf{r}_k)} \nabla w(\mathbf{r} - \mathbf{r}_k, h) m_k \qquad (3.50)$$

$$\nabla^2 A_s(\mathbf{r}) = \sum_{k=1}^{N} \frac{A(\mathbf{r}_k)}{\rho(\mathbf{r}_k)} \nabla^2 w(\mathbf{r} - \mathbf{r}_k, h) m_k \qquad (3.51)$$

Equation (3.50) is needed for computing pressure gradient and Eq. (3.51) is needed to calculate viscous forces based on the Laplacian of velocity field.

3.8.2 Kernel Selection for SPH

The choice of kernel $w(\mathbf{r}, h)$ plays an important role in accuracy and stability of SPH method [85]. In the work reported in this chapter and the next one we used two kernels: *i*) The $w_{poly6}(\mathbf{r}, h)$ suggested by Müller, Charypar and Gross [85], and *ii*) the $w_{spiky}(\mathbf{r}, h)$ suggested by Desburn [86]. The reasons for using two kernels are explained in the next paragraph.

$$w_{poly6}(\mathbf{r}, h) = \begin{cases} \frac{315}{64\pi h^9} \left(h^2 - r^2\right)^3 & \text{if } 0 \leq r \leq h \\ 0 & \text{otherwise} \end{cases} \qquad (3.52)$$
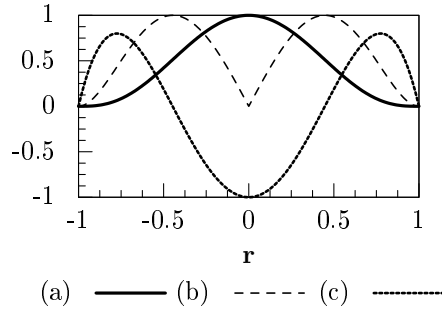
FIGURE 3.7: (a) w_{poly6}, (b) $|\nabla w_{poly6}|$ and (c) $\nabla^2 w_{poly6}$
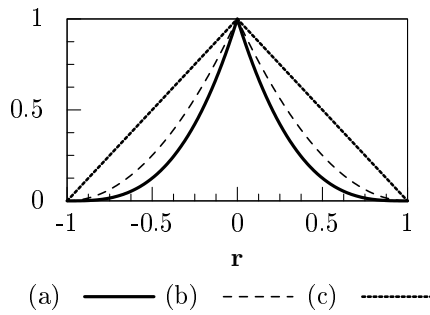
FIGURE 3.8: (a) w_{spiky}, (b) $|\nabla w_{spiky}|$ and (c) $\nabla^2 w_{spiky}$

$$w_{spiky}(\mathbf{r}, h) = \begin{cases} \frac{15}{\pi h^6} (h - r)^3 & \text{if } 0 \leq r \leq h \\ 0 & \text{otherwise} \end{cases} \qquad (3.53)$$

Where $r = \|\mathbf{r}\|_2 = \sqrt{r_1^2 + r_2^2 + r_3^2}$.

The kernel w_{poly6} uses r^2 and hence can reduce computational cost as it does not require the calculation of square roots [85]. This kernel has been used in Eq. (3.49) to estimate density due to its reduced computational cost. However, it might not be a good idea to use the same kernel for estimating pressure gradient [85], the reason becomes evident if we look at the information given in Fig. 3.7 and Fig. 3.8. Figure 3.7 shows a one dimensional kernel $w_{poly6}(\mathbf{r}, h)$ for $h = 1$, the magnitude of its gradient and its Laplacian, each normalised with respect to their maximum value. Figure 3.8 shows the same information but now for $w_{spiky}(\mathbf{r}, h)$. Note that the gradient of w_{poly6} approaches zero as $\mathbf{r} \to \mathbf{0}$. Therefore, when w_{poly6} is used to compute pressure gradient, if particles come too close to each other, the estimate of pressure gradient also tends to zero, which can cause the particle to form clusters [85]. For the problem under consideration cluster

formation in FPS is undesirable because it will translate into clusters of EDPs in EDPS. That is, a recharging schedule built using an EDPS with EDP clusters will cause sudden rise and fall in the flow of electric power from recharging sockets to the batteries of EVs. As a consequence of this, the energy demand will rise and fall periodically. In contrast, note that the gradient of w_{spiky} in Fig. 3.8 does not approach zero as $\mathbf{r} \to \mathbf{0}$. Therefore w_{spiky} is better suited for computing pressure gradients as it prevents clustering of particles [85].

Since we use a particle system in a plane and $\mathbf{r} = [r_1, \ r_2]^T \in \mathbf{R}^2$, we will use modified normalisation coefficients for the two kernels as suggested in [87].

$$
w_{poly6}(\mathbf{r}, h) = \begin{cases} \frac{4}{\pi h^8} \left(h^2 - r^2\right)^3 & \text{if } 0 \le r \le h \\ 0 & \text{otherwise} \end{cases} \tag{3.54}
$$

$$
w_{spiky}(\mathbf{r}, h) = \begin{cases} \frac{10}{\pi h^5} \left(h - r\right)^3 & \text{if } 0 \le r \le h \\ 0 & \text{otherwise} \end{cases} \tag{3.55}
$$

3.8.3 Algorithm of the SPH Method

The SPH method applied to the FPS is described using the pseudo code in Algorithm 1 where the following notation is used for properties of FPs and FPS:

- m = mass of a FP,

- $\mathbf{x} = [x_t, \ y_p]^T$ = the position of FP in FPS,

- $\mathbf{x}.x_t = x_t$ coordinate of $\mathbf{x}$,

- $\mathbf{v} = [v_x, v_y]^T$ = velocity of FP,

- $\mathbf{a} = [a_x, a_y]^T$ = net acceleration of FP,

- $\mathbf{a}_{i,q}$ = acceleration of FP i due to the force generated by pressure gradient,

- $\mathbf{a}_{i,e}$ = the acceleration of FP i due to the external force field, which typically is the force of gravitation,

- ρ = density of FPS,

- ρ_r = rest density of FPS,

- q = pressure in the FPS,

- τ = FPS simulation time,

- $\Delta\tau$ = a time step in FPS simulation time,

- x_l = minimum value of x_t coordinate of a FP defines the left boundary that the FP cannot cross,

- x_r = maximum value of x_t coordinate of a FP defines the right boundary that the FP cannot cross,

- K and L are constants, which are non-negative.

For properties of an FP shown here without subscript, a subscript i in the pseudo code in Algorithm 1 signifies that we are referring to the *ith* FP.

3.9   Evaluation of Proposed Approach

In this section we will present examples that highlight various aspects of the proposed approach. For these examples, we choose a 4 node secondary circuit as shown in Fig. 3.1 (on page 79), where $Z_{0,1} = Z_{1,1} = Z_{2.3} = 0.05 + j0.05$ (p.u), $V_s = 1\angle 0$ (p.u), $V_{base} = 415$ (V), S_{base}=1 (MVA). Three EVs are considered and EV i, for i= 1,2,3 is connected to a recharging socket at secondary circuit node i.

The EDPs are constructed using $p_{edp} = 1$ (kw) and $t_{edp} = 300$ (s) (which correspond to 5 minutes), and FPs are constructed using $K_{t,x} = 12$ (mm/h) (each hour in time maps to 12 (mm) in the system of fluids), $y_{P1} = 1$ (mm/kw), $K_{0,m} = 0.5$ (mg), and $K_{Z,m} = 0.707$ (mg/p.u).

For SPH method in Algorithm 1, the values of parameters used are: $h = 2$ (mm), $\rho_r = 0.2$ (mg/mm^3), $\Delta\tau = 0.1$ (s), $K = 1(mm^2/s^2)$, and $L = 0.2 \times m_i$ (mm/s^2) where m_i is the mass of FP for which L is to be used in Algorithm 1. These values have been used for SPH method throughout this thesis.

Algorithm 1 Pseudo code for SPH method

loop
   $\tau \leftarrow \tau + \Delta\tau$
   for each FP i in the FPS **do**
      //find current neighbours
      $\mathcal{N}_i = \{j|\ \|\mathbf{x_j} - \mathbf{x_i}\| \leq h\}$
      //calculate density at FP i's position
      $\rho_i \leftarrow \sum_{j \in \mathcal{N}_i} m_j w_{poly6}(\mathbf{x_j} - \mathbf{x_i}, h)$
      //calculate pressure at FP i's position
      $q_i \leftarrow K(\rho - \rho_r)$
   end for
   for each FP i in the FPS **do**
      //calculate acceleration of FP due to pressure
      //acceleration of FP is calculated directly without calculating force
      $\mathbf{a}_{i,q} \leftarrow -\sum_{j \in \mathcal{N}_i} \left(\frac{q_i}{\rho_i^2} + \frac{q_j}{\rho_j^2}\right) w_{spiky}(\mathbf{x_j} - \mathbf{x_i}, h)\frac{\mathbf{x_j} - \mathbf{x_i}}{\|\mathbf{x_j} - \mathbf{x_i}\|}$
      //calculate acceleration of FP due to external force field (gravitational force)
      $\mathbf{a}_{i,e} \leftarrow [0, -L]^T$
      //calculate net acceleration of FP i
      $\mathbf{a}_i \leftarrow \mathbf{a}_{i,q} + \mathbf{a}_{i,e}$
   end for
   for each FP i in the FPS **do**
      //calculate velocity of particle i using Euler integration method.
      $\mathbf{v}_i \leftarrow \mathbf{v}_i + \mathbf{a}_i \Delta\tau$
      //calculate position of particle i
      $\mathbf{x}_i \leftarrow \mathbf{x}_i + \mathbf{v}_i \Delta\tau$
      //check boundaries for this FP. If FP has moved outside its allowed boundaries,
      assign it boundary a position.
      if $\mathbf{x_i}.x_t < x_{l,i}$ **then**
         $\mathbf{x_i}.x_t \leftarrow x_{l,i}$
      end if
      if $\mathbf{x_i}.x_t > x_{r,i}$ **then**
         $\mathbf{x_i}.x_t \leftarrow x_{r,i}$
      end if
   end for
end loop

3.9.1 Remarks About Parameter Values

Without loss of generality, for mapping an EPDS to FPS using equations (3.32) and (3.32), we have selected the two systems such that an hour in time in EDPS is mapped to a few millimetres in FPS, and a kilowatt in EDPS is mapped a millimetre in FPS. This choice is not strictly necessary, but it is convenient to deal with a volume of few cubic centimetres of fluids when using particle based methods.

In the selection of $K_{0,m}$ and $K_{Z,m}$ introduced in Eq. 3.34, we map the typical range of

per unit values of impedance in a distribution system to a typical range of densities of real fluids. Although it is not necessary to choose densities of simulated fluids to be close to the densities of real fluids, it is a convenient choice because literature on simulation of real fluids can be easily consulted.

In respect to the parameters for the SPH method, we have noticed that the FPS simulation time step $\Delta\tau$ is the only critical parameter to be considered carefully. Other parameters values also affect the dynamics of simulated fluid, but our aim is to reach equilibrium and not necessarily to accurately simulate the exact dynamics of a real fluid. Therefore, as long as the choice of parameters does not make the method unstable, we can choose convenient values. The value of $\Delta\tau$ is a choice that can make the method unstable especially by introducing oscillations at the boundaries of the FPS. Such effects of instability can be avoided by selecting a small value of $\Delta\tau$ and decreasing it until stability is achieved. Using smaller values of $\Delta\tau$ can decrease the simulation speed, therefore, $\Delta\tau$ should not be selected too small unless the choice is necessary to ensure stability.

3.9.2 Performance Metric

In order to compare previously published approaches and the proposed one, we suggest a performance metric that measures the voltage deviation in a secondary circuit for given recharging schedule.

$$J = \int_0^T \left(10 \max_i (|V_s| - |V_i|)\right)^6 dt \tag{3.56}$$

where T is the total time for which recharging schedule is constructed, V_s is the voltage at the output of distribution transformer, V_i is the voltage at secondary circuit node i, and $\max_i(|V_s| - |V_i|)$ is the maximum of all voltage drops that can occur between the distribution transformers and a the secondary circuit node. Hence, J in Eq. (3.56) grows very rapidly if $\max_i(|V_s| - |V_i|)$ exceeds 0.1 p.u or 10 % of voltage at the output of the distribution transformer, thus smaller values of J indicate better schedules.

In all the examples studied here, the performance of schedule is measured by computing the performance metric J in Eq. (3.57).

$$J = \int_0^T \left(10(|Vs(t)| - |V_3(t)|)\right)^6 dt \tag{3.57}$$

where V_3 is selected because it is the lowest of all voltages on secondary circuit nodes.

3.9.3 Example 1 : Using a Maximum Load Factor Schedule as Initial Schedule

In this example, we use an initial feasible recharging schedule (the output of Stage 1) with the maximum load factor [72]. Since there can be multiple maximum load factor schedules, this particular initial schedule recharges the three EVs one after the other as if the EVs are in a queue and are served one by one. We then improve the initial schedule using Stage 2 of the proposed approach and compare the improved schedule to the initial schedule.

Figure 3.9 shows the FPS corresponding to the initial schedule. This figure show the positions of FPs for the three EVs at the start of FPS simulation time $\tau = \tau_0$. The FPs are plotted in the (x_t, y_p) plane. Figure 3.10 shows an intermediate configuration of the FPS at FPS simulation time $\tau = \tau_0 + \tau_1$. The FPS has been reconfigured but has not reached equilibrium. Figure 3.11 shows a configurations of FPS at FPS simulation time $\tau = \tau_0 + \tau_1 + \tau_2$. At this stage the rate of change in FPS is very low and FPS has reached near equilibrium. The recharging schedule corresponding to this configuration of the FPS can be considered the final recharging schedule.

In this example and the next, the time is divided into time slots. Each time slot has a duration of 5 minutes. The total time duration of schedule is assumed to be 3 hours and 20 minutes which results in 40 time slots. In this example, all 3 EVs under consideration will remain connected to their respective recharging sockets for 40 time slots.

In relation to the same example, Fig. 3.12 shows the initial and the final recharging rates of each of the EVs in each of the time slots. These recharging rates have been calculated from the corresponding configurations of FPS. It is evident from Fig. 3.12 that initial recharging schedule will recharge EVs one by one in a sequence, whereas, as shown in Fig. 3.13, the final recharging schedule will recharge EVs simultaneously but with reduced recharging rate for each of the EVs.
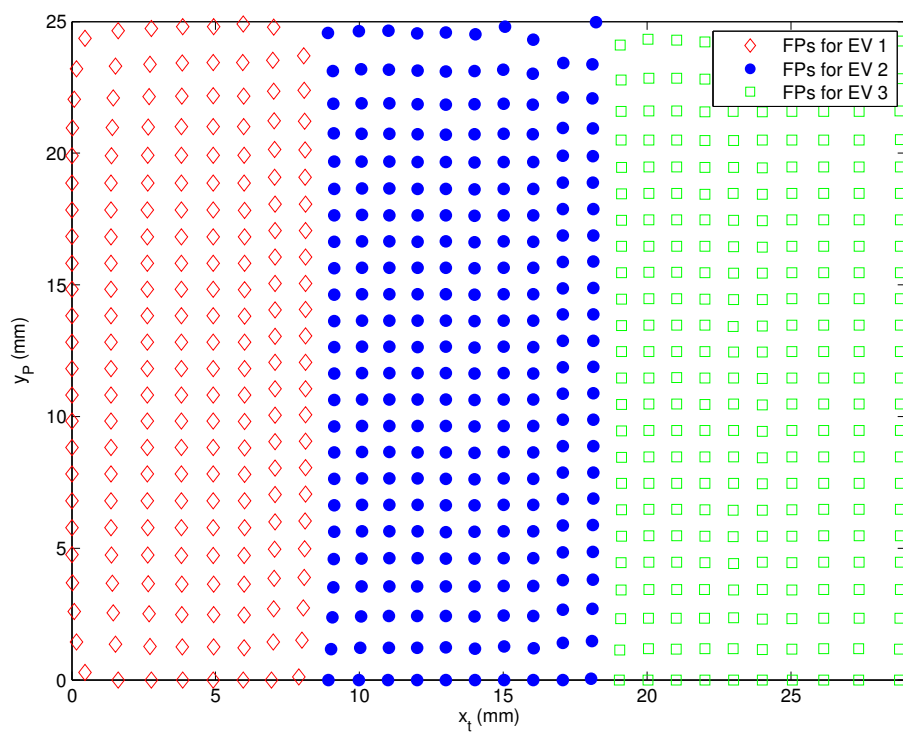
FIGURE 3.9: The FPS for the initial recharging schedule for three EVs
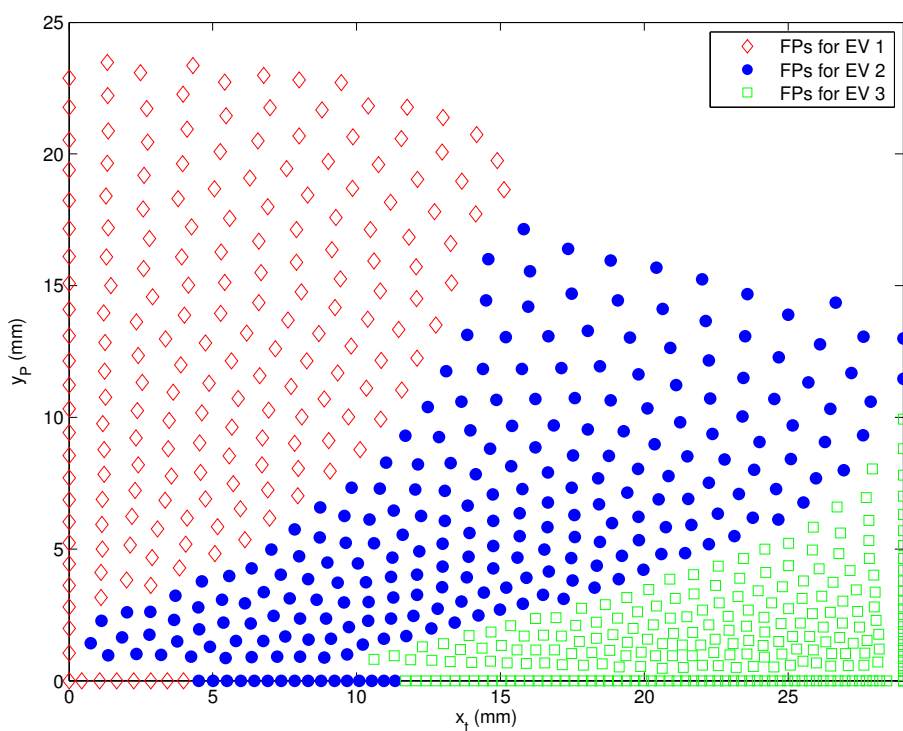
FIGURE 3.10: The FPS seeking equilibrium
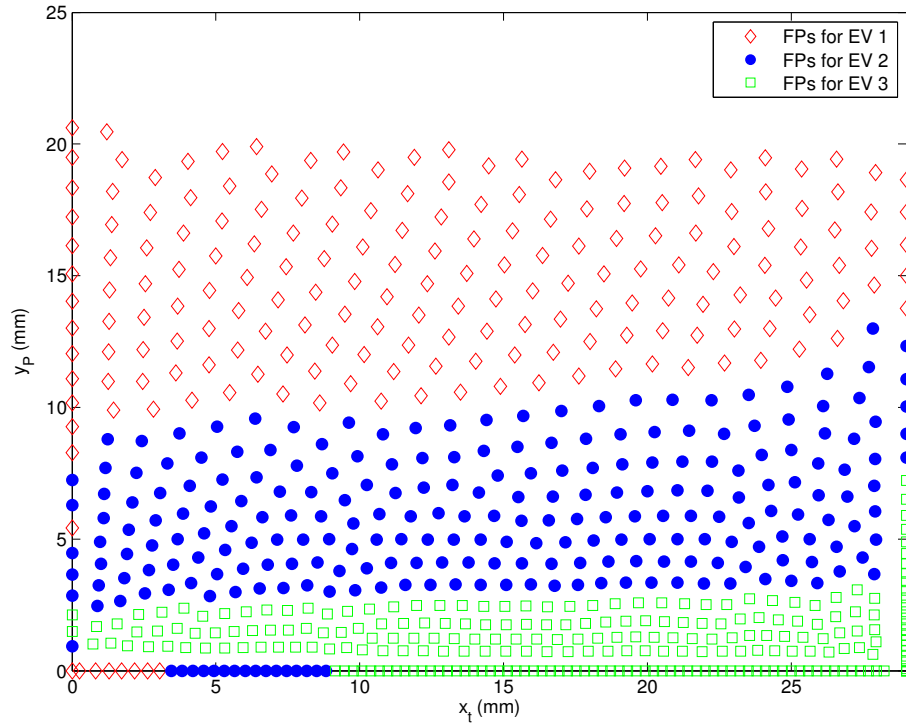
FIGURE 3.11: The FPS near equilibrium
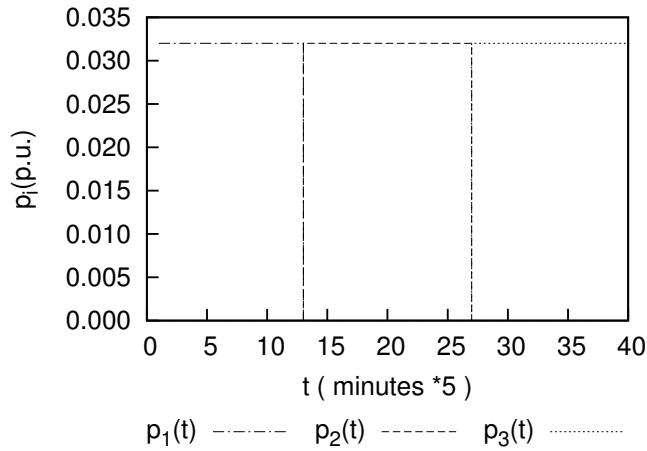
FIGURE 3.12: Recharging rates for the initial recharging schedule

In Fig. 3.14 the voltage at secondary circuit node 3 for the initial and the final recharging schedules are shown. It can be seen from the Fig. 3.14 that final recharging schedule reduces the maximum voltage drop between the distribution transformer and the secondary circuit node 3, especially in time slots 26 to 40.

Figures 3.15 and 3.16 show the mean and standard deviation of voltage drops at all of the three secondary circuit nodes. It can see seen that the mean of voltage drops is similar for
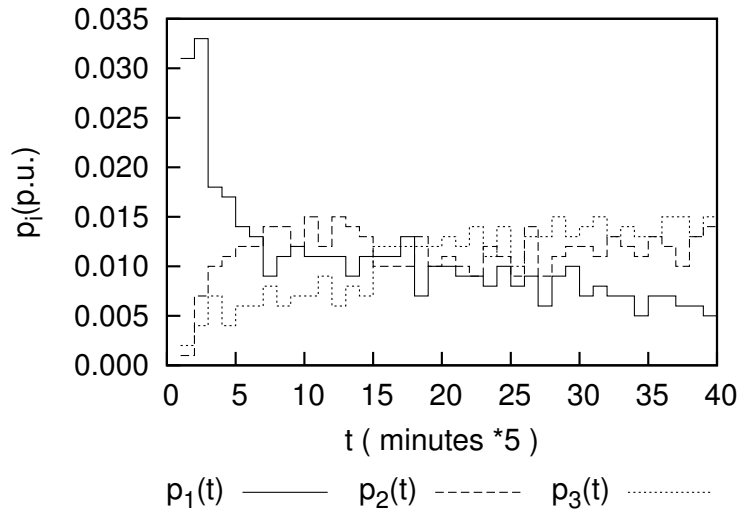
FIGURE 3.13: Recharging rates for the final recharging schedule
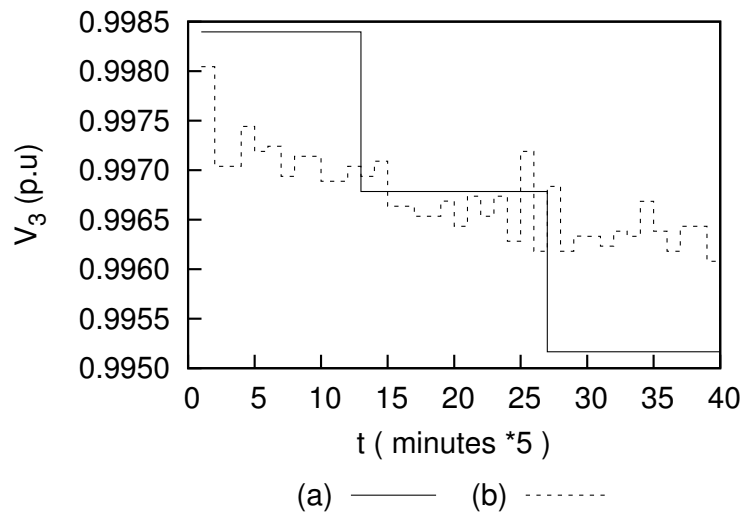
FIGURE 3.14: $|V_3(t)|$ for (a) Initial schedule, (b) schedule constructed from near equilibrium particle system

both schedules, however the standard deviation of voltage drops is significantly smaller for the final schedule as compared to the initial schedule.

Finally, in Fig. 3.17, the performance metric introduced by Eq. (3.57) for the initial J_i and the final enhanced recharging schedules J_e are shown. Using this performance metric, since $(J_e = 5.4 \times 10^{-7}) < (J_i = 15.3 \times 10^{-7})$, the final recharging schedule will perform better as compared to the initial recharging schedule.
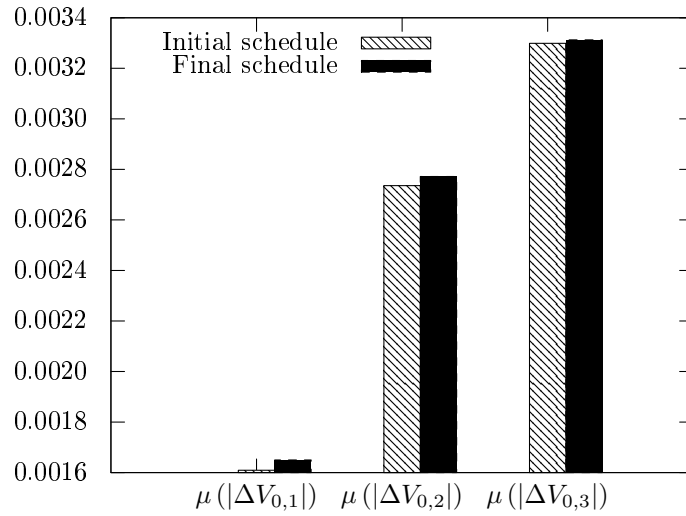
FIGURE 3.15: Mean of voltage drops
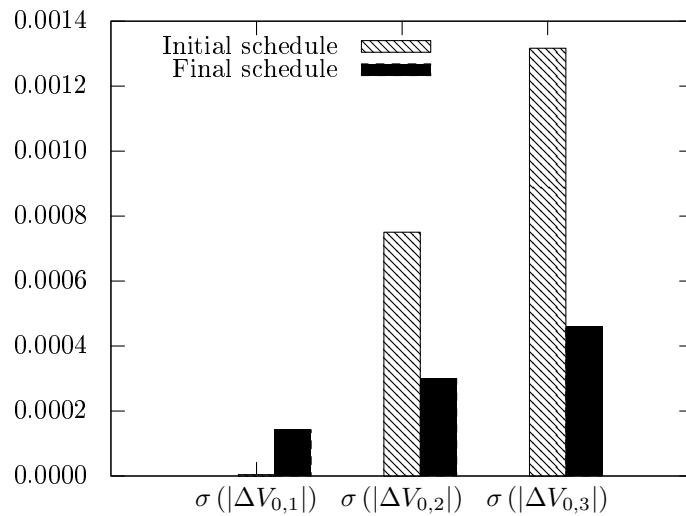
FIGURE 3.16: Standard deviation of voltage drops

3.9.4 Example 2: Using Admission Control Based Schedule as Initial Schedule

In this example an initial recharging schedule used that is based on admission control as suggested in [73]. The initial schedule is a feasible schedule that tries to recharge each EV as soon as possible after the EV connects to a recharging socket. Stage 2 of the proposed approach is then used to enhance the initial schedule. In this example, all EVs connect to their respective recharging sockets at $t = 0$. EV 2 needs to depart after 2 hours and 45 minutes, hence EV 2 will depart at the end of time slot 33. EV 1 and
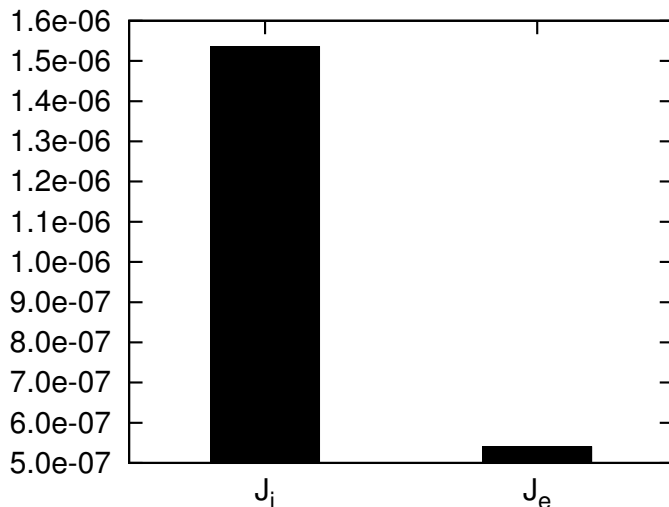
FIGURE 3.17: $J_i = J$ for the initial schedule [72] and $J_e = J$ for the final recharging schedule
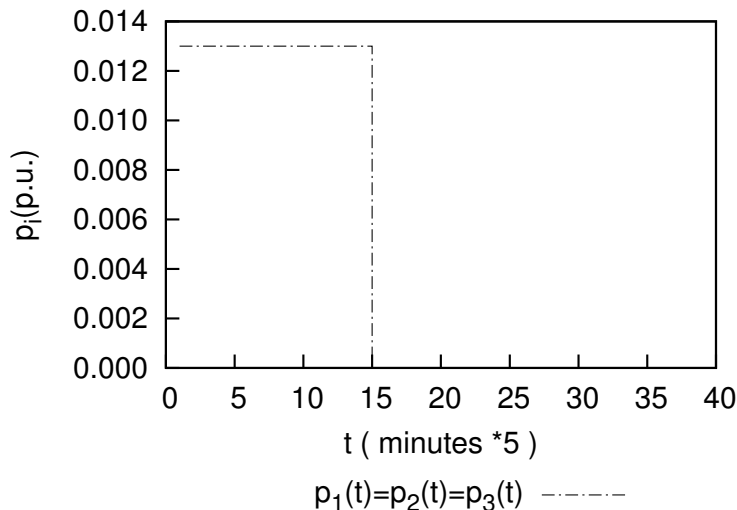
FIGURE 3.18: Recharging rates for the initial recharging schedule

EV 3 will remain connected for approximately 3 hours and 20 minutes, hence they will remain connected for 40 time slots.

In Fig. 3.18, the recharging rates are shown for the initial schedule and in Fig. 3.19 the recharging rates for the final schedule are shown. The initial recharging schedule, which is based on admission control scheme, starts recharging all EVs at time slots 0 and finishes recharging at time slot 15. In the case of this example, it is feasible to recharge all EVs at maximum recharging rates simultaneously. Therefore, initial recharging schedule will recharge all 3 EVs simultaneously at the maximum recharging rates. In contrast, the final recharging schedule will recharge EVs simultaneously but with reduced recharging
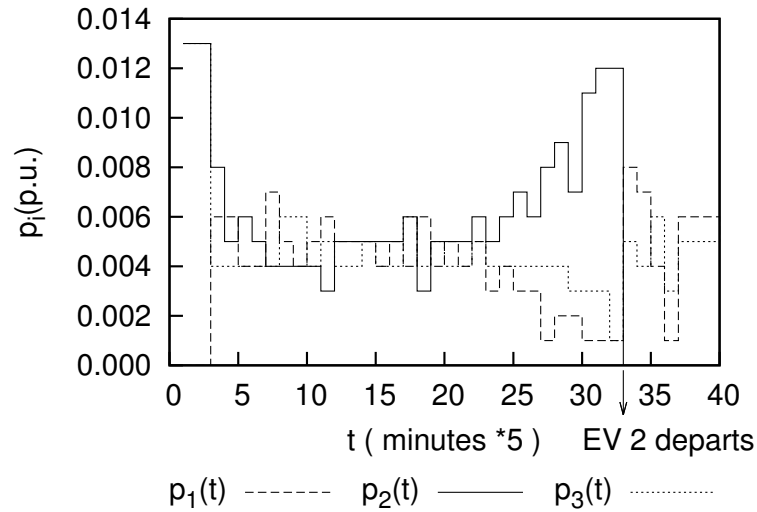
FIGURE 3.19: Recharging rates for the final recharging schedule
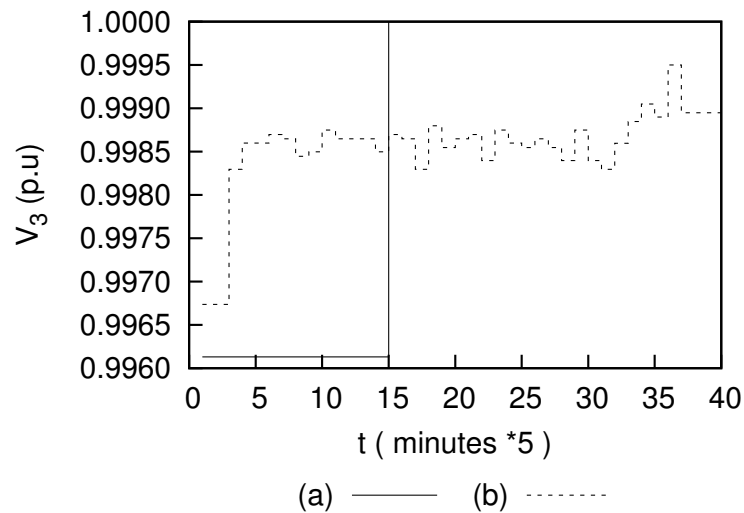
FIGURE 3.20: $|V_3(t)|$ for (a) the initial recharging schedule and (b) the final recharging schedule

rates. It will finish recharging EV 1 at time slot 33, and it will finish recharging EV 2 and EV 3 at the end of time slot 40.

In Fig. 3.20, the voltage at secondary circuit node 3 for the initial and the final recharging schedules are shown. The initial recharging schedule causes $|V_3| = 0.9961$ (p.u) (a 0.4% voltage drop in the secondary circuit) in the time slots 1 to 15 and then it causes voltage drops in time slots 15 to 40. In contrast, the final recharging schedule causes an almost uniform $|V_3| \approx 0.9985$ (p.u) (approximately 0.15% voltage drop in secondary circuit) in almost all time slots.
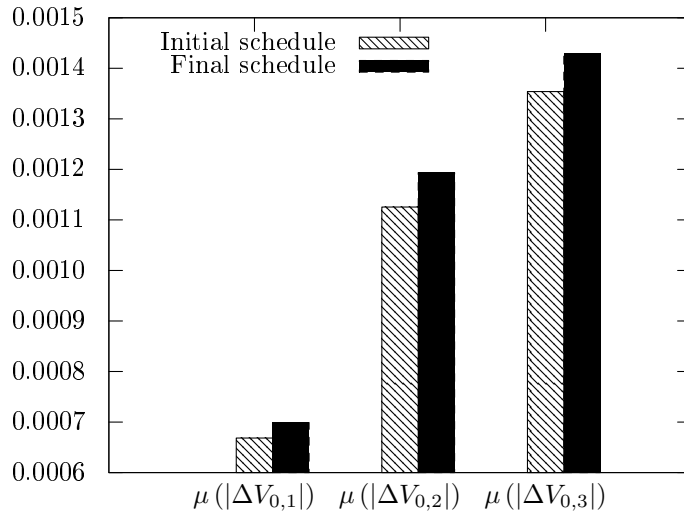
FIGURE 3.21: Mean of voltage drops
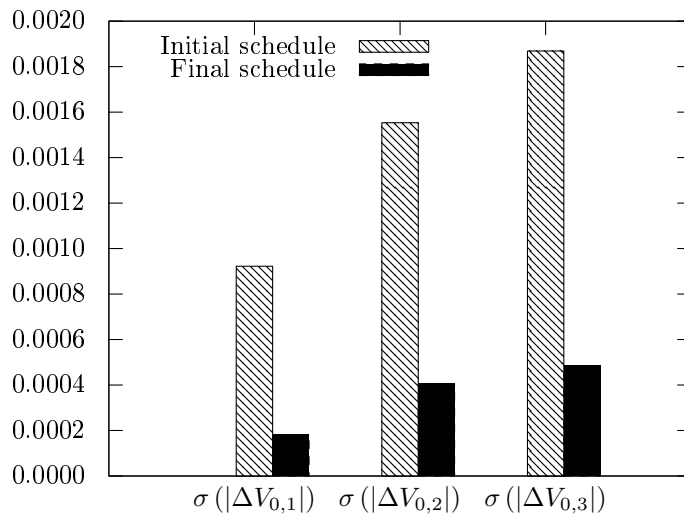
FIGURE 3.22: Standard deviation of voltage drops

Figures 3.21 and 3.22 show the mean and standard deviation of voltage drops at all three secondary circuit nodes. In this case too, the mean of voltage drops is similar for both schedules with the final schedule having slightly larger mean voltage drops. The standard deviation of voltage drops is significantly smaller for the final schedule as compared to the initial schedule.

Finally, Fig. 3.23 shows the performance of the initial and the final enhanced recharging schedules as measured in terms of the performance metric in Eq. (3.57). Since $J_e < J_i$, the final schedule performs better as compared to the initial recharging schedule.
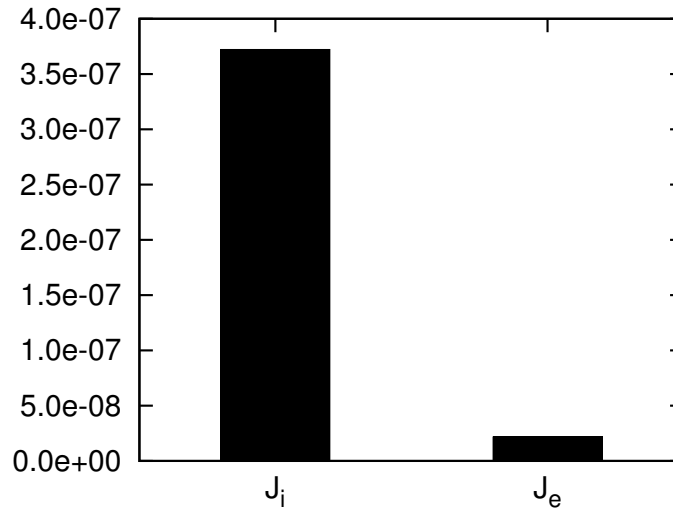
FIGURE 3.23: $J_i = J$ for the initial recharging schedule [73] and $J_e = J$ for the final recharging schedule

3.10 Final Remarks

In this chapter we present an approach that modifies any feasible initial recharging schedule to a schedule for coordinated recharging of EVs that reduces the voltage drops between the distribution transformer and the secondary circuit nodes. Recharging schedules are constructed in two stages. The first stage does not need to consider the impacts on voltages and, for example, builds an initial schedule for maximising load factor. The second stage uses information about topology of the distribution system and enhances the initial schedule with respect to impact on voltages at secondary circuit nodes. Two example cases are presented, which show that the presented approach can construct recharging schedules which have only small impacts on the voltages when compared with other approaches in state of the art literature.

In the next chapter, we will show that the approach proposed in this chapter can dynamically reschedule EV loads in order to accommodate unexpected events (for example, unexpected load arrival or drop in frequency), and can reduce the potential impacts of such unexpected events on the voltage in the distribution system.

Chapter 4

Voltage Congestion Aware Frequency Control Service

4.1 Introduction

Let us consider again the scenario of several EVs recharging at the same time in a secondary circuit. If this schedule has been obtained using the approach in Chapter 3, the EVs will be recharged according to the recharging schedule that avoids voltage congestion. If the schedule is planned at the start of the planning period and never changed during its execution, then energy delivered to each EV will satisfy its energy needs when the schedule has been executed. However, in a real world environment, power system operations is continuously facing episodes of uncertainty, and the outset and evolution of such episodes is very difficult to predict in advance. For example, there can be sudden changes in the amount of generated electric power because of an unexpected event like a failure of a large generator. Therefore, even though a planned schedule will recharge EVs and reduce the impact of recharging on secondary circuit, it might not appropriately respond to spontaneously changing conditions in the electric power system. EVs have the intrinsic capacity to store energy and ability to defer energy demand. Therefore, in this chapter we investigate a particle system based mechanism that aims at reducing the impact of uncertainties on operation of electric power system by exploiting the intrinsic elastic nature of the energy demand of the majority of parked EVs.

In this chapter, we will use the particle system introduced in Chapter 3 to dynamically rebuild the recharging schedule if unexpected events occur. The aim is to devise the capability of an on-line schedule building process so that it can respond to unexpected changes as well as deliver the right amount of energy to EVs before a given deadline, and avoid congesting the secondary circuits.

4.2   Motivation

If an EV recharging policy only considers the frequency regulation (either with the aim of improving security of the electric power system with respect to a sudden loss of an electric generator, or with the aim of neutralising the impact of uncertain availability of renewable sources) without considering the voltage profile in the underlying distribution system, then congestion may arise in the distribution system. In contrast, if EVs are recharged considering only the impacts on utilisation voltages with the aim of improving adequacy of the secondary circuits in the distribution system (but without allowing EVs to take part in demand response (DR) schemes), then their ability to defer demand and their ability to store energy will not be optimised in respect to security of electric power system. Therefore, to investigate scheduling algorithms that will allow EVs to recharge and improve both security and adequacy of electric power system is worth further research.

4.3   Organisation of the Chapter

In Section 4.4, background information about frequency control services is presented. In Section 4.5, the context of the problem addressed in this chapter is established by reviewing research that has used dynamic demand control to provide frequency control services. In Section 4.6 and 4.7 the particle system mechanism, introduced in Chapter 3, is extended to non-elastic loads that spontaneously become active in the system. These loads are different from EV loads because their service cannot be delayed. In Section 4.8, the extended particle system mechanism is used to dynamically add virtual non-elastic load that emulate a portion of primary frequency control reserve. In Section 4.8 another alternative approach is presented that uses the shift in boundary of the particle system to emulate a portion of primary frequency control reserve. In Section 4.9 it is shown

that the usage of the mechanisms of virtual non-elastic load or shifting the boundary of the particle system, can avoid congestion in the distribution system by re-planning the recharging schedule.

4.4   Frequency Control Services

Frequency control services are generally used at three levels. The exact definitions and properties of frequency control services vary from country to country [88]. To enable a consistent use of terms, we use the terms as specified in Table 4.1. These terms can be mapped to country specific terms, where applicable, using Table. II on page 351 of [88].

	Primary	**Secondary**	**Tertiary**
Purpose	Arrest frequency fall or rise	Restoration of: (a) frequency; (b) tie line flow.	(a) Transmission congestion management (b) economic operation
Control	Local automatic	Centralised automatic	Centralised manual
Deployment start	0–30 (s)	10–30 (m)	60 (m)

TABLE 4.1: Frequency control services

Some of the terms of used in Table 4.1 are now explained in the following text. When a frequency control service is activated, the delivery of active power will start with a delay that depends on the type of the frequency control service. *Deployment start* is the time interval of maximum size between the time of activation of service and the time of delivery of active power by the service. *Transmission congestion management* refers to the process of regulating the power flow over transmission lines, which is needed if, during the restoration of frequency by primary and secondary frequency control service, some transmission lines had been overloaded. *Economic operation* refers to the use of most cost effective generators to supply a given load within the operational constraints.

Primary frequency control service is provided by on-line generators that are fitted with speed governors and are normally not operating at full capacity. These generators can

change their output power within a few seconds. These are essential to maintain stability of electric power system as they prevent large sudden changes in frequency. The secondary frequency control service is provided by generators that can either increases their output or can be brought on-line within a few minutes [88]. Secondary frequency control service is used to relieve primary frequency control reserves, and to restore the frequency and the interchange of electric power with other systems to their target values [89, 90]. The tertiary frequency control is generally provided to manage congestion in the transmission system, ensure economic operation and to bring the flow on tie lines to their target values if the secondary frequency control failed to do so.

The usage of frequency control services varies from country to country. For example, the U.K. electric power transmission system is not interconnected to other systems. Therefore, the electric power system in the U.K. is subject to larger and faster frequency deviations as compared to the frequency deviations of interconnected systems like the mainland Europe and North America [88]. In the U.K. secondary frequency control service is not used. Instead primary frequency control service is provided by using three types of frequency control reserves. The *primary reserves* and *secondary reserves* are used as positive frequency control reserve, and *high frequency reserve* is used as negative frequency control reserve.

In the U.K., the electric power transmission system is managed by the National Grid, which has an obligation to control frequency within the limits specified in the *Electricity Supply Regulations*. The frequency must remain within a band of $\pm 1\%$ of the nominal frequency of 50 Hz under normal circumstances.

In this chapter, we use the particle system approach presented in Chapter 3 to recharge EVs, but now with a composite objectives of improving both; i) the security of electric power system with respect to unexpected changes in generated electric power, and ii) the adequacy of secondary circuits in the distribution system. We will use EVs to provide a share of the primary frequency control reserve by delaying the recharging of those EVs that can accept delayed recharging. Those EVs will eventually start recharging again after the secondary frequency control service start delivering electric power. The underlying aim is to reduce the impact of disturbance caused by, for example, a sudden failure of an on-line electric generator.

4.5 Dynamic Demand Response and Frequency Control

Traditionally frequency control services have been provided by electric power generators. However, there has been increasing interest recently in allowing demand side participation in frequency control services, and several interesting dynamic demand response schemes have been proposed and used in case studies. In this section, we are going to review the existing literature on dynamic demand response schemes for frequency control which are most relevant to the work presented in this chapter.

One way to provide dynamic demand response is to switch off certain devices belonging to a certain class of loads (for example, air conditioners and refrigerators) and switch them on at a later time. Such schemes can be implemented in a completely distributed manner but often result in so called *rebound effect* [91] where the loads that try to *catch up* (for example, to restore the temperature that rose when the refrigerator was switched off) create a peak in demand when they are switched on again. Some works also refer to *rebound effect* as *recovery peak.*

In [92] refrigerators are used to respond to changes in frequency where the target temperature inside refrigerator compartment varies as a linear function of frequency deviation. Refrigerators use a hysteresis switch to turn on and off periodically in order to keep the temperature inside the compartment within a specified range. If a drop in frequency is detected by the refrigerators, their target temperature is increased. Therefore, a certain percentage of population of refrigerators temporarily switch off. The electric generators that provide secondary frequency control service then restore the frequency to its nominal value. After the frequency has been restored, the refrigerator's target temperature is reduced and refrigerators start turning on at roughly the same time resulting in a rebound effect. We note that, in this case, there might be several such refrigerators using the same secondary circuit or distribution feeder, hence the rebound effect might also introduce congestion in the distribution system and increase the voltage drops on distribution feeders and secondary circuits. To the best of our knowledge, the problem of potential congestion in the distribution system caused by the rebound effect has not be explicitly addressed in the existing literature, although the mitigation of rebound effect through de-synchronisation of switching times and diversification of duty cycles of

periodic switching has been highlighted as a valuable research topic that is worth further investigation. Centralised and distributed de-synchronisation schemes have been recently investigated [93].

In [93], the authors have used a stochastic approach to manage the switching on/off of refrigerator loads using a Markov chain with the state transition probabilities linked to the frequency deviation of the electric power system. The work in [93] aims at de-synchronising the duty cycle of refrigerators and thus reduce the periodic oscillations and the recovery peak. This approach can manage the recovery peak or the *rebound effect* in a completely distributed manner with no communication requirement. We will refer to this approach as *"stochastic de-synchronisation"*.

An important difference between the work presented in this chapter and the existing published work on frequency control using dynamic demand, is that our proposed mechanism is not a frequency controller in the strict sense, but provides a fixed amount of reduction in load in response to a drop in frequency. The proposed mechanism provides a share of frequency control reserve, that could be interpreted as a complementary frequency control service. Such service can be provided by simply switching off some loads for a short duration of time (for example, 15 minutes) and switching them on again. However, our contribution here is not simply to switch off recharging sockets and switch them on again, but also to re-plan the recharging schedule so that the recharging does not cause a recovery peak; and that the secondary circuits do not get congested after the frequency has been restored and recharging sockets are switched on again. In addition, compared to stochastic de-synchronisation, our proposed approach also aims at managing the recovery peak as well but from the different perspective of reducing congestion in the distribution system. Furthermore, we also note that the population of loads may be small for a given secondary circuit and hence, if there are 50 refrigerators that use the same distribution transformer and the same secondary circuit, then a randomisation of their duty cycles may not produce sufficient de-synchronisation. In contrast, even a small population of EVs can be scheduled for recharging without causing congestion by using the particle system. The particle system, however, requires communication between recharging sockets and the FPS solver.
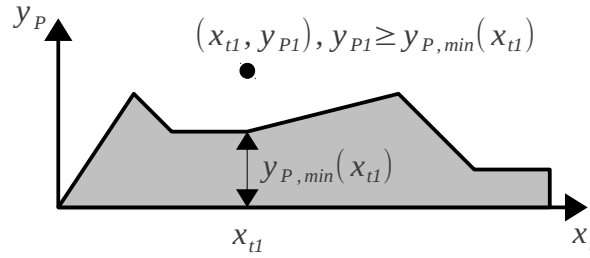
FIGURE 4.1: Non-elastic load as terrain of FPS

4.6 Representing Non-Elastic Loads in Particle System

In this section, the FPS introduced in Chapter 3 is extended to non-elastic loads. We can represent non-elastic loads in the FPS in two ways: 1) Terrain of the FPS, and 2) Particle groups in the FPS.

4.6.1 Terrain of the Particle System

The aggregate non-elastic load can be incorporated as the terrain over which the FPs of the FPS move. Let $P_{NE}(t)$ be the aggregate non-elastic load in a secondary circuit. We can define a terrain $y_{P,min}(x_t)$ where x_t in FPS and t in EDPS are related by Eq. (3.32) (on page 88) and y_P in FPS and P_{NE} in EDPS are related by Eq. (3.33). The terrain is defined such that for each FP in FPS with position (x_{t1}, y_{P1}), it must be the case that $y_{P1} > y_{P,min}(x_{t1})$ as shown in Fig. 4.1.

This representation is not used in this thesis, but can be used in the future work. Using aggregate non-elastic load as terrain of FPS simplifies the handling of non-elastic load and its impact on the scheduling of EVs for recharging. However, it is not possible to distinguish between the non-elastic loads at different secondary circuit nodes because all non-elastic load is aggregated without considering the secondary circuit nodes to which non-elastic loads are connected. The recharging schedules might be improved if we could distinguish between the non-elastic loads that are at different secondary circuit nodes. In the following section an alternative representation that can model non-elastic load on different secondary circuit nodes is presented.
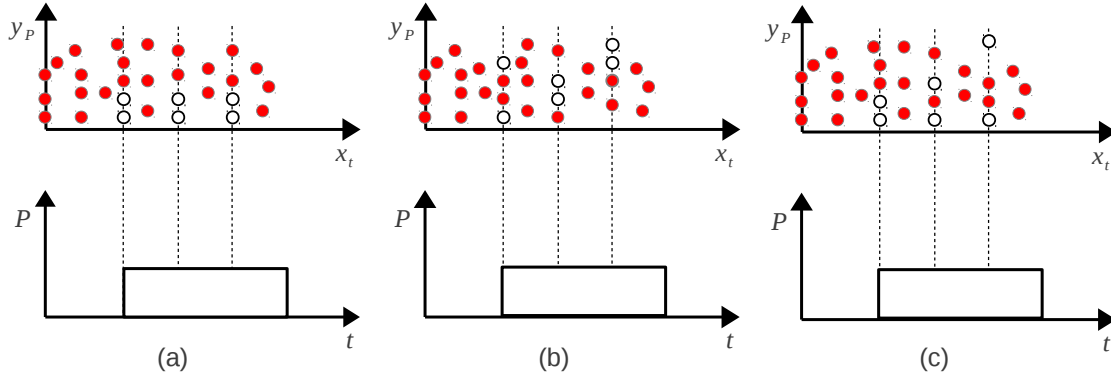
FIGURE 4.2: Various FP groups (shown as white), whose corresponding EDPs construct
the same non-elastic load profile

4.6.2 Particle Groups in the Particle System

Figure 4.2 shows an alternative way of representing non-elastic loads in FPS. In this case
a non-elastic load can be seen as a group of FPs in the FPS. Each FP in the group has
a fixed x-coordinate that does not change during the application of the SPH method to
the FPS. In the SPH algorithm these FPs are handled as ordinary FPs but with $v_x = 0$,
where $v = [v_x, v_y]^T$ is the velocity of the FP in the FPS. This representation is used in
the remainder of this chapter.

When compared with the representation of non-elastic loads as in Section 4.6.1, this
representation has the advantage that the properties assigned to the FPs can distinguish
between non-elastic loads on different secondary circuit nodes, and hence, could be
used to build schedules that reduce voltage drops in the secondary circuits. We note,
however, that a FPS (FPS 1) that represents all non-elastic loads as groups of FPs might
not always produce recharging schedules that are better than the recharging schedule
produced by another FPS (FPS 2) that represents all non-elastic loads as terrain of the
FPS. This is due to the fact that, in the FPS 1, FPs for non-elastic loads have very
restricted mobility and can block the FPs for elastic loads.

The two representations of non-elastic loads introduced in this section and Section 4.6.1
are not mutually exclusive. We could use a combination of the two representations
where the non-elastic loads (whose switching times can be predicted with high degree
of certainty) are represented as terrain of FPS and some (especially those that arrive
unexpectedly) are represented as groups of FPs in the FPS.
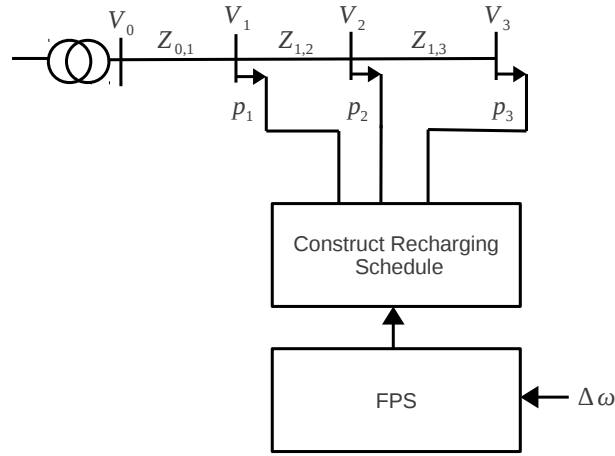
FIGURE 4.3: Particle system and its relation to a secondary circuit

4.7 Dynamically Adding Non-elastic Loads

Using either of the representations discussed in Section 4.6, non-elastic loads can be added dynamically to FPS and the FPS will respond by reconfiguring itself. Using the reconfigured FPS, a modified recharging schedule can be dynamically built such that the modified schedule will include the consideration for the newly added non-elastic load.

In this section, we use an example that shows the dynamic addition of non-elastic loads that are represented by particle groups in the FPS.

4.7.1 Example 1: Non-elastic Loads in the Particle System

Consider a secondary circuit shown in Fig. 4.3 which has the same parameters values as in Chapter 3: $Z_{0,1} = Z_{1,2} = Z_{2,3} = 0.05 + j0.05$ and $V_0 = 1\angle 0$. Furthermore, let us consider 3 EVs: EV 1, EV 2, and EV 3. Let EV i be connected to secondary circuit node i for $i = 1, 2, 3$.

As explained in Chapter 3, a two stage process is used to build a recharging schedule for the three EVs. In the Stage 2 of the two stage process, a FPS is used in the same manner as discussed in Chapter 3. To explain the impact of dynamically adding a non-elastic load, a sequence of four figures (4.4–4.7) is presented here. This sequence of four figures shows the FPS at four different times in the FPS simulation time τ (at, say, τ_0, $\tau_0 + \Delta\tau_1$, $\tau_0 + \sum_{i=1}^{2} \Delta\tau_i$, and $\tau_0 + \sum_{i=1}^{3} \Delta\tau_i$). At any time τ_k in the FPS simulation time τ, the configuration of the FPS can be used to construct a feasible recharging rescheduled plan,

which can be executed in real world time t. Thus, the sequence of four figures shows the variable of interest if four recharging plans are constructed (at four instances of the FPS simulation time τ), and executed in the real world time t.

Let us consider Fig. 4.4, which is composed of three sub-figures. Fig. 4.4 (A) shows the FPS used for this example. The positions of FPs in the FPS are plotted in the (x_t, y_p) plane. Three types of FPs can be seen in the FPS, where each type of FPs is associated to one of the EVs. For example, the FPs plotted as red diamond shapes are FPs that belong to EV 1. The key for associating each type of FP to an EV is given in the caption of Fig. 4.4. Figure 4.4 (B) shows the recharging rate profiles for all EVs under consideration, which are constructed[1] from the FPS in Fig. 4.4 (A).

Note that x_t in Fig. 4.4 (A) and t in Fig. 4.4 (B) are related by the expression in Eq. (3.32), that is, $x_t = K_{t,x}t$. Here $K_{t,x}$ is 1/300 (mm/s) or 12 (mm/h), which is the same as in Section 3.9. Figure 4.4 (C) shows the voltage $|V_3|$ at the secondary circuit node 3. Note that the recharging rate profile of EV i, for $i = 1, 2, 3$, acts as a load on secondary circuit node i. We calculate the voltage by first calculating the loads at all secondary circuit nodes and then solving a load flow problem using forward backward sweep method (see, for example, [94]).[2]

The key to the Fig. 4.4 will be also used for subsequent figures 4.5–4.7.

We use an initial recharging schedule which is a maximum load factor schedule [72] built by Stage 1 of the two stage process described in Section 3.7.1 in Chapter 3. Figure 4.4 corresponds to the initial schedule at $\tau = \tau_0$ (s). It can be seen from Fig. 4.4 (A) that the FPs for EV 1 are positioned between $x_t = 0$ (mm) and $x_t = 10$ (mm), which means that EV 1 will recharge in the time interval between $t = 0$ (s) to $t = 3000$ (s). Similarly, EV 2 and EV 3 will recharge in the time intervals $t \in [3000,\ 6000]$ (s) and $t \in [6000,\ 9000]$ (s) respectively. Figure 4.4 (B) shows the recharging rates for $\tau = \tau_0$. Figure 4.4 (C) shows the voltage V_3 at secondary circuit node 3 at $\tau = \tau_0$, which shows that when EV 3 is recharging in the interval $t \in [6000,\ 9000]$ (s), it causes large voltage drops between secondary circuit node 0 and secondary circuit node 3 (approximately 0.75% of $|V_0|$) as compared to the same voltage drops when only EV 1 is recharging in the interval $t \in [0,\ 3000]$ (s) (approximately 0.25% of the $|V_0|$).

---

[1]The construction process has been discussed in Section 3.6.4 (on page 89) and Section 3.6.2.

[2]methods for solving the load flow problem are very mature and well known, and therefore are not repeated in the thesis
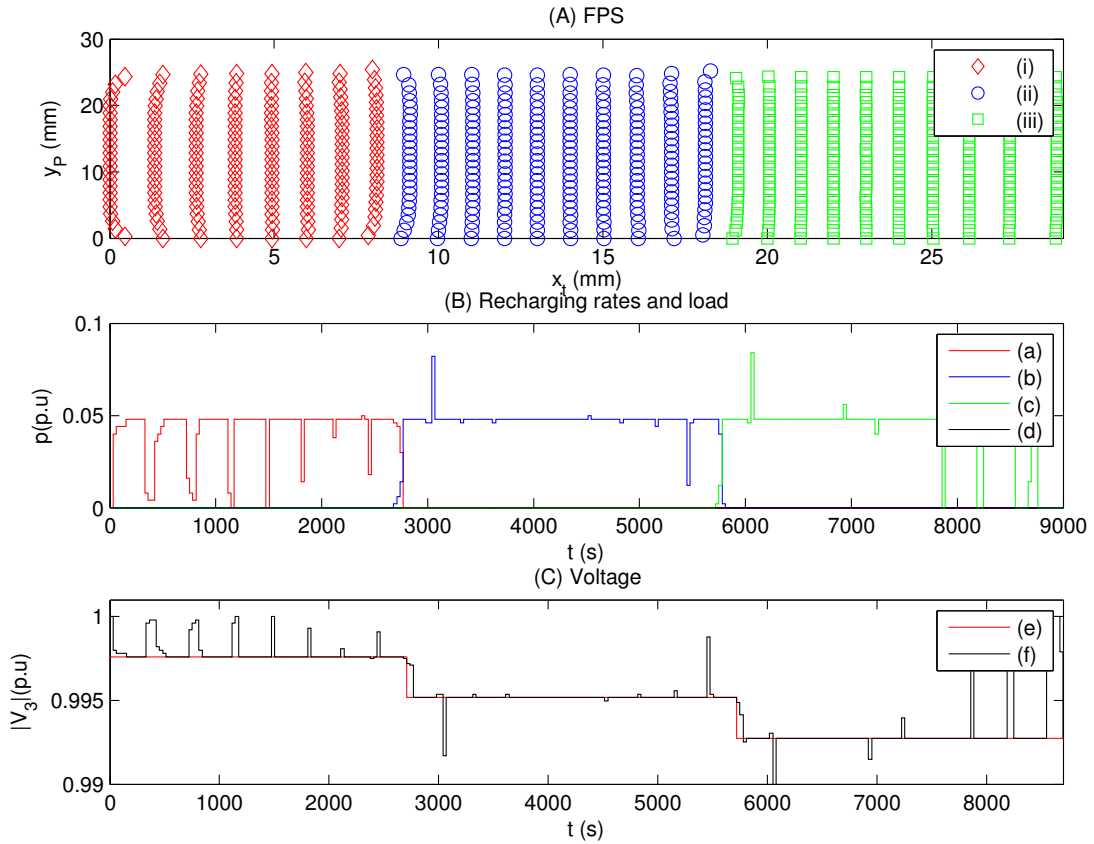
FIGURE 4.4: A snapshot at the start of FPS simulation time $\tau = \tau_0$
Key: (A): FPS where (i) FPs for EV 1, (ii) FPs for EV 2, and (iii) FPs for EV 3 (iv)
FPs for non-elastic load;
(B): Recharging rates and non-elastic load where (a) $p_1(t)$, (b) $p_2(t)$, (c) $p_3(t)$, and (d)
electric power consumed by non-elastic load; and
(C): voltage at secondary circuit node 3 for (e) initial schedule, and (f) final schedule

Starting from the FPS in Fig. 4.4 (A) at the FPS simulation time $\tau = \tau_0 = 0$, if we apply the SPH method in Algorithm 1 in Chapter 3 to the FPS and increment τ by $\Delta\tau$, the SPH method will start to reconfigure the FPS. Figure 4.5 (A) shows a snapshot of the FPs at a later time in the FPS simulation time, say at $\tau = \tau_0 + \Delta\tau_1$ after the SPH method has been applied to the FPS. Figure 4.5 (B) shows that EVs are no longer recharged one after the another, but their recharging time windows start overlapping. Figure 4.5 (B) shows that the voltage drop in $|V_3|$ is starting to reduce in time window $t \in [6000,\ 9000]$ (s) where the largest voltage drops had been at $\tau = \tau_0$.

Figure 4.6 (A) shows a snapshot of the FPs at the FPS simulation time $\tau = \tau_0 + \sum_{i=1}^{2} \Delta\tau_i$. At this time τ new FPs are being introduced into the FPS, which represent a non-elastic load (as explained in Section 4.6.2) at the secondary circuit node 1. The newly added
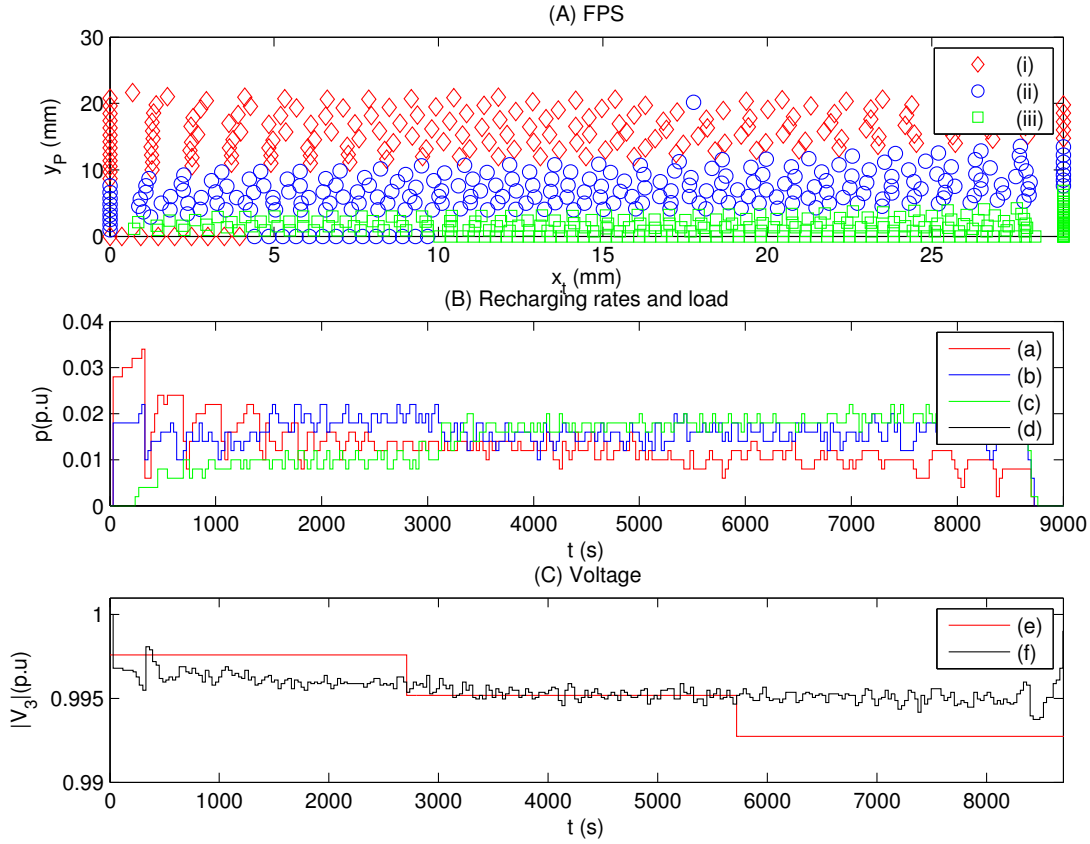
FIGURE 4.5: A snapshot where FPS is in the process of seeking equilibrium

FPs are assigned the same mass as that assigned to all FPs that represent load at the secondary circuit node 1.

Figure 4.7 (A) shows a snapshot of the FPs at simulation time $\tau = \tau_0 + \sum_{i=1}^{3} \Delta\tau_i$. Note from Fig. 4.7 (B) that the recharging rate of EV 1 ((a) in the figure) has been reduced to nearly zero in the time interval $t = [2700, 5700]$ (s). This is the time interval where the non-elastic load has been switched on. We note that EV 1 and non-elastic load are connected to the same secondary circuit node, hence the SPH method has reconfigured the FPS such that the EV 1 produces a load that is complementary to the non-elastic load. Figure 4.7 (C) shows that at this FPS simulation time τ, the extremes values of voltage drop are lower than the extreme values of voltage drop for the initial schedule, even though the initial schedule is supplying less load.

This sequence of figures shows the ability of the proposed approach to dynamically absorb non-elastic loads and avoid voltage congestion.
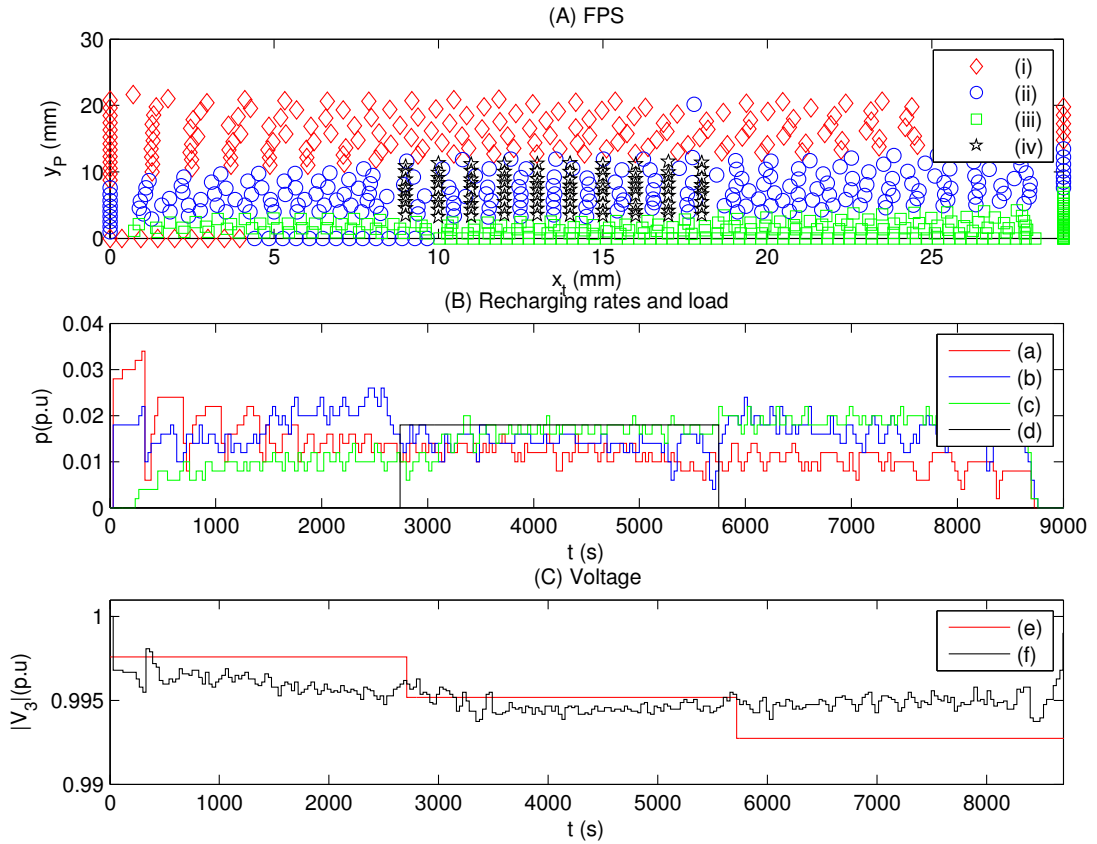
FIGURE 4.6: A snapshot where FPs for a non-elastic load, which is introduced at secondary circuit node 1, are added to FPS

4.8 Voltage Congestion Aware Frequency Control Service Using FPS

In this section, we present two approaches for providing primary frequency control reserve using the particle system, which are: 1) using FPs that represents a virtual non-elastic load, and 2) dynamically shifting the boundary of the FPS. These two approaches are described in the following sections.

4.8.1 Using FPs That Represent Virtual Non-Elastic Load

In this approach, the frequency control reserve is activated by adding FPs in the FPS for a virtual non-elastic load. The addition of FPs for virtual non-elastic loads causes FPs for EV loads to move sideways (towards right) in the (x_t, y_P) plane. Such movement of FPs for EV load either defers the recharging of EVs or reduces their recharging rates.
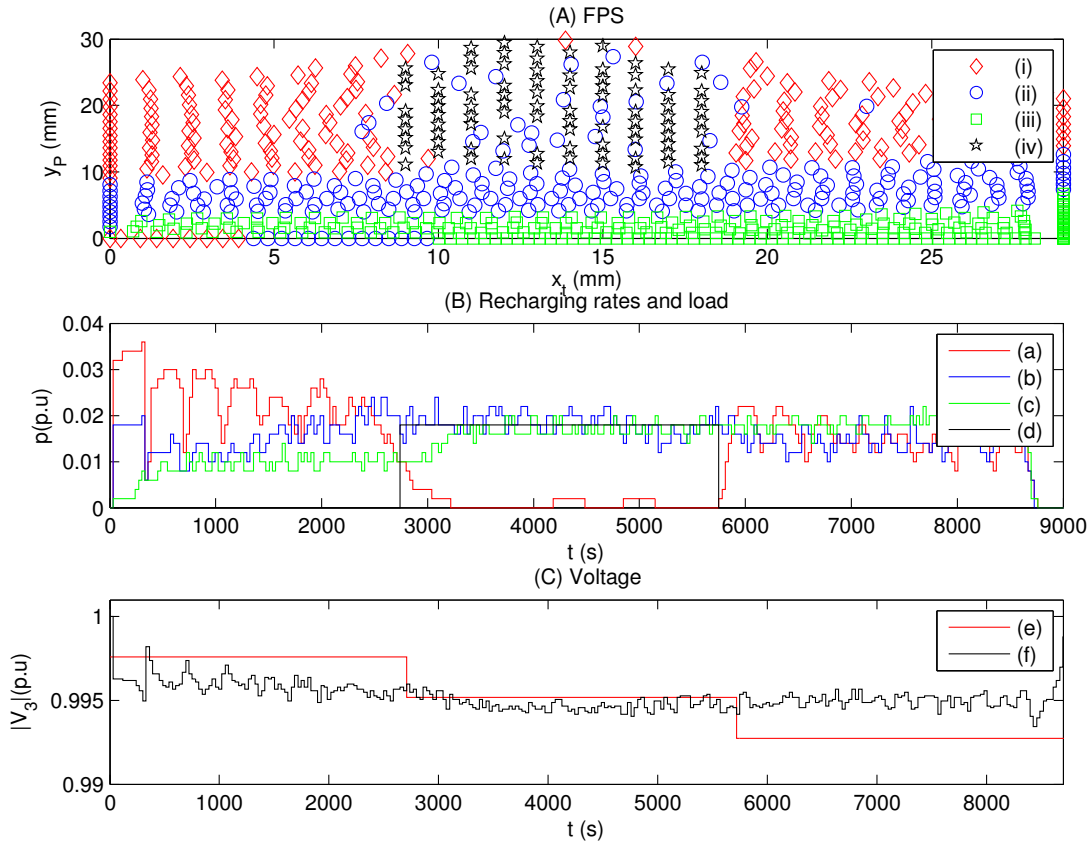
FIGURE 4.7: A snapshot where FPS seeks equilibrium after addition of new FPs

In this way, we can emulate a virtual non-elastic loads to provide a portion of primary frequency control reserve.

Example 2: Using Virtual Non-elastic Load to Provide Frequency Control Reserve

In this example, we highlight the impact of a virtual non-elastic load that is added in response to a drop in frequency, on the voltage at secondary circuit node 3, and on the frequency of the underlying electric power system. To calculate the impact on the voltage we use the secondary circuit shown in Fig. 4.3, which has the same parameters values as in Chapter 3: $Z_{0,1} = Z_{1,2} = Z_{2,3} = 0.05 + j0.05$ and $V_0 = 1\angle 0$. Let us also consider three EVs (EV 1, EV 2, and EV 3). Let EV i be connected to secondary circuit node i for $i = 1, 2, 3$. The test system used for the frequency control is shown in Fig. 4.8. Since we are using a very small population of EVs, we have used a scaled down electric power system where a loss of a 100 kw generator can affect the frequency. Also each energy demand particle (EDP) causes a load of 2 (kw). The test system in
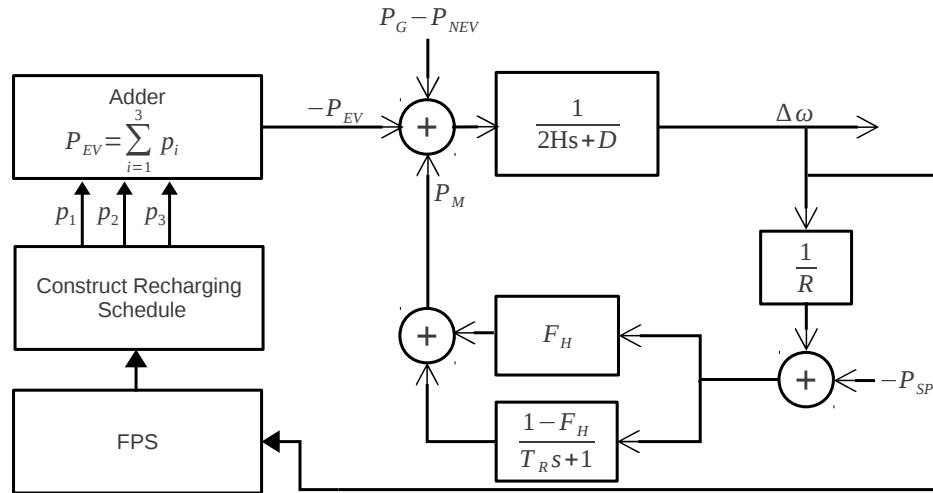
FIGURE 4.8: Particle system and its relation to the frequency control service

Fig. 4.8 has the same parameter values as in Chapter 2: $H = 3.5$, $D = 1$, $R = 0.05$, $F_h = 0.3$, $T_R = 8$, and $PSP = 0$. Here $P_{base} = 1\ MVA$. In the initial schedule, the total instantaneous EVs load is 48 (kw) on average which is 0.048 (p.u) with respect to P_{base}, thus non-EV load[3] is 0.952 (p.u) or 952 (kw). We assume that all of the non-EV load is non-responsive to change in frequency. The primary frequency regulation is mainly provided by a generator driven by a steam reheat turbine, which is fitted with a speed governor with droop of 5%. At $t = 0$ (s), an electric power generator of size 100 kw or 0.1 (p.u) fails suddenly causing a 10% loss in the electric power generation. A secondary generator starts producing 100 (kw), at $t = 600$ (s) or $t = 10$ (m), to compensate the the earlier loss in the electric power generation.

Similar to Example 1, once again we will use a sequence of figures 4.9–4.12) to demonstrate the evolution of the FPS in the FPS simulation time τ. We recall that at any time τ_k in the FPS simulation time τ, the configuration of the FPS (the positions of FPs in the FPS) can be used to construct a recharging schedule which is a plan that can be executed in real world time t. Thus, the sequence of figures shows the variable of interest if four different plans are constructed, (at, say, τ_0, $\tau_0 + \Delta\tau_1$, $\tau_0 + \sum_{i=1}^{2} \Delta\tau_i$, and $\tau_0 + \sum_{i=1}^{3} \Delta\tau_i$) and executed in the real world time t. All figures in the sequence are plotted in the same manner. For example, let us consider Fig. 4.9, which is composed of three sub-figures (A), (B), and (C). Figure. 4.9 (A) shows the FPS in the (x_t, y_P)

---

[3]In calculating voltage on secondary circuit node 3 for this example, we have assumed that the this non-EV load is not in the secondary circuit used by the EVs. The non-EV load is assumed to be either in a different distribution system or in other secondary circuits of the distribution system.
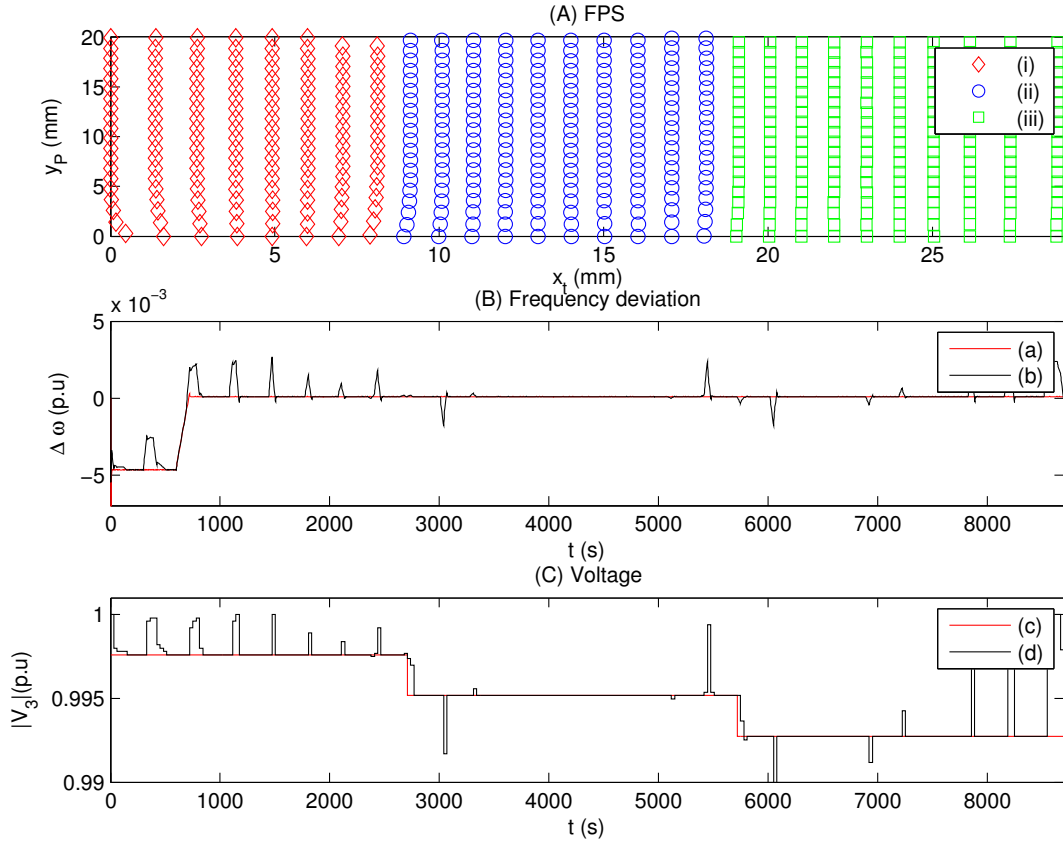
FIGURE 4.9: A snapshot at the start of FPS simulation time $\tau = \tau_0$
key: (A): the FPS where (i) FPs for EV 1, (ii) FPs for EV 2, (iii) FPs for EV 3;
(B): frequency deviation $\Delta\omega$ for (a) the initial schedule (b) current schedule; and
(C): the voltage $|V_3|$ for (c) the initial schedule at $\tau = \tau_0$ and (d) the current schedule

plane. A key is provided in the caption of Fig. 4.9 that should be used for interpreting the sequence of figures.[4] Figure. 4.9 (B) shows the frequency response of electric power system. The frequency response is obtained by solving the differential equations corresponding to the test system shown in Fig. 4.8. Figure 4.4 (C) shows the voltage $|V_3|$ at secondary circuit node 3.

Let us now observe the figures in the sequence one by one starting from Fig. 4.9. Fig. 4.9(A) shows a snapshot at the start of FPS simulation time, that is, $\tau = \tau_0$. It can be observed from the positions of the FPs that EV 1 is recharged first, then EV 2 is recharged, and finally, EV 3 is recharged. Figure 4.9(B) shows that frequency drops below its nominal value in the time interval $t \in [0, \ 600]$ (s) where $\Delta\omega \approx -0.005$ (p.u) in the interval $t \in [0, \ 600]$ (s). Figure 4.9(C) shows the voltage at secondary circuit node 3, which shows that when EV 3 is recharging in the interval $t \in [6000, 9000]$ (s),

---

[4]The key in the caption of Fig. 4.9 will be also used for subsequent figures 4.10–4.12. These figures should be interpreted in the same manner as described above for Fig. 4.9.
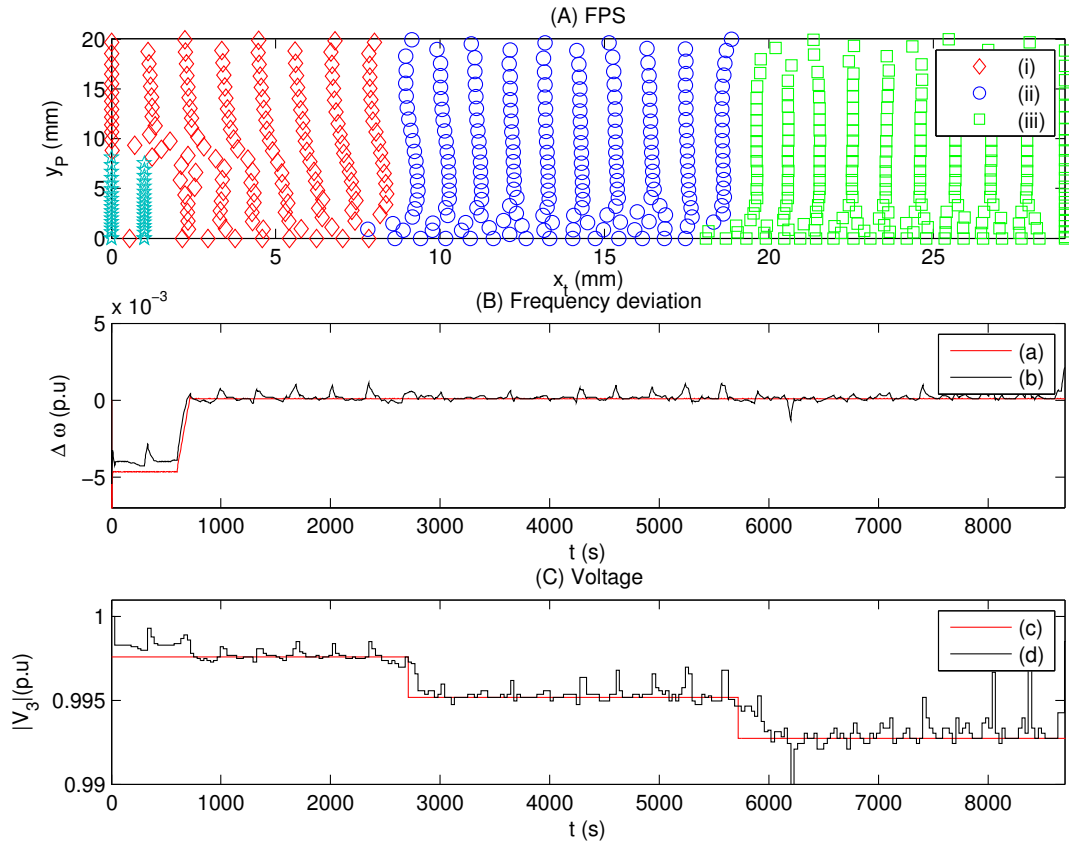
FIGURE 4.10: If a drop in frequency is detected, a virtual non-elastic load is added
The load is assumed to be switched on for 10 minutes

$|V_3| \approx 0.9925$ (p.u), which indicates a voltage drop 0.0075 (p.u) or 0.75% of the voltage
at the output of the distribution transformer.

Figure 4.10 (A) shows a snapshot of the FPs at the FPS simulation time $\tau = \tau_0 + \Delta\tau_1$
when primary frequency control reserve is activated as a drop in frequency is detected.
The FPS responds by adding FPs for virtual non-elastic load. Recall that it is assumed
that secondary frequency control service will start delivering active power after 10 min-
utes. Therefore, the virtual non-elastic load is assumed to have a duration of 10 minutes.
Figure 4.10 (B) shows that the frequency deviation will start to decrease as the FPS
starts to accept FPs for the virtual non-elastic load.

Figure 4.11 (A) shows a snapshot of the FPs at the FPS simulation time $\tau_0 + \sum_{i=1}^{2} \Delta\tau_i$.
The FPS has finished accepting the FPs for virtual non-elastic load. Figure 4.11 (B)
shows that the maximum frequency deviation has been decreased and now $\Delta\omega \approx$
-0.0025 (p.u). Finally, Fig. 4.12 (A) shows a snapshot of the FPs at FPS simulation
time $\tau_0 + \sum_{i=1}^{3} \Delta\tau_i$, when FPS has reached near equilibrium. Figure 4.12 (B) shows that
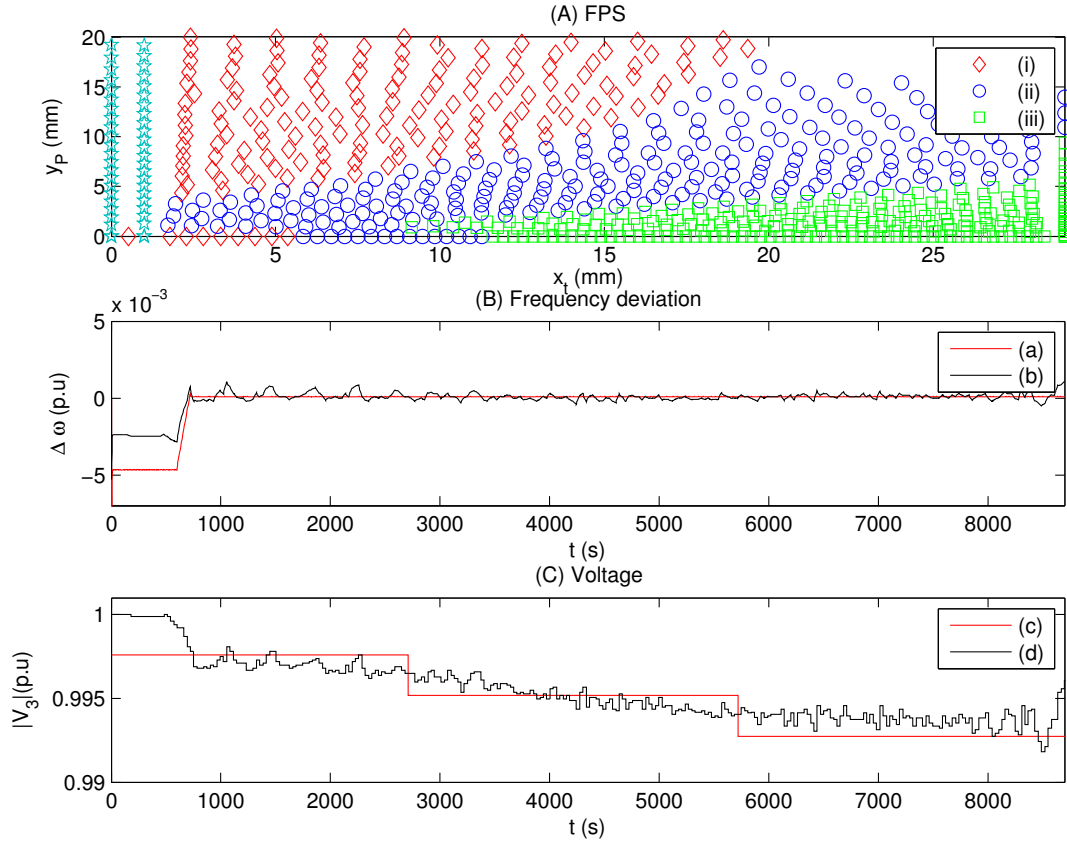
FIGURE 4.11: After the virtual non-elastic load has been added, the maximum frequency deviation is reduced.

the magnitude of frequency deviation (shown as (b)) has increased slightly as compared to the frequency deviation in Figure 4.11 (B). However, at this FPS simulation time τ, the voltage drops in the interval $t \in [6000,\ 9000]$ (s) have been reduced as shown in Fig. 4.12 (C). When compared with Fig. 4.9, Fig. 4.12 shows that the approach based on the particle system can be used to decrease both the frequency deviation and extreme values of voltage drops in the secondary circuit.

We note that to respond to a drop in frequency, the FPS must first detect it. This is due to the fact that a drop in frequency cannot be predicted in advance, it can only be detected after it has occurred. Therefore, while the FPS simulation will be running in the FPS simulation time τ (after having detected a drop in frequency), the frequency would already have dropped and $\Delta\omega \approx -0.005$ (p.u) by the time the remedial action takes place. In this example, as soon as the FPS responds to the drop in frequency, the frequency deviation will be brought back to $\Delta\omega \approx -0.0025$ (p.u) in the interval $t \in [0,\ 600]$ (s). The time it will take to decrease the magnitude of frequency deviation
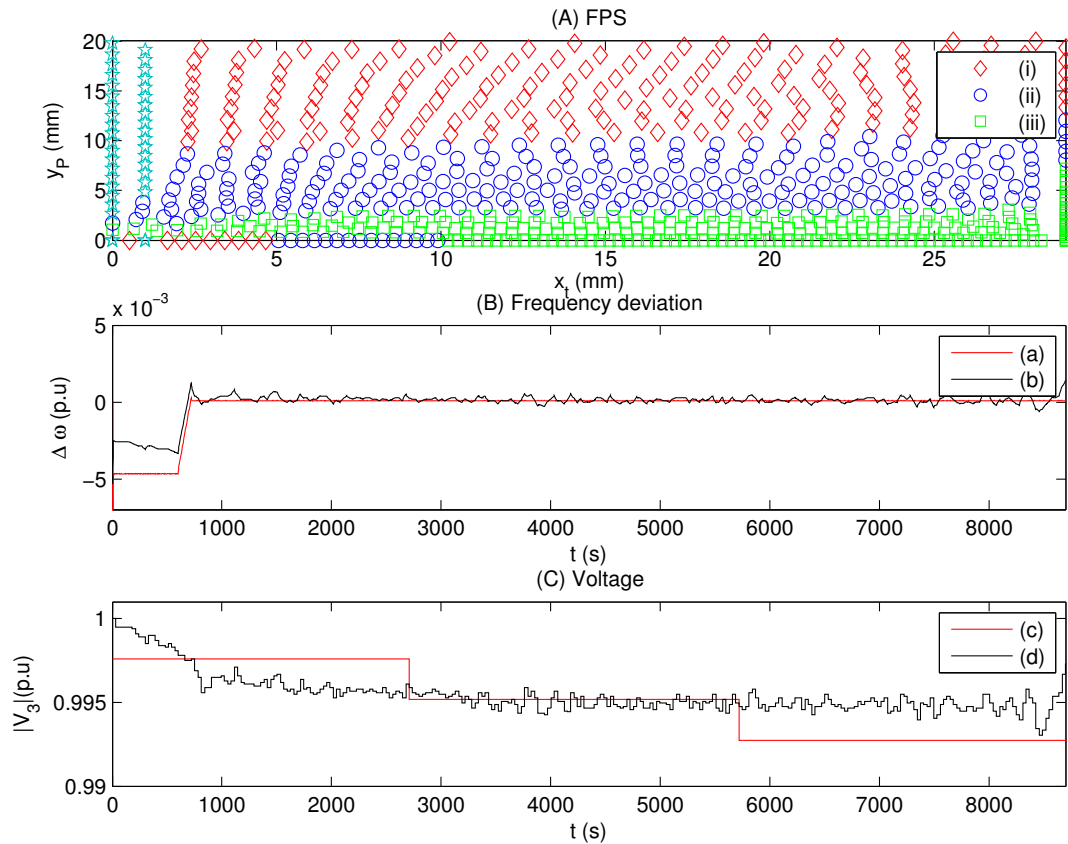
FIGURE 4.12: FPS reaches equilibrium and reduces maximum voltage drop in the secondary circuit

depends on the speed at which the FPS can be simulated.

4.8.2   Voltage Congestion Aware Frequency Control Service Using Shift in the Boundary of FPS

An alternative mechanism to provide frequency control reserve is to shift the boundary of the FPS. For example, when a drop in frequency is detected, the left boundary of FPS is shifted to the right. With the help of Fig. 4.13, we will show the mechanism for a shift in the boundary of the FPS. Figure 4.13(a) shows the FPS which corresponds to, say a EV that is planned to recharge at a constant recharging rate. Suppose that as soon as the recharging starts, a significant drop in the frequency of electric power is detected. As a result, the boundary of the FPS is shifted which in turn shifts to the right all the FPs near the origin of the (x_t, y_p). As the FPs shift towards right, they form a secondary peak as shown in Fig. 4.13(b). After the boundary of the FPS has been shifted, the FPS is no longer at equilibrium. Figure 4.13(c) shows that FPS has reached

y_P

x_t

(a) Initial FPS

Frequency drop is detected: Secondary frequency control service is activated

Secondary peak: Similar to "rebound effect"

y_P

Boundary of FPS is shifted: Contributes to primary frequency control reserve

x_t

(b) FPS after a shift in boundary

Secondary frequency control service start delivering active power

y_P

FPS settles to new equilibrium

x_t

(c) FPS at new equilibrium

Secondary frequency control service start delivering active power

FIGURE 4.13: A shift in the boundary of the FPS

a new equilibrium. A recharging rate profile corresponding to new equilibrium of the FPS will recharge the EV with a delay but at increased recharging rate as compared the original recharging rate profile.

Example 3: Frequency Control Service Using Shift in the Boundary of FPS

In this example, we emulate a shift in boundary of the FPS to provide a primary frequency control reserve. In exactly the same manner as described previously, we will use a sequence of figures (4.14–4.16). All the figures in this example can be interpreted in the same manner as described in Example 2.
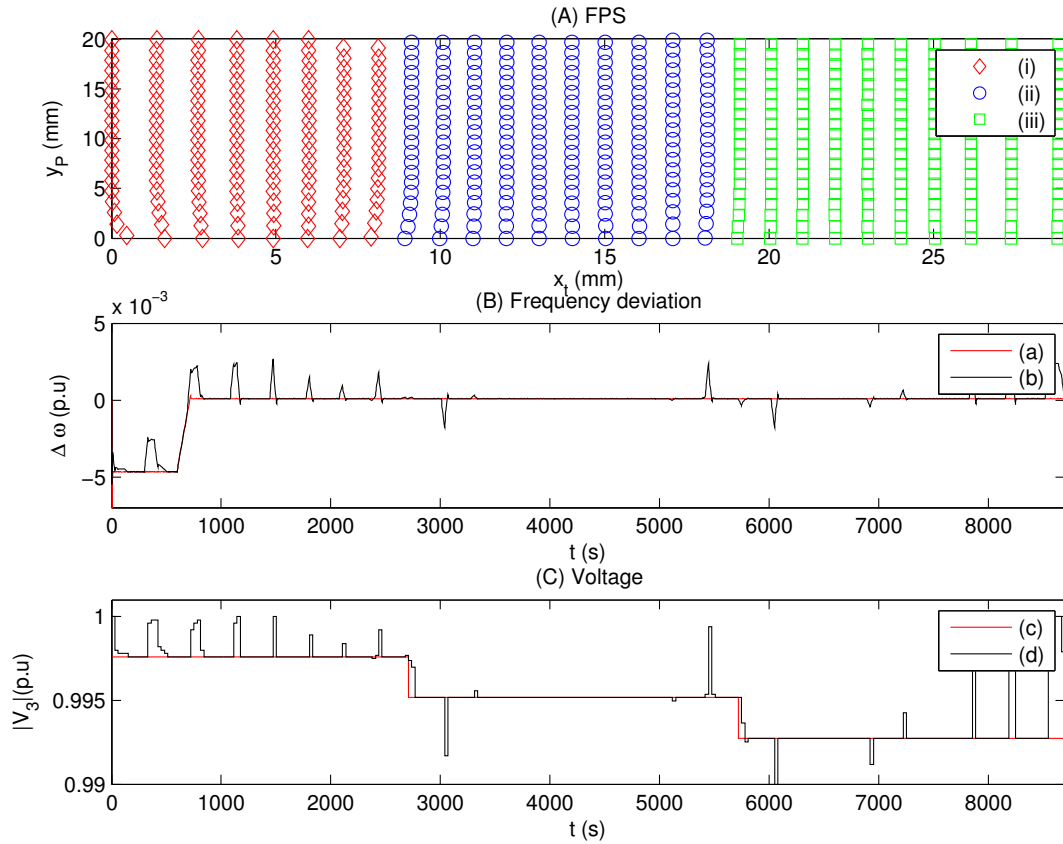
FIGURE 4.14: A snapshot at the start of FPS simulation time $\tau = \tau_0$
Key: **(A):** FPS for current schedule where (i) FPs for EV 1, (ii) FPs for EV 2, (iii)
FPs for EV 3;
(B): frequency deviation where (a) $\Delta\omega$ for initial schedule, (b) $\Delta\omega$ for current schedule;
and
(C): voltage where (c) $|V_3|$ for initial schedule, and (d) $|V_3|$ for current schedule con-
structed from FPS

Figure 4.14 shows a snapshot at the start of the FPS simulation time $\tau = \tau_0$. This figure
is very similar to Fig. 4.9 and hence the description for Fig 4.9 applies here.

Figure 4.15 (A) shows a snapshot of the FPs at the FPS simulation time $\tau = \tau_0 + \Delta\tau_1$
when primary frequency control reserve is activated as the drop in the frequency of
electric power is detected. The FPS responds by shifting its left boundary towards
right. In this example, it is assumed that secondary service will start delivering active
power after 10 minutes. Therefore, this example also shows that Figure 4.15 (B) shows
that the magnitude of frequency deviation starts decreasing and $\Delta\omega \approx -0.0025$ (p.u)
for $t \in [0, \ 300]$ (s) but still $\Delta\omega < -0.005$ (p.u) some time $t \in [500, \ 600]$ (s).

Figure 4.16 (A) shows a snapshot of the FPs at the FPS simulation time $\tau = \tau_0 + \Delta\tau_1$
when the boundary of the FPS has been moved to the desired position and also the FPS
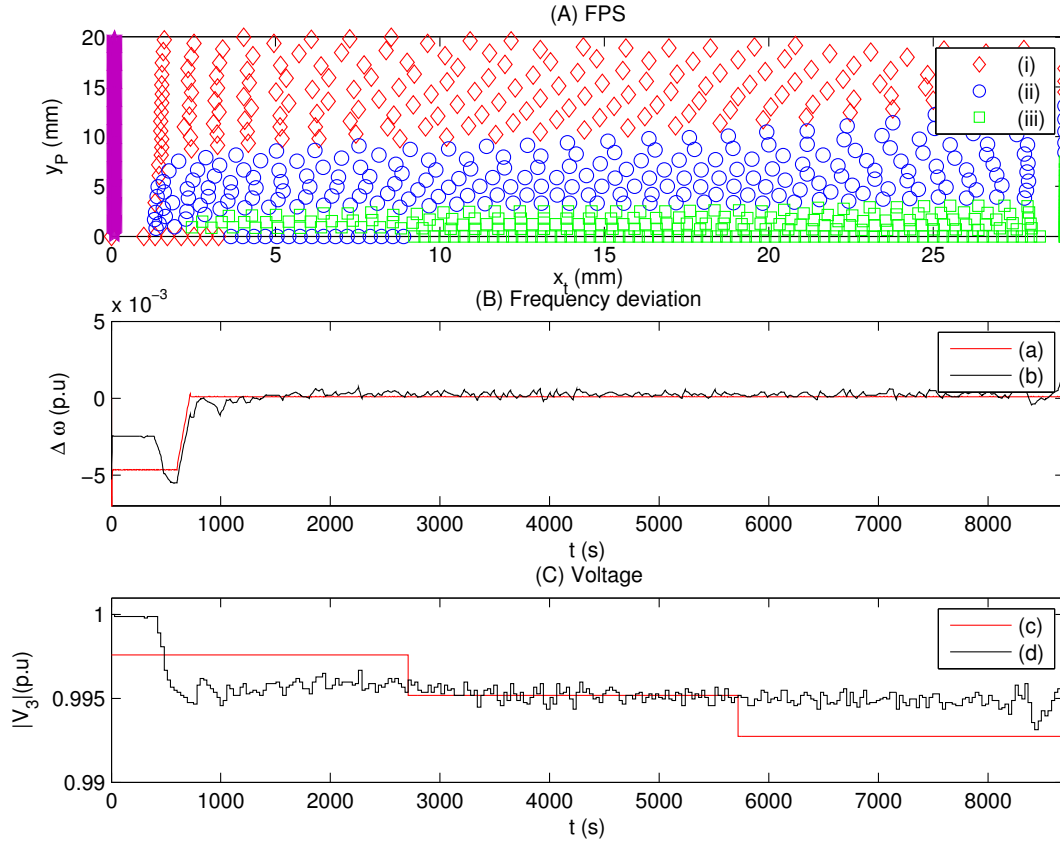
FIGURE 4.15: The boundary of FPS is shifted

has reached equilibrium. Figure 4.16 (B) shows that the magnitude of the frequency deviation has been reduced and $\Delta\omega \approx -0.0025$ for $t \in [0,\ 600]$ (s). Therefore, this example also shows that the recharging schedule constructed at this point in the FPS simulation time τ, reduces both the maximum frequency deviation and the maximum drop in voltage in secondary circuit.

4.9   Advantage of Using Particle System

In this section four recharging schedules are compared in terms of their performance as measured by performance metric J introduced in Section 3.9.2 (in Chapter 3) and their impact on frequency response of electric power system. The settings are the same for testing all four schedules and are the same as used in Example 2 in Section 4.8. The four schedules that have been selected for the purpose of comparison are:
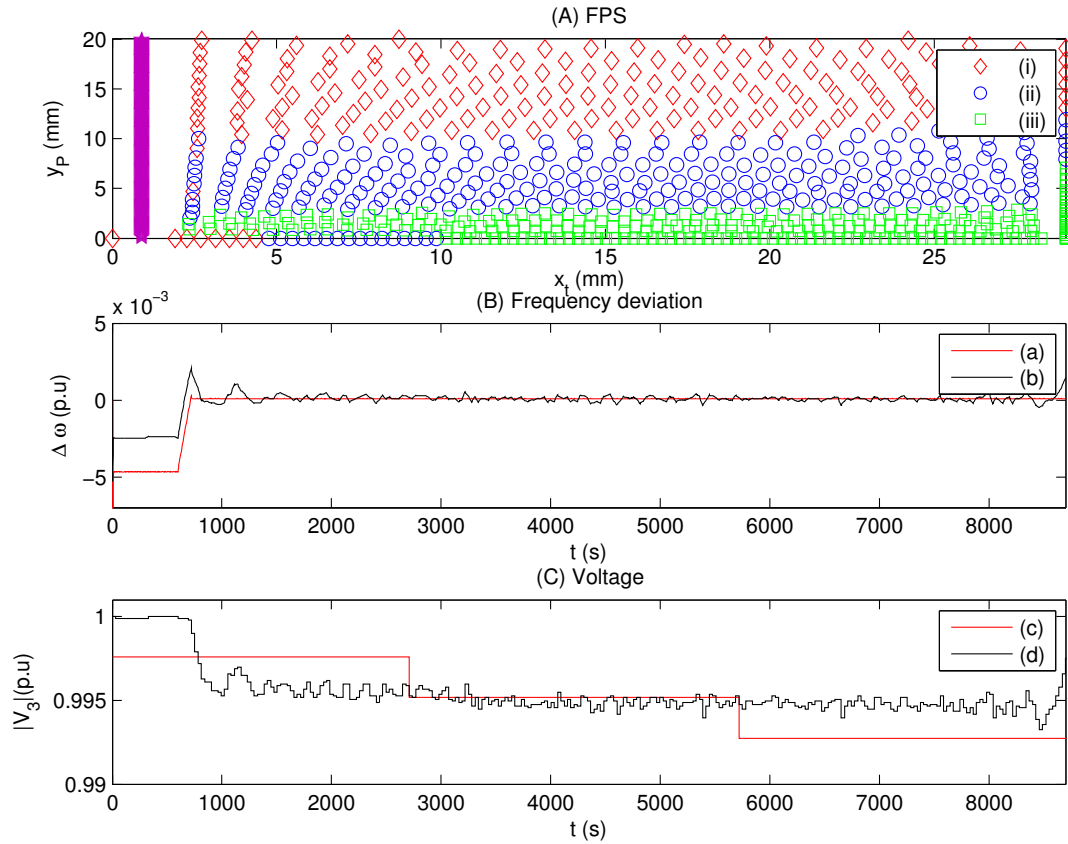
FIGURE 4.16: FPS reaches near equilibrium after the boundary has been shifted

1. **Schedule A:** This schedule is constructed by the Stage 1 of the two stage framework introduced in Section 3.7 (in Chapter 3) and is never improved by Stage 2. It is a maximum load factor schedule [72] where EV 1, EV 2 and EV 3 are recharged in a sequence such that EV i starts recharging when EV $(i-1)$ finishes. The schedule is never changed during execution and hence it does not respond to a drop in frequency.

2. **Schedule B:** This schedule is constructed by taking Schedule A as an initial schedule and apply Stage 2 of the two stage framework in Section 3.7.1. A FPS is constructed for the Schedule A, SPH method is applied to the FPS, and a schedule is constructed from the equilibrium configuration of FPs in the FPS. Schedule B is never changed during its execution and hence it does not respond to a drop in frequency.

3. **Schedule C:** This schedule is constructed by taking Schedule B as the initial schedule and it differs from schedule B in one aspect in that it responds to a
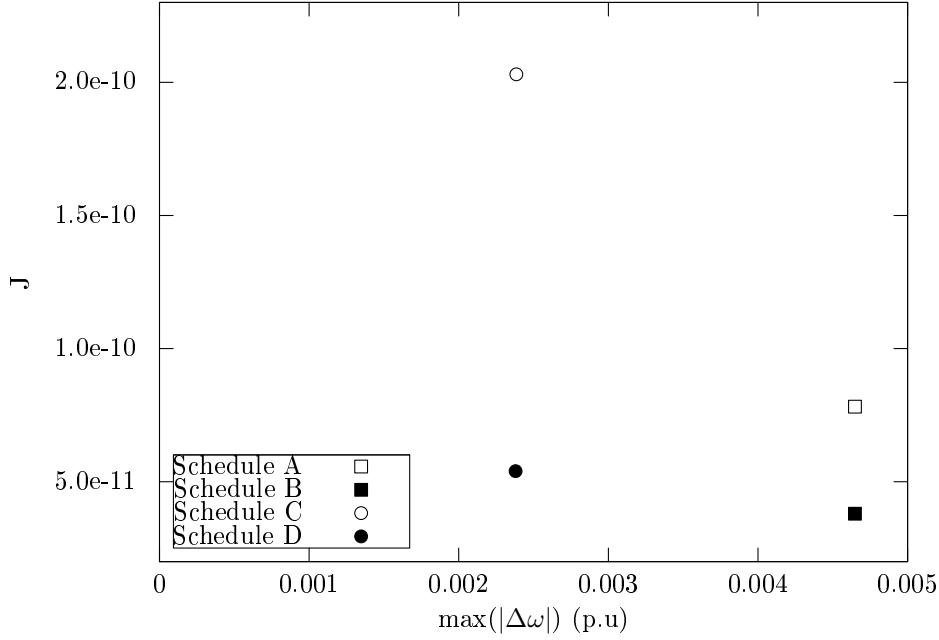
FIGURE 4.17: $\max(|\Delta\omega|)$ as maintained by primary frequency control before restoration of frequency vs J for the four schedules

drop in frequency by simply delaying the demand for 10 minutes. Any demand scheduled at times later than 10 minutes after the drop in frequency is not affected.

4. **Schedule D:** This schedule is also constructed by taking Schedule B as the initial schedule. It uses the same FPS as used by Schedule B, however in contrast to Schedule B, Schedule D responds to a drop in frequency by shifting the boundary of the FPS and allowing the FPS to reach a new equilibrium. After the FPS has reached new equilibrium, a new schedule is constructed and executed.

Note that similar results are obtained if the FPS reacts to a drop in frequency by adding a virtual non-elastic virtual load. Therefore, the results for Schedule D are also representative of results for a schedule that could have been constructed from the equilibrium configuration of FPs in the FPS after a virtual non-elastic load had been added.

Figure 4.17 shows the comparative performance of the four selected schedules, where J is given in Eq. (3.57), which is:

$$J = \int_0^T \left(10(|Vs(t)| - |V_3(t)|)\right)^6 dt$$

It can be seen that Schedule B achieves better performance as compared to Schedule A in terms of voltage impacts but is otherwise equivalent to Schedule A in terms of frequency response. Schedule C improves the frequency response but increases voltage impacts and can potentially cause congestion. In this case it does not cause congestion because there are only 3 EVs in the secondary circuit. Schedule D manages to improve the frequency response as well as manages to avoid potential congestion.

4.10   Final Remarks

In this chapter we have extended the particle system, introduced in Chapter 3, to handle non-elastic loads and the impact of their arrival on recharging schedules of EVs. Using the particle system approach, two mechanisms have been presented that can enable EVs to participate in frequency control services. When using particle systems for scheduling EVs energy demands, the demand can be deferred with the addition of virtual non-elastic loads, or by a simple shift of boundary of FPS. It is clear from the Fig. 4.17 that using particle system, both frequency response and voltage performance of schedules can be improved. Furthermore, we have shown with a simple example that using the particle system to provide a frequency control reserve has an advantage over the approach of simply delaying the demand. This is due to the fact that the particle system also avoids potential congestion in the distribution system.

In the context of dynamic demand response using stochastic de-synchronisation, we further note that the nature of EV loads is more flexible as compared to the refrigerator loads. It would be interesting to further investigate the possibility of combining the stochastic de-synchronisation approach using refrigerator load (which addresses a global problem of frequency control) with the particle system based congestion avoidance using EV loads (which addresses a local problem of improving utilisation voltage).

Chapter 5

Conclusions and Future Work

5.1 Summary and Conclusions

The aim of this thesis is to investigate recharging schemes for energy demand management of electric vehicles. The contributions made in this research can be summarised as follows.

Chapter 2: Distributed Recharging Rate Control

In Chapter 2, we have presented a distributed recharging rate controller that combines the objectives of regulating frequency and improving utilisation of electric generators. The controller creates an incentive policy for autonomous EV that are randomly connecting to and disconnecting from the electric grid. Furthermore, we note that the proposed recharging rate controller can be used to realise a DM solution to, for example, reconcile EVs energy demand profiles with the output of available energy sources.

The features of the controller and its implementation can be summarised as follows.

- EVs act as frequency regulators which can control their participation role by modifying their respective payment rates as individual EVs connect and disconnect at arbitrary times.

- The incentive policy encourages EVs to demand energy when non-EV demand is low and utilisation of electric generators needs to be improved. A simple game is

used to show that the incentive policy would encourage some EVs to defer their demand relative to the other EVs.

- The controller is able to allocate proportionally fair recharging rate to EVs and requires only binary information about frequency of electric power system.

- The controller is implemented for a single synchronous machine. It is shown that the frequency deviation can be used as a proxy to the imbalance between the generation and consumption of the electric power.

- The controller is modified and a protocol is discussed that can be used to implement the modified controller in a multi-machine electric power system. It is shown, via simulation, that in the multi-machine system, the controller allocates proportionally fair recharging rates and also regulates the frequency of electric power system.

- The integration of the controller with the legacy protection system was also suggested, which causes the controller to shed all EV load if the frequency drops below the statutory limits of operation.

- It is also shown that the distributed billing for recharging EVs is possible using the proposed recharging rate controller.

The proposed controller enables EVs to learn by safely experimenting with their recharging rates and the payment rates, and at the same time ensures that the EVs improve the frequency stability of the electric power system. Furthermore, the results presented in the thesis show that the proposed recharging rate control algorithm can help to decrease the required size of frequency regulating turbines.

Chapter 3: Distribution Voltage Congestion Avoidance

In Chapter 3, we have presented a novel recharging schedule building approach that modifies a given feasible initial recharging schedule to a recharging schedule that reduces the voltage drops between the distribution transformer and the recharging sockets at secondary circuit nodes. The work in this chapter can be summarised as follows.

- An analogy is highlighted between the voltage drops in the secondary circuit and the pressure in a system of fluids. Using a simple example, expected properties of desired voltage avoiding schedule are verified analytically.

- A correspondence is established between a fluid particle system and a recharging schedule by transforming the recharging schedule to an energy demand particle system.

- A two stage framework is presented, where the first stage does not need to consider the impacts of recharging schedule on voltages in the distribution system and, for example, builds an initial recharging schedule for maximising the load factor. The second stage uses a particle system that includes information about topology of the distribution system, and enhances the initial schedule with respect to the impacts on voltages at secondary circuit nodes. The second stage is based on the smoothed particle hydrodynamics method, which had been previously used for simulation of fluid dynamics.

- A metric for comparing recharging schedules built by existing approaches and the proposed approach is developed.

- Two example cases are presented, which show that the proposed approach can construct recharging schedules which have only small impacts on the voltages when compared with other approaches in state of the art literature.

In summary, the particle system based approach is an alternative to the scheduling methods (reported in the literature for recharging EVs) that aim at avoiding voltage congestion in the distribution system.

Chapter 4: Voltage Congestion Aware Frequency Control Service

In Chapter 4 we extended particle system presented in Chapter 3 with the aim of deferring EV energy demand to respond to a drop in frequency of electric power system. The deferment of EV energy demand is achieved in a manner that is aware of subsequent voltage congestion in the distribution system. The work in this chapter can be summarised as follows.

- Two representations of non-elastic loads in the fluid particle system are discussed. The first representations is by means of terrain of fluid particle system. The second representation is by means of groups of FPs with restricted mobility in the fluid particle system. The relative benefits and disadvantages of the two representations are discussed.

- The particle system is then extended to handle non-elastic loads and the impact of their arrival on recharging schedules of EVs.

- Using the extended particle system, two mechanisms are presented that can enable EVs to participate in frequency control services. The deferment of the recharging of EVs can be achieved by adding virtual non-elastic load or by shifting the boundary of the FPS.

- To highlight the advantage of providing a frequency control reserve using the particle system, four schedules are compared in terms of their impact on the frequency of electric power system and the voltage drops in the distribution system.

In summary, the approach presented in Chapter 3 and extended in Chapter 4 is shown to be very useful when providing a congestion aware frequency control reserve.

5.2   Future Work

The work reported in this thesis highlighted some further developments in implementation of the recharging schemes that should realise the full benefits of electric vehicles. However, much remains to be done in order to further develop, analyse and deploy the recharging schemes in real world settings.

Chapter 2: Distributed Recharging Rate Control

A large body of work already exists that addresses most of outstanding aspects in this chapter, but there could be specific issues related to EVs that haven't been addressed in the existing literature.

- The emergent behaviour of the population of the EV agents could be further investigated as a function of their demand submission strategies when their reward and cost functions are defined.

- The capacity control for recharging EVs that is to be solved as a revenue management problem.

- The quantification of decrease in the required size of frequency regulating turbines as a function of parked and recharging EVs.

- Alternative methods that use the frequency deviations to allocate rechargine rates in a distributed manner.

Chapter 3: Distribution Voltage Congestion Avoidance

- The performance of proposed approach can be tested with large populations of EVs and IEEE test distribution systems. It would be necessary to explore optimisation of SPH method for this purpose.

- To compare recharging schedule in terms of voltage congestion, other metrics can be proposed and used. For example, the mean and variance of voltage drops over the planning period might also indicate the preference for different schedules.

- The optimisation and implementation of the SPH method on parallel computing platforms is also an interesting research direction in itself. The optimisation is required to speedily simulate a large number of FPs in the FPS.

- Dynamically adapting the value FPS simulation time τ to achieve faster convergence of the FPS to equilibrium is also a very interesting problem.

- The recharging sockets can take decisions about individual EDPs before activating them. This feature can be used to build more sophisticated mechanisms for energy demand management. For example, instead of applying admission control to EVs, admission control could be applied to individual EDPs (as there may be more than one EDPs for a given EV), which could result in fair admission control policies for EVs, because an EV will not be completely blocked and made to wait while other EVs are recharged at maximum recharging rates.

.

Chapter 4: Voltage Congestion Aware Frequency Control Service

- The mechanisms in Chapter 4 could be extended to selectively defer the demand of EVs based on their energy demand and the time of departure. Thus the mechanism could have the ability to dynamically filter and choose the EVs whose demand can be safely deferred.

- Alternative representations of non-elastic load in the particle system, for example, as a terrain of the fluid particle system could be investigated and their relative benefits and disadvantages could be further researched.

- It would be interesting to explore ways in which the mechanism in Chapter 4 could be integrated with dynamic demand control schemes.

Appendices

Appendix A

Supplementary Proofs for Chapter 2

Convergence of control laws in Eq. (2.3)

For the problems of the form

$$
\begin{aligned}
\underset{\mathbf{x}}{\text{maximize}} \quad & f(\mathbf{x}) \\
\text{subject to} \quad & g_i(\mathbf{x}) \leq 0, \ i = 1, 2, \ldots, \text{m}
\end{aligned}
\tag{A.1}
$$

where $\mathbf{x} \in \mathbb{R}^n$, $f : \mathbb{R}^n \to \mathbb{R}$ and $g_i : \mathbb{R}^n \to \mathbb{R}$, i=1, 2, ..., m. Let us define

$$
\Omega = \bigcap_{i=1}^{m} \{\mathbf{x} : g_i(\mathbf{x}) \leq 0\}
$$

and

$$
J(\mathbf{x}) = \{i : g_i(\mathbf{x}) > 0\}
$$

In [60] it is shown that the differential inclusions of the form

$$
\tau \dot{\mathbf{x}}(t) =
\begin{cases}
\nabla f(\mathbf{x}(t)) & \text{if } \mathbf{x}(t) \in \Omega, \\
-\mu \sum_{i \in J(\mathbf{x}(t))} \nabla g_i(\mathbf{x}(t)) & \text{if } \mathbf{x}(t) \notin \Omega
\end{cases}
\tag{A.2}
$$

have an equilibrium point that is the maximizer for Eq. (A.1).

Taking

$$f(\mathbf{P}) = \sum_{i|\nu_i \in \nu} w_{i,1} log(p_i) \tag{A.3}$$

and

$$g_1(\mathbf{P}) = \sum_{i|\nu_i \in \nu} p_i - C \tag{A.4}$$

$$g_{i+1}(\mathbf{P}) = p_i - p_{imax} \text{ for } i = 1, \ldots, \ N \tag{A.5}$$

and

$$g_{i+N+1}(\mathbf{P}) = -p_i \text{ for } i = 1, \ldots, \ N \tag{A.6}$$

and $m = 2N+1$, where N is the number of EVs connected to recharging sockets we can see that problem (2.1) has the form (A.1).

Clearly

$$[\nabla f(\mathbf{P})]_i = \frac{w_{i,1}}{p_i} \tag{A.7}$$

Also

$$[\nabla g_{i+1}(\mathbf{P})]_i = 1, \ [\nabla g_{i+N+1}(\mathbf{P})]_i = -1 \text{ for } i = 1, \ldots, \ N \tag{A.8}$$

We also note that

$$[\nabla g_{i+1}(\mathbf{P})]_j = 0, \ [\nabla g_{i+N+1}(\mathbf{P})]_j = 0 \text{ for } i \neq j \tag{A.9}$$

Now define

$$\theta_1 = \begin{cases} 1 & \text{if } g_1(\mathbf{P}) > 0 \\ 0 & \text{otherwise} \end{cases} \tag{A.10}$$

$$\phi_1(p_i) = \begin{cases} 1 & \text{if } g_{i+1}(\mathbf{P}) > 0, \\ -1 & \text{if } g_{i+N+1}(\mathbf{P}) > 0 \\ 0 & \text{otherwise} \end{cases} \tag{A.11}$$

$$\text{for } i = 1, \ldots, \ N$$

$$\bar{\theta}_1 = \begin{cases} 1 & \text{if } \theta = 0 \\ 0 & \text{otherwise} \end{cases} \tag{A.12}$$

and

$$\overline{\phi_1(p_i)} = \begin{cases} 1 & \text{if } \phi(p_i) = 0 \\ 0 & \text{otherwise} \end{cases} \tag{A.13}$$

Using these values in equation Eq. (A.2) and writing $\mathbf{x}(t) = \mathbf{P}(t)$, $\alpha = \frac{1}{\tau}$, $\beta = \frac{\mu}{\tau}$, we get:

$$\frac{d(p_i(t))}{dt} = \frac{\alpha w_{i,1}(t)}{p_i(t)} \bar{\theta}_1 \overline{\phi_1(p_i(t))} - \beta(\theta_1 + \phi_1(p_i(t))) \tag{A.14}$$

Which is same as Eq. (2.3)

Thus the differential inclusions Eq. (2.3) have the equilibrium point that is the solution of Eq. (2.1).

Intermediate Results For Procedure A

This section shows that $k_{j+1} \geq k_j$ in procedure A on page 50.

Proof. From Eq. (2.17) we have

$$\kappa_j = \frac{C_j}{\sum_{k=0}^{N_j} w_{k,1}} \tag{A.15}$$

$$\kappa_{j+1} = \frac{C_{j+1}}{\sum_{k=0}^{N_{j+1}} w_{k,1}} \tag{A.16}$$

At step 2 of jth iteration we assign EVs to $G_{1,j}$ or $G_{2,j}$ and set of EV for $(j + 1)th$ iteration is reduced to $G_{1,j}$ hence we can rewrite Equations (A.15) and (A.16) as

$$\kappa_j = \frac{C_j}{\sum_{k|v_k \in G_{1,j} \cup G_{2,j}} w_{k,1}} \tag{A.17}$$

hence

$$\kappa_j = \frac{C_j}{\displaystyle\sum_{k|v_k\in G_{1,j}} w_{k,1} + \sum_{l|v_l\in G_{2,j}} w_{l,1}} \tag{A.18}$$

$$\kappa_{j+1} = \frac{C_{j+1}}{\displaystyle\sum_{k|v_k\in G_{1,j}} w_{k,1}} \tag{A.19}$$

and

$$C_{j+1} = C_j - \sum_{k|v_k\in G_{2,j}} p_{k,max} \tag{A.20}$$

Using Eq. (A.20) in Eq. (A.18) and dividing the numerator and denominator by $\displaystyle\sum_{k|v_k\in G_1} w_{k,1}$, we get

$$\kappa_j = \frac{\dfrac{C_{j+1} + \displaystyle\sum_{k|v_k\in G_{2,j}} p_{k,max}}{\displaystyle\sum_{k|v_k\in G_{1,j}} w_{k,1}}}{1 + \dfrac{\displaystyle\sum_{k|v_k\in G_{2,j}} w_{k,1}}{\displaystyle\sum_{k|v_k\in G_{1,j}} w_{k,1}}} \tag{A.21}$$

Now using Eq. (A.19) and simplifying we get

$$\kappa_j + \frac{\displaystyle\sum_{k|v_k\in G_{2,j}} \kappa_j w_{k,1}}{\displaystyle\sum_{k|v_k\in G_{1,j}} w_{k,1}} - \frac{\displaystyle\sum_{k|v_k\in G_{2,j}} p_{k,max}}{\displaystyle\sum_{k|v_k\in G_{1,j}} w_{k,1}} = \kappa_{j+1} \tag{A.22}$$

Now clearly for $v_i \in G_{2,j}$, $\kappa w_i \geq p_{i,max}$. It immediately follows that

$$\frac{\displaystyle\sum_{k|v_k\in G_{2,j}} \kappa_j w_{k,1}}{\displaystyle\sum_{k|v_k\in G_{1,j}} w_{k,1}} - \frac{\displaystyle\sum_{k|v_k\in G_{2,j}} p_{k,max}}{\displaystyle\sum_{k|v_k\in G_{1,j}} w_{k,1}} \geq 0 \tag{A.23}$$

combining Eq. (A.22) and Eq. (A.23) we get

$$k_{j+1} \geq k_j \tag{A.24}$$

which is required. $\square$

Pareto Efficiency

The following argument to show Pareto efficiency is based on work by Arrow [61].

Consider a two resource economy. Each agent has two resources: money and energy. The agents can trade these resources as they consider appropriate. The agents are rational and autonomous. Each agent wishes to accumulate resources in order to maximise its own utility. The price of money is 1 [\$/\$]. The price of energy is $\frac{1}{\kappa}$ [\$/kwh]. All agents observe the same value of these prices.

Let us assume that each agent is initially endowed with some quantity of each of the resources. For instance, here EVs are endowed with money and wish to exchange it for energy. The generators are endowed with energy and wish to exchange it for money. Consider this economy in a given second. An EV receives an amount of energy $p_i/3600$ [kwh] if it pays $w_i/3600$ [\$].

For the sake of convenience in notation we introduce,

E_i = energy held by the *ith* agent

M_i = money owned by the *ith* agent

If *ith* EV spends 1 [\$], it reduces M_i by 1 [\$] and increases E_i by κ [kwh]. Let $(E_{i,e}, M_{i,e})$ be the initial endowments of ith agent. At equilibrium, given $\frac{1}{\kappa}$, the *ith* EV would select $(\tilde{E}_i, \tilde{M}_i)$ that maximises its utility $U_i(E_i, M_i)$ which is a function increasing in both E_i and M_i.

$$\text{maximise} \qquad U_i(E_i, M_i)$$

$$\text{subject to} \qquad\qquad\qquad\qquad\qquad\qquad (A.25)$$

$$\frac{1}{\kappa}E_i + M_i = \frac{1}{\kappa}E_{i,e} + M_{i,e}$$

Let $(\tilde{E}_q, \tilde{M}_q)$ be the solution to Eq. (A.25). Then,

$$\frac{1}{\kappa}\tilde{E}_i + \tilde{M}_i = \frac{1}{\kappa}E_{i,e} + M_{i,e} \qquad\qquad (A.26)$$

Suppose we claim that for the *qth* EV, there exists $(\hat{E}_q, \hat{M}_q) \neq (\tilde{E}_q, \tilde{M}_q)$ such that

$$U_q(\hat{E}_q, \hat{M}_q) > U_q(\tilde{E}_q, \tilde{M}_q)$$

and

$$U_i(\hat{E}_i, \hat{M}_i) \geq U_i(\tilde{E}_i, \tilde{M}_i) \ \forall i \neq q$$

It can be shown that this claim is false because it leads to a contradiction.

To show this, note that

$$\frac{1}{\kappa}\hat{E}_q + \hat{M}_q > \frac{1}{\kappa}\tilde{E}_q + \tilde{M}_q = \frac{1}{\kappa}E_{q,e} + M_{q,e}$$

and

$$\frac{1}{\kappa}\hat{E}_i + \hat{M}_i \geq \frac{1}{\kappa}\tilde{E}_i + \tilde{M}_i = \frac{1}{\kappa}E_{q,e} + M_{q,e} \ \forall i \neq q$$

Performing a sum over the whole population of EVs and generators

$$\frac{1}{\kappa}\sum \hat{E}_i + \sum \hat{M}_i > \frac{1}{\kappa}\sum E_{i,e} + \sum M_{i,e} \tag{A.27}$$

but

$$\sum \hat{E}_i = \sum E_{i,e}$$

and

$$\sum \hat{M}_i = \sum M_{i,e}$$

Because the total energy and the total money are conserved in the transaction process.

Thus, the two sides of Eq. (A.27) must have the same value. Hence, we have a contradiction.

Proportional Fairness

Proportional fairness was introduced by Kelly [55] and we use similar steps to prove it.

Let $\mathbf{P_0} = [p_{01}, p_{02}, \ldots, p_{0N}]$ be a recharging rate vector for N EVs that is feasible. For a given payment rate vector $\mathbf{W_1} = [w_{1,1}, w_{2,1}, \ldots, w_{N,1}]$, we say that $\mathbf{P_0}$ is proportional fair if for any other feasible $\mathbf{P_1} \neq \mathbf{P_0}$ the aggregate weighted proportional change is negative. *i.e.,*

$$\sum_{i=1}^{N} w_{0i} \frac{p_{1i} - p_{0i}}{p_{0i}} < 0 \tag{A.28}$$

Let $\mathbf{P_0}$ be some feasible recharging rate vector for a given $\mathbf{W_1}$. It can be shown that if it is optimal, then it is proportionally fair [55]. To show this, consider a small perturbation $\Delta \mathbf{P_0} = \mathbf{P_1} - \mathbf{P_0}$. The perturbation causes the value of objective to change. Note that the objective is

$$\sum_{i=1}^{N} w_{i,1} log(p_i) \tag{A.29}$$

The change in objective by the small perturbation in $\mathbf{P_0}$ is given by

$$\sum_{i=1}^{N} w_{i,1} \frac{\Delta p_{0i}}{p_{0i}} = \sum_{i=1}^{N} w_{i,1} \frac{p_{1i} - p_{0i}}{p_{0i}} \tag{A.30}$$

Note that if $\mathbf{P_0}$ is optimal, then the concavity of the objective implies that

$$\sum_{i=1}^{N} w_{i,1} \frac{p_{1i} - p_{0i}}{p_{0i}} < 0 \tag{A.31}$$

for all feasible $\mathbf{P_1}$. Hence $\mathbf{P_0}$ is proportionally fair.

List of Publications

[1] Q. Hamid and J. Barria, "Distributed recharging rate control for energy demand management of electric vehicles," *Power Systems, IEEE Transactions on*, vol. 28, no. 3, pp. 2688–2699, 2013.

[2] ——, "Distribution voltage congestion avoidance in recharging electric vehicles using smoothed particle hydrodynamics," *Transactions journal*, 2014, submitted.

Bibliography

[1] R. Singh and Y. Sood, "Policies for promotion of renewable energy sources for restructured power sector," in *Electric Utility Deregulation and Restructuring and Power Technologies, 2008. DRPT 2008. Third International Conference on*, 2008, pp. 1–5.

[2] G. Boyle, Ed., *Renewable electricity and the grid: the challenge of variability.* 8–12 Camden High Street, London, NW1 0JH, U.K.: Earthscan, 2007.

[3] L. C. Henriksen, "Wind energy literature survey no. 13," *Wind Energy*, vol. 12, no. 5, pp. 524–526, 2009. [Online]. Available: http://dx.doi.org/10.1002/we.350

[4] C. L. Archer and M. Z. Jacobson, "Evaluation of global wind power," *Journal of Geophysical Research: Atmospheres*, vol. 110, no. D12, pp. n/a–n/a, 2005. [Online]. Available: http://dx.doi.org/10.1029/2004JD005462

[5] WWEA, "World wind energy report 2008," World Wind Energy Association, WWEA Head Office, Charles-de-Gaulle-Str. 5,53113 Bonn, Germany, Tech. Rep., 2009. [Online]. Available: http://www.wwindea.org/home/images/stories/worldwindenergyreport2008_s.pdf

[6] G. Dany, "Power reserve in interconnected systems with high wind power production," in *Power Tech Proceedings, 2001 IEEE Porto*, vol. 4, 2001, pp. 6 pp. vol.4–.

[7] J. Momoh, *Renewable Energy and Storage.* John Wiley & Sons, Inc., 2012, pp. 140–159. [Online]. Available: http://dx.doi.org/10.1002/9781118156117.ch7

[8] G. Strbac, "Demand side management: Benefits and challenges," *Energy Policy*, vol. 36, no. 12, pp. 4419 – 4426, 2008, ¡ce:title¿Foresight Sustainable Energy Management and the Built Environment Project¡/ce:title¿. [Online]. Available: http://www.sciencedirect.com/science/article/pii/S0301421508004606

[9] W. Kempton and J. Tomić, "Vehicle-to-grid power implementation: From stabilizing the grid to supporting large-scale renewable energy," *Journal of Power Sources*, vol. 144, no. 1, pp. 280 – 294, 2005. [Online]. Available: http://www.sciencedirect.com/science/article/pii/S0378775305000212

[10] M. D. Galus and G. Andersson, "Demand management of grid connected plug-in hybrid electric vehicles (PHEV)," in *Energy 2030 Conference, 2008. ENERGY 2008. IEEE*, 2008, pp. 1–8.

[11] H. Lund and W. Kempton, "Integration of renewable energy into the transport and electricity sectors through V2G," *Energy Policy*, vol. 36, no. 9, pp. 3578 – 3587, 2008. [Online]. Available: http://www.sciencedirect.com/science/article/pii/S0301421508002838

[12] J. Taylor, A. Maitra, M. Alexander, D. Brooks, and M. Duvall, "Evaluations of plug-in electric vehicle distribution system impacts," in *Power and Energy Society General Meeting, 2010 IEEE*, 2010, pp. 1–6.

[13] R. C. Green, L. Wang, and M. Alam, "The impact of plug-in hybrid electric vehicles on distribution networks: A review and outlook," *Renewable and Sustainable Energy Reviews*, vol. 15, no. 1, pp. 544 – 553, 2011. [Online]. Available: http://www.sciencedirect.com/science/article/pii/S1364032110002674

[14] R. Verzijlbergh, M. Grond, Z. Lukszo, J. Slootweg, and M. Ilic, "Network impacts and cost savings of controlled ev charging," *Smart Grid, IEEE Transactions on*, vol. 3, no. 3, pp. 1203–1212, 2012.

[15] M. Albadi and E. El-Saadany, "Overview of wind power intermittency impacts on power systems," *Electric Power Systems Research*, vol. 80, no. 6, pp. 627 – 632, 2010. [Online]. Available: http://www.sciencedirect.com/science/article/pii/S0378779609002764

[16] S. W. Hadley and A. A. Tsvetkova, "Potential impacts of plug-in hybrid electric vehicles on regional power generation," *The Electricity Journal*, vol. 22, no. 10, pp. 56 – 68, 2009. [Online]. Available: http://www.sciencedirect.com/science/article/pii/S104061900900267X

[17] W. Kempton and S. E. Letendre, "Electric vehicles as a new power source for electric utilities," *Transportation Research Part D: Transport and*

Environment, vol. 2, no. 3, pp. 157 – 175, 1997. [Online]. Available: http://www.sciencedirect.com/science/article/pii/S1361920997000011

[18] W. Kempton and J. Tomić, "Vehicle-to-grid power fundamentals: Calculating capacity and net revenue," *Journal of Power Sources*, vol. 144, no. 1, pp. 268 – 279, 2005. [Online]. Available: http://www.sciencedirect.com/science/article/pii/S0378775305000352

[19] S. Han, S. Han, and K. Sezaki, "Development of an optimal vehicle-to-grid aggregator for frequency regulation," *Smart Grid, IEEE Transactions on*, vol. 1, no. 1, pp. 65–72, 2010.

[20] M. Kisacikoglu, B. Ozpineci, and L. Tolbert, "Examination of a PHEV bidirectional charger system for V2G reactive power compensation," in *Applied Power Electronics Conference and Exposition (APEC), 2010 Twenty-Fifth Annual IEEE*, 2010, pp. 458–465.

[21] C. D. White and K. M. Zhang, "Using vehicle-to-grid technology for frequency regulation and peak-load reduction," *Journal of Power Sources*, vol. 196, no. 8, pp. 3972 – 3980, 2011. [Online]. Available: http://www.sciencedirect.com/science/article/pii/S0378775310019142

[22] M. Tran, D. Banister, J. D. K. Bishop, and M. D. McCulloch, "Realizing the electric-vehicle revolution," *Nature Clim. Change*, vol. 2, no. 5, pp. 328–333, May 2012. [Online]. Available: http://dx.doi.org/10.1038/nclimate1429

[23] O. Sundstrom and C. Binding, "Flexible charging optimization for electric vehicles considering distribution grid constraints," *Smart Grid, IEEE Transactions on*, vol. 3, no. 1, pp. 26–37, 2012.

[24] W. Su, H. Eichi, W. Zeng, and M.-Y. Chow, "A survey on the electrification of transportation in a smart grid environment," *Industrial Informatics, IEEE Transactions on*, vol. 8, no. 1, pp. 1–10, 2012.

[25] OECD. (2010) Reducing transport greenhouse gas emissions: Trends and data. International Transport Forum, OECD. [Online]. Available: http://www.internationaltransportforum.org/Pub/pdf/10GHGTrends.pdf

[26] F. Birol. (2010) "World energy outlook 2010". International Energy Agency. [Online]. Available: http://www.worldenergy.org/documents/weo_2010_berlin_birol.pdf

[27] P. Denholm and W. Short, "An evaluation of utility system impacts and benefits of optimally dispatched plug-in hybrid electric vehicles," National Renewable Energy Laboratory, Tech. Rep., October 2006.

[28] S. Wirasingha, N. Schofield, and A. Emadi, "Plug-in hybrid electric vehicle developments in the us: Trends, barriers, and economic feasibility," in *Vehicle Power and Propulsion Conference, 2008. VPPC '08. IEEE*, 2008, pp. 1–8.

[29] B. K. Sovacool and R. F. Hirsh, "Beyond batteries: An examination of the benefits and barriers to plug-in hybrid electric vehicles (PHEVs) and a vehicle-to-grid (V2G) transition," *Energy Policy*, vol. 37, no. 3, pp. 1095 – 1103, 2009. [Online]. Available: http://www.sciencedirect.com/science/article/pii/S0301421508005934

[30] J. Romm, "The car and fuel of the future," *Energy Policy*, vol. 34, no. 17, pp. 2609 – 2614, 2006. [Online]. Available: http://www.sciencedirect.com/science/article/pii/S0301421505001734

[31] S. Lukic, J. Cao, R. Bansal, F. Rodriguez, and A. Emadi, "Energy storage systems for automotive applications," *Industrial Electronics, IEEE Transactions on*, vol. 55, no. 6, pp. 2258–2267, 2008.

[32] V. Marano, S. Onori, Y. Guezennec, G. Rizzoni, and N. Madella, "Lithium-ion batteries life estimation for plug-in hybrid electric vehicles," in *Vehicle Power and Propulsion Conference, 2009. VPPC '09. IEEE*, 2009, pp. 536–543.

[33] L. Serrao, Z. Chehab, Y. Guezennee, and G. Rizzoni, "An aging model of ni-mh batteries for hybrid electric vehicles," in *Vehicle Power and Propulsion, 2005 IEEE Conference*, 2005, pp. 78–85.

[34] H. Chan, "A new battery model for use with battery energy storage systems and electric vehicles power systems," in *Power Engineering Society Winter Meeting, 2000. IEEE*, vol. 1, 2000, pp. 470–475.

[35] T. Franke, I. Neumann, F. Bhler, P. Cocron, and J. F. Krems, "Experiencing range in an electric vehicle: Understanding psychological barriers," *Applied*

Psychology, vol. 61, no. 3, pp. 368–391, 2012. [Online]. Available: http://dx.doi.org/10.1111/j.1464-0597.2011.00474.x

[36] T. B. Christensen, P. Wells, and L. Cipcigan, "Can innovative business models overcome resistance to electric vehicles? better place and battery electric cars in denmark," *Energy Policy*, vol. 48, no. 0, pp. 498 – 505, 2012, ¡ce:title¿Special Section: Frontiers of Sustainability¡/ce:title¿. [Online]. Available: http://www.sciencedirect.com/science/article/pii/S0301421512004673

[37] T. Trigg and P. Telleen, "Global EV outlook, understanding the electric vehicle landscape to 2020," International Energy Agency, Tech. Rep., April 2013. [Online]. Available: http://www.iea.org/topics/transport/electricvehiclesinitiative/EVI_GEO_2013_FullReport.PDF

[38] C. Zhu and N. Nigro, "Plug-in electric vehicle deployment in the Northeast: A market overview and literature review," U.S. Department of Energy, Tech. Rep., 2012.

[39] Q. Hamid and J. Barria, "Distributed recharging rate control for energy demand management of electric vehicles," *Power Systems, IEEE Transactions on*, vol. 28, no. 3, pp. 2688–2699, 2013.

[40] H. L. Willis, *Power distribution planning reference book*, 2nd ed. CRC press, 2010.

[41] W. Li and R. Billington, *Reliability assessment of electrical power systems using Monte Carlo methods.* 233 Spring Street, New York, N.Y. 10013: Springer, 1994.

[42] "Benefits of demand response in electricity markets and recommendations for achieving them: report to U.S. congress pursuant to section 1252 of the energypolicy act of 2005," U.S. Department of Energy, Washington, DC 20585, Tech. Rep., February 2006, last accessed: August 2013. [Online]. Available: http://eetd.lbl.gov/ea/EMP/reports/congress-1252d.pdf

[43] J. Lopes, F. Soares, and P. Almeida, "Identifying management procedures to deal with connection of electric vehicles in the grid," in *PowerTech, 2009 IEEE Bucharest*, Jul. 2009, pp. 1 –8.

[44] S. Acha, T. Green, and N. Shah, "Optimal charging strategies of electric vehicles in the uk power market," in *Innovative Smart Grid Technologies (ISGT), 2011 IEEE PES*, 2011, pp. 1–8.

[45] Z. Ma, D. Callaway, and I. Hiskens, "Optimal charging control for plug-in electric vehicles," in *Control and Optimization Methods for Electric Smart Grids*, ser. Power Electronics and Power Systems. Springer US, 2012, vol. 3, pp. 259–273.

[46] L. Gan, U. Topcu, and S. Low, "Optimal decentralized protocol for electric vehicle charging," in *Decision and Control and European Control Conference (CDC-ECC), 2011 50th IEEE Conference on*, 2011, pp. 5798–5804.

[47] ——, "Optimal decentralized protocol for electric vehicle charging," *Power Systems, IEEE Transactions on*, vol. 28, no. 2, pp. 940–951, 2013.

[48] P. Vytelingum, T. D. Voice, S. D. Ramchurn, A. Rogers, and N. R. Jennings, "Agent-based micro-storage management for the smart grid," in *Proceedings of the 9th International Conference on Autonomous Agents and Multiagent Systems: volume 1 - Volume 1*, ser. AAMAS '10. Richland, SC: International Foundation for Autonomous Agents and Multiagent Systems, 2010, pp. 39–46. [Online]. Available: http://dl.acm.org/citation.cfm?id=1838206.1838212

[49] C. Wei, H. Hu, Q. Chen, and G. Yang, "Learning agents for storage devices management in the smart grid," in *Computational Intelligence and Software Engineering (CiSE), 2010 International Conference on*, 2010, pp. 1–4.

[50] Y. Wang, R. Zhou, and C. Wen, "Robust controller design for power system load frequency control ," in *Control Applications, 1992., First IEEE Conference on*, vol. 2, Sep. 1992, pp. 642–646.

[51] M. D. Galus, S. Koch, and G. Andersson, "Provision of load frequency control by phevs, controllable loads, and a cogeneration unit," *Industrial Electronics, IEEE Transactions on*, vol. 58, no. 10, pp. 4568–4582, 2011.

[52] J. Von Neumann, O. Morgenstern, A. Rubinstein, and H. Kuhn, *Theory of games and economic behavior*. Princeton Univ Pr, 2007.

[53] C. Touati, E. Altman, and J. Galtier, "Generalized nash bargaining solution for bandwidth allocation," *Computer Networks*, vol. 50, no. 17, pp. 3242 –

3263, 2006. [Online]. Available: http://www.sciencedirect.com/science/article/pii/
S1389128605004275

[54] H. Yaïche, R. R. Mazumdar, and C. Rosenberg, "A game theoretic framework for bandwidth allocation and pricing in broadband networks," *IEEE/ACM Trans. Netw.*, vol. 8, no. 5, pp. 667–678, Oct. 2000.

[55] F. Kelly, "Charging and rate control for elastic traffic," *European Transactions on Telecommunications*, vol. 8, no. 1, pp. 33–37, 1997. [Online]. Available: http://dx.doi.org/10.1002/ett.4460080106

[56] R. M. Salles and J. A. Barria, "Fair and efficient dynamic bandwidth allocation for multi-application networks," *Computer Networks*, vol. 49, no. 6, pp. 856 – 877, 2005.

[57] ——, "Lexicographic maximin optimisation for fair bandwidth allocation in computer networks," *European Journal of Operational Research*, vol. 185, no. 2, pp. 778 – 794, 2008.

[58] S. Boyd and L. Vandenberghe, *Convex optimization*.   Cambridge Univ Pr, 2004.

[59] V. Utkin, *Sliding modes in control and optimization*.   Springer-Verlag Berlin, 1992.

[60] M. Glazos, S. Hui, and S. Zak, "Sliding modes in solving convex programming problems," *SIAM Journal on Control and Optimization*, vol. 36, no. 2, pp. 680–697, 1998.

[61] K. Arrow, *An extension of the basic theorems of classical welfare economics*. Cowles Commission for Research in Economics, The University of Chicago, 1952.

[62] P. Anderson and A. Fouad, *Power System Control and Stability*.   Iowa State University Press, Ames IA, 1977.

[63] P. Anderson, J. Farquhar, J. Medalia, A. Chayes, J. Wiesner, M. Raskin, W. Reinicke, L. Haus, W. Wang, S. Tantawi *et al.*, *Power system protection*.   Wiley, 1998.

[64] X. Wang and T. Sandholm, "Learning near-pareto-optimal conventions in polynomial time," in *Advances in Neural Information Processing Systems 16*, S. Thrun, L. Saul, and B. Schölkopf, Eds.   Cambridge, MA: MIT Press, 2004.

[65] W. Usaha and J. Barria, "Reinforcement learning for resource allocation in LEO satellite networks," *Systems, Man, and Cybernetics, Part B: Cybernetics, IEEE Transactions on*, vol. 37, no. 3, pp. 515–527, 2007.

[66] P. Moses, M. A. S. Masoum, and S. Hajforoosh, "Overloading of distribution transformers in smart grid due to uncoordinated charging of plug-in electric vehicles," in *Innovative Smart Grid Technologies (ISGT), 2012 IEEE PES*, 2012, pp. 1–6.

[67] P. Richardson, D. Flynn, and A. Keane, "Local versus centralized charging strategies for electric vehicles in low voltage distribution systems," *Smart Grid, IEEE Transactions on*, vol. 3, no. 2, pp. 1020–1028, 2012.

[68] P. Zhang, K. Qian, C. Zhou, B. Stewart, and D. Hepburn, "A methodology for optimization of power systems demand due to electric vehicle charging load," *Power Systems, IEEE Transactions on*, vol. 27, no. 3, pp. 1628–1636, 2012.

[69] K. Valentine, W. G. Temple, and K. M. Zhang, "Intelligent electric vehicle charging: Rethinking the valley-fill," *Journal of Power Sources*, vol. 196, no. 24, pp. 10 717 – 10 726, 2011. [Online]. Available: http://www.sciencedirect.com/science/article/pii/S0378775311016223

[70] J. Taylor, A. Maitra, M. Alexander, D. Brooks, and M. Duvall, "Evaluations of plug-in electric vehicle distribution system impacts," in *Power and Energy Society General Meeting, 2010 IEEE*, 2010, pp. 1–6.

[71] K. Clement, E. Haesen, and J. Driesen, "Coordinated charging of multiple plug-in hybrid electric vehicles in residential distribution grids," in *Power Systems Conference and Exposition, 2009. PSCE '09. IEEE/PES*, Mar. 2009, pp. 1 –7.

[72] E. Sortomme, M. M. Hindi, S. J. MacPherson, and S. Venkata, "Coordinated charging of plug-in hybrid electric vehicles to minimize distribution system losses," *Smart Grid, IEEE Transactions on*, vol. 2, no. 1, pp. 198–205, 2011.

[73] S. Deilami, A. S. Masoum, P. S. Moses, and M. A. Masoum, "Real-time coordination of plug-in electric vehicle charging in smart grids to minimize power losses and improve voltage profile," *Smart Grid, IEEE Transactions on*, vol. 2, no. 3, pp. 456–467, 2011.

[74] K. Clement-Nyns, E. Haesen, and J. Driesen, "The impact of charging plug-in hybrid electric vehicles on a residential distribution grid," *Power Systems, IEEE Transactions on*, vol. 25, no. 1, pp. 371–380, 2010.

[75] M. Gustafson, J. Baylor, and S. Mulnix, "The equivalent hours loss factor revisited [power systems]," *Power Systems, IEEE Transactions on*, vol. 3, no. 4, pp. 1502–1508, 1988.

[76] O. M. Mikic, "Variance-based energy loss computation in low voltage distribution networks," *Power Systems, IEEE Transactions on*, vol. 22, no. 1, pp. 179–187, 2007.

[77] R. Taleski and D. Rajicic, "Energy summation method for energy loss computation in radial distribution networks," *Power Systems, IEEE Transactions on*, vol. 11, no. 2, pp. 1104–1111, 1996.

[78] A. Masoum, S. Deilami, P. Moses, M. Masoum, and A. Abu-Siada, "Smart load management of plug-in electric vehicles in distribution and residential networks with charging stations for peak shaving and loss minimisation considering voltage regulation," *Generation, Transmission Distribution, IET*, vol. 5, no. 8, pp. 877–888, 2011.

[79] F. Zhang, J. Wu, and X. Shen, "Sph-based fluid simulation: A survey," in *Virtual Reality and Visualization (ICVRV), 2011 International Conference on*, 2011, pp. 164–171.

[80] K. Zhan, Z. Hu, Y. Song, Z. Luo, Z. Xu, and L. Jia, "Coordinated electric vehicle charging strategy for optimal operation of distribution network," in *Innovative Smart Grid Technologies (ISGT Europe), 2012 3rd IEEE PES International Conference and Exhibition on*, 2012, pp. 1–6.

[81] V. Gungor, D. Sahin, T. Kocak, S. Ergut, C. Buccella, C. Cecati, and G. Hancke, "Smart grid technologies: Communication technologies and standards," *Industrial Informatics, IEEE Transactions on*, vol. 7, no. 4, pp. 529–539, 2011.

[82] ——, "A survey on smart grid potential applications and communication requirements," *Industrial Informatics, IEEE Transactions on*, vol. 9, no. 1, pp. 28–42, 2013.

[83] J. Monaghan, "An introduction to SPH," *Computer Physics Communications*, vol. 48, no. 1, pp. 89 – 96, 1988. [Online]. Available: http://www.sciencedirect.com/science/article/pii/0010465588900264

[84] J. J. Monaghan, "Smoothed particle hydrodynamics," *Reports on progress in physics*, vol. 68, no. 8, p. 1703, 2005.

[85] M. Müller, D. Charypar, and M. Gross, "Particle-based fluid simulation for interactive applications," in *Proceedings of the 2003 ACM SIGGRAPH/Eurographics symposium on Computer animation*, ser. SCA '03. Aire-la-Ville, Switzerland, Switzerland: Eurographics Association, 2003, pp. 154–159. [Online]. Available: http://dl.acm.org/citation.cfm?id=846276.846298

[86] M. Desbrun and M. paule Gascuel, "Smoothed particles: A new paradigm for animating highly deformable bodies," in *In Computer Animation and Simulation 96 (Proceedings of EG Workshop on Animation and Simulation*. Springer-Verlag, 1996, pp. 61–76.

[87] H. Lee and S. Han, "Solving the shallow water equations using 2d sph particles forinteractive applications," *The Visual Computer*, vol. 26, no. 6-8, pp. 865–872, 2010. [Online]. Available: http://dx.doi.org/10.1007/s00371-010-0439-9

[88] Y. Rebours, D. Kirschen, M. Trotignon, and S. Rossignol, "A survey of frequency and voltage control ancillary services — part I: Technical features," *Power Systems, IEEE Transactions on*, vol. 22, no. 1, pp. 350–357, 2007.

[89] M. D. Galus, S. Koch, and G. Andersson, "Provision of load frequency control by phevs, controllable loads, and a cogeneration unit," *Industrial Electronics, IEEE Transactions on*, vol. 58, no. 10, pp. 4568–4582, 2011.

[90] N. Jaleeli, L. S. VanSlyck, D. Ewart, L. Fink, and A. Hoffmann, "Understanding automatic generation control," *Power Systems, IEEE Transactions on*, vol. 7, no. 3, pp. 1106–1122, 1992.

[91] P. Palensky and D. Dietrich, "Demand side management: Demand response, intelligent energy systems, and smart loads," *Industrial Informatics, IEEE Transactions on*, vol. 7, no. 3, pp. 381–388, 2011.

[92] J. Short, D. Infield, and L. Freris, "Stabilization of grid frequency through dynamic demand control," *Power Systems, IEEE Transactions on*, vol. 22, no. 3, pp. 1284–1293, 2007.

[93] D. Angeli and P.-A. Kountouriotis, "A stochastic approach to 'dynamic-demand' refrigerator control," *Control Systems Technology, IEEE Transactions on*, vol. 20, no. 3, pp. 581–592, 2012.

[94] G. Chang, S. Chu, and H. Wang, "An improved backward/forward sweep load flow algorithm for radial distribution systems," *Power Systems, IEEE Transactions on*, vol. 22, no. 2, pp. 882–884, 2007.